Journal of Science & Technology in the Tropics

Volume 1 Number 2 Dec 2005

COSTAM

Journal of Science & Technology in the Tropics

JOSTT

DEDICATED TO THE ADVANCEMENT OF SCIENCE AND TECHNOLOGY RELATED TO THE TROPICS

Volume 1 Number 2
Dec 2005
ISSN 1823-5034

Journal of
Science & Technology
in the Tropics Volume 1 Number 2 Dec 2005

CONTENTS

Journal of Science and Technology in the Tropics (2005) 1: 95-101

Table 3. Twenty-four hour energy expenditure of normal and obese subjects on habitual calorie intake and similar physical activity level.

Subject		Age (y)	Ht (m)	Wt (kg)	BMI (kg/m^2)	Bf (%)	24-h EI (kcal) 1st trial	24-h EI (kcal) 2nd trial	24-h EE (kcal) 1st trial	24-h EE (kcal) 2nd trial
Lean	1	27	1.60	56	21.9	15.5	2382	2332	1479	1520
	2	26	1.63	63	23.7	16.6	2564	2591	1942	1919
	3	27	1.64	67	24.9	16.3	2410	2433	2157	2039
Obese	4	23	1.72	97	32.8	24.1	2833	2857	2134	2199
	5	22	1.69	98	34.3	23.6	2695	2672	2425	2641
	6	22	1.72	110	37.2	28.5	2963	2998	2636	2579
	7	22	1.78	117	36.9	34.3	3052	3028	2655	2561

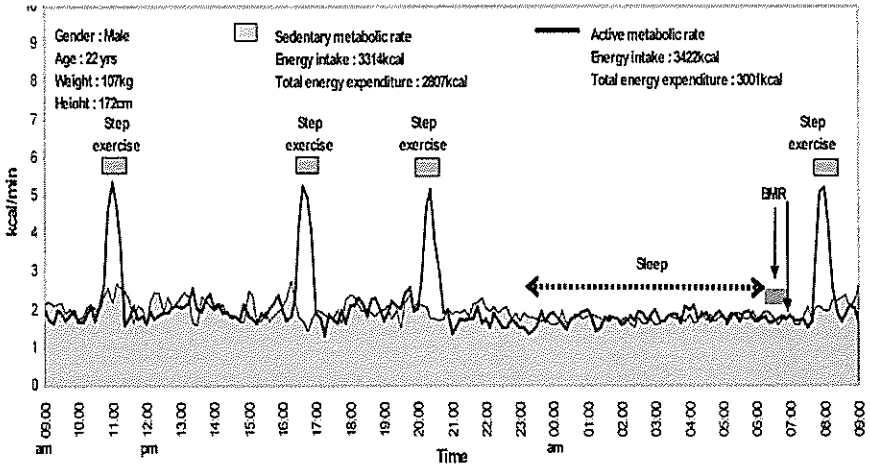

Figure 3. Twenty-four-hour energy expenditure pattern during a control (sedentary) day and during a more active day, which included four 30-min bouts of step-test exercise.

complaints were recorded by the subjects regarding its set-up. An example of a recording of a 24-h energy expenditure (sedentary and active runs) of a 22 year-old obese male subject weighing 107 kg is shown in Figure 3.

A recent study in a country with four seasons, suggested that the measured daily EE in human calorimeter was significantly lower than the FAO/WHO/UNU [8] estimated daily EE in both sedentary and active men [14]. As far as people living in temperate region have higher basal metabolic rate than their counterparts in tropical region with the same weight [15] is accepted, studies on daily energy requirements in tropical people using accurate and reliable technique, such as human calorimeter, would be more appreciated.

Furthermore, with the development of a human calorimeter, it is now possible for us to investigate some of the factors responsible for the variations in daily energy expenditure with respect to food intake, exercise and use of drugs. In addition, the basal metabolic rate (BMR) could be conveniently and accurately determined while the subjects spend a 24 h period in the calorimeter.

In conclusion, it is fair to claim that with a relatively modest expenditure, it is possible to convert an ordinary room into a calorimeter suitable for long-term studies on energy expenditure in man without sacrificing accuracy.

Acknowledgement – This research was funded by Intensified Research in Priority Area (IRPA) grant 06-02-02-0026 from the Ministry of Science and Technology of Malaysia. We are indebted to Universiti Kebangsaan Malaysia and the subjects who volunteered in this study.

REFERENCES

1 WHO (2004) Energy requirements. *Report of a joint FAO/WHO/UNU Expert Consultation*, WHO, Geneva.

2 Atwater W.O. and Benedict F.G. (1905) A respiration calorimeter with appliances for the direct determination of oxygen. *Carnegie Institute of Washington D.C.* Publication No.42.

3 Ismail M.N. and Miller D.S. (1985) A simple and inexpensive respirometer for energy expenditure studies in man. *ASEAN Food J.* **1**(4): 170-172.

4 Dulloo A.G., Ismail M.N., Ryall M., Melas G., Geissler C.A. and Miller D.S. (1988) A low-budget and easy-to-operate room respirometer for measuring daily energy expenditure in man. *Am. J. Clin. Nutr.* **48**:1367-1374.

5 Rumpler W.V., Seale J.L., Conway J.M. and Moe P.W. (1990) Repeatability of 24-h energy expenditure measurements in humans by indirect calorimetry. *Am. J. Clin. Nutr.* **51**: 147-152.

6 Toubro S., Christensen N.J. and Astrup A. (1995) Reproducibility of 24-h energy expenditure, substrate utilization and spontaneous physical activity in obesity measured in a respiration chamber. *Int. J. Obes.* **19**: 544-549.

7. Ismail M.N., Ng K.K., Chee S.S., Roslee R. and Zawiah H. (1998) Predictive equations for the estimation of basal metabolic rate in Malaysian adults. *Mal. J. Nutr.* **4**:81-90.

8. FAO/WHO/UNU (1985) Energy and protein requirements. *Technical Report Series* 724, WHO, Geneva.

9. Henry C.J.K. and Rees A.G. (1991) New predictive equations for the estimation of basal metabolic rate in tropical people. *Europ. J. Clin. Nutr.* **45**:177-185.

10. Ismail M.N. (1983) Variations in daily energy expenditure in animals and man. *PhD Thesis.* University of London, UK.

11. Weir J.B.de V. (1949) New methods for calculation metabolic rate with special reference to protein metabolism. *J. Physiol.* **109**: 1-9.

12. Brown G.A., Bennetto H.P., Miller D.S., Rigby M., Stock M.J. and Stirling J.L. (1977) A DIY human calorimeter for £100. *Proc. Nutr. Soc.* **36**: 13A(abstr.).

13. Boroumand M. (1977) Nutrition and genetics: a study of obesity and leanness in rats. *PhD Thesis.* University of London,UK.

14. Alfonzo-González G., Doucet E., Alméras N., Bouchard C. and Tremblay A. (2004) Estimation of daily energy needs with the FAO/WHO/UNU 1985 procedures in adults: comparison to whole-body indirect calorimetry measurements. *Europ. J. Clin. Nutr.* **58**: 1125-1131.

15. Hayter J.E. and Henry C.J.K. (1993) Basal metabolic rate in human subjects migrating between tropical and temperate regions: a longitudinal study and review of previous work. *Europ. J. Clin. Nutr.* **47**: 724-734.

Journal of Science and Technology in the Tropics (2005) 1: 103-107

Antioxidative properties of red palm fat blended with celery and tomato extracts in MDCM sausages

A. S. Babji, Y. J. Ee, A. A. Rahim and N. Abdullah
School of Chemical Sciences and Food Technology, Faculty of Science and Technology, Universiti Kebangsaan Malaysia, Bangi, Selangor, Malaysia

Received 15 May 2005; accepted 1 December 2005

Abstract Extracts obtained from celery and tomato were evaluated for the antioxidative effects in delaying lipid oxidation in mechanically deboned chicken meat (MDCM) sausages during chilled storage (4°C) for 12 days. There were significant differences in the thiobarbituric acid (TBA) values ($p<0.05$) between the control sample and samples treated with red palm fat plus celery extract and tomato extract respectively. Differences in the peroxide value (PV) between the control sample and the samples treated with red palm fat plus celery and tomato extracts were significant ($p<0.05$) particularly after 8-12 days of storage. Sausages blended with red palm fat and tomato extracts showed the lowest TBA and PV throughout storage, indicating synergistic effects of natural carotenoids and tocopherols acting with plant extracts in delaying lipid oxidation effectively. The pH values for all treatments decreased as the storage time increased. There were significant differences ($p<0.05$) between treatments in total plate count (TPC) from 0-12 days throughout chilled storage.

Keywords antioxidants – red palm fat – sausage

INTRODUCTION

Rapid lipid oxidation is the major cause of quality deterioration in meat products and may shorten the product's life span [1]. It is also responsible for changes in colour, texture as well as wholesomeness of food quality. Lipid oxidation not only lowers the nutritive value of food but is also associated with aging, membrane damage, heart disease, stroke and cancer in living organisms [2]. Meat products such as frankfurters which contain high unsaturated fat are particularly susceptible to oxidation.

In recent years, mechanically deboned chicken meat (MDCM) has been utilized in the processing of precooked, restructured meat products in order to lower the cost besides providing uniform textures to these products. However, the stress and aeration to which MDCM is subjected during mechanical deboning as well as its compositional nature (bone marrow, heme and lipids) contribute to its high oxidative potential [3]. Thus the inclusion of MDCM in processed products can further induce oxidative deterioration of lipids and results in shorter shelf life [4].

The addition of antioxidants to food is effective in retarding the lipid oxidation in food systems. Antioxidants disrupt the mechanism of free radical formation, thus inhibiting the reaction chain and deactivating the reactive oxygen species (ROS) in lipid oxidation. There is currently a strong interest in replacing synthetic antioxidants such as butylated hydroxyanisole (BHA) and butylated hydroxytoluene (BHT) with natural alternatives in food system due to safety concerns about potential health risks associated with these synthetic antioxidants [5]. Plant-derived substances which are known as phytochemicals act as natural antioxidants in scavenging oxygen. Phytochemicals are chemicals present naturally in plants that include essential oils, oleoresins, alkaloids, carotenoids, flavonoids, glycosides, phenolic compounds and other bioactive compounds. A variety

of spices, herbs, vegetables, fruits, oilseed, leaves, roots and grains are being investigated as potential sources of natural antioxidants [6]. Lycopene, a carotenoid with particularly effective antioxidant activity, is present mainly in tomatoes [7] and has been found to be a more powerful antioxidant than β- and α-carotene [8].

Red palm oil is made by a patented and nonchemical process and its distinctive red colour is due to this refining process where more than 80% of the natural carotenes and vitamin E is retained. Red palm oil is cholesterol-free and is a rich source of natural antioxidants such as β-carotene, tocopherols and co-enzyme Q10. β-carotene and vitamin E are powerful antioxidants which act as scavengers of damaging free radicals while the co-enzyme Q10 revitalises the body's immune system and protects against ageing-related diseases. The red palm oil also contains high levels of tocotrienols which are part of viatmin E and suppresses the formation of cholesterol in liver and reduce the harmful LDL cholesterol level in blood.

The primary objective of this study was to explore the antioxidative properties of red palm fat as well as the extracts from commonly used vegetables, namely celery and tomato in MDCM sausages. The study also evaluated the synergistic effects of red palm fat with celery and tomato extracts respectively on their antioxidative and antimicrobial properties in MDCM sausages during chilled storage (4°C) for 12 days.

MATERIALS AND METHODS

Chicken sausages were prepared using mechanically deboned meat and allotted into five treatments namely chicken fat, chicken fat with red palm fat, red palm fat, red palm fat with either celery or tomato extracts, respectively. Mechanically deboned chicken meat were obtained from a local commercial processing plant (Dinding's Poultry Processing Sdn. Bhd.) while red palm fat were purchased from Carotino Sdn. Bhd.

Preparation of natural antioxidant extract

Celery and tomato purchased from the local markets were washed, cut and dried in an oven at 50°C. Dried samples were then blended and 300 g of each sample were soaked in ethanol for 72 hours. After soaking, ethanol was removed using a vacuum rotary evaporator to obtain the extracts.

Analytical methods

Thiobarbituric acid numbers (TBA) was determined following the distillation method described by Tarladgis *et al.* [9]. Peroxide value (PV) was measured using AOAC method [10]. The pH value was determined using a Hanna Instrument model 8519 pH meter at 27°C. The colour changes of sausages during chill storage were determined for L (lightness), a (redness) and b (yellowness) using a Chromameter (Minolta Model CR-100). Total plate count (TPC) was carried out using the pour plate technique, with Plate Count Agar and incubation at 37°C for 48 hours. Counts reported were calculated from the mean of duplicate plates with colonies in the range of 30-300.

Statistical analysis

The data were analyzed using the Statistical Analysis Systems (SAS) program version 6.12 (SAS 1995). Treatments showing significant differences ($p<0.05$) were subjected to the Duncan's Multiple Range Test.

RESULTS AND DISCUSSION

The TBA values of five treatments of MDCM sausages stored at 4°C for 12 days are shown in Figure 1. The control (chicken fat) showed the highest TBA value throughout the storage period. There were significant differences ($p<0.05$) between the control and samples treated with red palm fat, with red palm fat plus 0.1% celery and 0.1% tomato extracts respectively from 4-12 days storage. Sausages blended with red palm fat plus tomato showed the lowest TBA value from 0-12 days of storage. It indicated that tomato extract was most effective in inhibiting the formation of malonaldehyde (MDA), thus delaying lipid oxidation

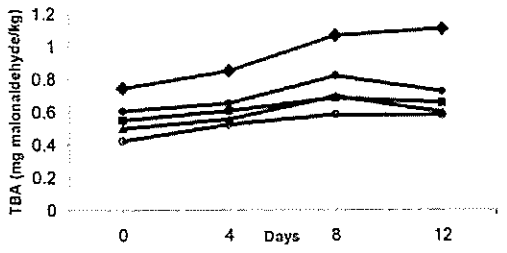

Figure 1. TBA values of five types of MDCM sausages stored at 4°C for 12 days. ◆control (chicken fat); ●sausage + chicken fat + red palm fat; ■ sausage + red palm fat; ▲ sausage + red palm fat + celery extract; ○ sausage + red palm fat + tomato extract.

in MDCM sausages. Sausages with red palm fat plus celery extract also showed strong antioxidative property by recording lower TBA values throughout the chill storage It is believed that natural antioxidants such as carotenoids and tocopherols in red palm fat also contributed to the low TBA values in sausages treated with red palm fat compared to the control using chicken fat. Thus, there may be synergistic effects of natural carotenoids and tocopherols acting with plant extracts such as celery and tomato in sausages (Fig.1). Carotenoids have been shown to interact synergistically with tocopherols in preventing oxidation and α-tocopherol is found to protect β-carotene from being degraded [11]. Babji *et al.* [12,13] have reported the improved nutritional properties of chicken frankfurter, when chicken fat was substituted with red palm fat.

All the samples showed increase in TBA values with storage time between 0 to 8 days. However, TBA values for all the samples except the control sample decreased at 12 day storage. In most cases, TBA numbers of meat products tend to increase over the storage period, and reach a maximum value and then start to decline [14]. This decline may be due to further reaction of MDA with the meat constituents such as the amino group. Kim and Labella [15] suggested that the reduction of TBA values observed in the later stages of oxidation is probably associated with the formation of highly polar product (as well as carbonyl and fluorescent), resulting from polymerisation of secondary oxidation products. Gutteridge [16] reported losses of substantial amounts of TBA-reactivity by MDA during the process of polymerisation. The secondary oxidation products, especially the aldehydes, have the off flavours associated with rancid oil.

The peroxide values (PV) for all the five treatments over the chilled storage for 12 days are shown in Figure 2. The control (chicken fat) showed high PV compared to samples with red palm fat and plant extracts added to the sausage. Sausages that contained red palm fat plus 0.1% tomato extracts showed the lowest PV values during the test period. Differences in PV values amongst treatments were significant ($p<0.05$), particularly after 8-12 days of storage. The peroxide value is a good guide to the quality of a fat and is indeed a most common method to measure the primary initial product formed by oxidation such as peroxide or hydroperoxide [17]. PV is reported in units of miliequivalents of oxygen per kilogram fat and it is claimed that PVs ranging from 0.06 to 20 units are acceptable. All treatments showed decrease in PV values from 8 to12 days of storage. Wang *et al.* [18] reported that the decrease of PV values is probably due to the degradation of hydroperoxides. Hydroperoxides are essentially odourless and can potentially decompose into a variety of volatile and non-volatile secondary products [19].

Colour changes to the sausages during chilled storage (4°C) for 12 days are shown in Figures 3, 4 and 5. The control (chicken fat) possessed lighter surface

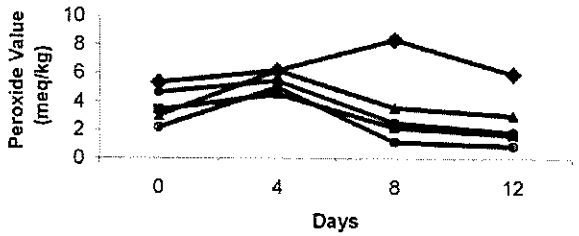

Figure 2. Peroxide values (PV) of five types of MDCM sausages stored at 4°C for 12 days. ◆ control (chicken fat); ● saudage + chicken fat + red palm fat; ■ sausage + red palm fat; ▲ sausage + red palm fat + celery extract; ○ sausage + red palm fat + tomato extract

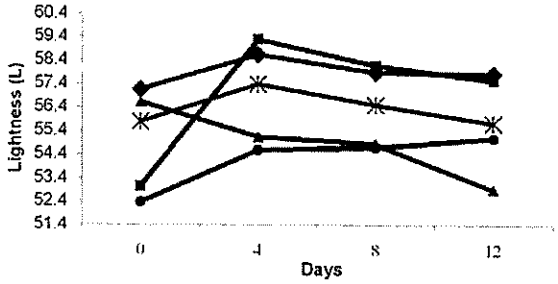

Figure 3. Lightness (L) values of five types of MDCM sausages stored at 4°C for 12 days. ◆ control (chicken fat); ● sausage + chicken fat + red palm fat; ■ sausage + red palm fat; ▲ sausage + red pal fat + celery extract; ✳ sausage + red palm fat + tomato extract

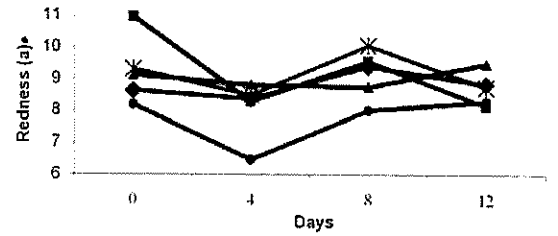

Figure 4. Redness values (a) for five types of MDCM sausages stored at 4°C for 12 days. ◆ control (chicken fat); ● sausage + chicken fat + red palm fat; ■ sausage + red palm fat; ▲ sausage + red palm fat + celery extract; ✳ sausage + red palm fat + tomato extract

Journal of Science and Technology in the Tropics (2005) 1: 103-107

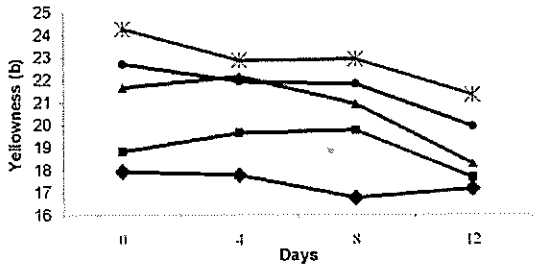

Figure 5. Yellowness (b) values for five types of MDCM sausages stored at 4°C for 12 days. ◆ control (chicken fat); ● sausage + chicken fat + red palm fat; ■ sausage + red palm fat; ▲ sausage + red palm fat + celery extract; ✳ sausage + red palm fat + tomato extract

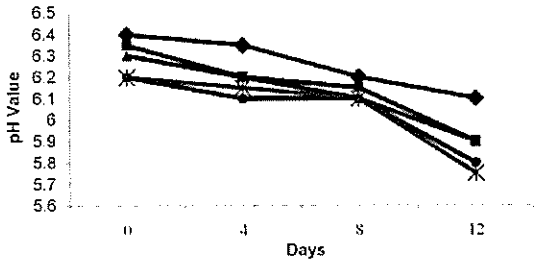

Figure 6. The pH values of five types of MDCM sausages stored at 4°C for 12 days. ◆ control (chicken fat); ■ sausage + chicken fat + red palm fat; ▲ sausage + red palm fat; ● sausage + red palm fat + celery extract; ✳ sausage + red palm fat + tomato extract

colour compared to those blended with red palm fat exhibiting darker surface (lower L value) and more reddish yellow colour intensities (higher a and b values). Sausages with red palm fat plus tomato extract also exhibited higher b value (more yellowness), giving the surface an attractive pinkish yellow colour.

The pH values of five treatments of MDCM sausages stored over 12 days at 4°C are shown in Figure 6. Due to its relationship to bacterial growth, pH was monitored in this study. The samples treated with red palm fat and plant extracts had lower pH throughout the chilled period, while the control sample had higher overall pH. Sausages with red palm fat showed a significant reduction ($p<0.05$) in pH values during the 12 days chilled storage. Rhee *et al.* [20] suggested that the reduction of pH values was due to the release of fatty acid from the phospholipids fraction which changed the lipid molecule into free fatty acid and triglyceride. During chilled storage, microbes tend to use more oxygen and acidic products such as hydrogen sulfide are formed, thus lowering the pH value. Blickstard and Molin [21] found a slight decrease in the pH of frankfurter sausages after storage in vacuum at 4°C.

The total plate count (TPC) for all the five formulated sausages are shown in Table 1. During chilled storage (4°C) from 0-12 days, all the samples showed increase in TPC, with the control (chicken fat) recording the highest count ($3.2x10^6$ per g) at day 12. Sausages treated with red palm fat plus tomato extract showed strong synergistic relationship in being antibacterial followed by celery extract with red palm fat, respectively. Differences between samples for TPC were significant ($p<0.05$). The antimicrobial effectiveness of phenolic compounds has been associated with their surface-active properties [22]. A strong chemical interaction may occur between the antioxidants and the medium matrix.

Table 1. Total Plate Count (per g) for five formulation of MDCM sausages stored at 4°C for 12 days.

Days	Formulation				
	T1	T2	T3	T4	T5
0	$^{D}3.5x10^{3a}$	$^{D}2.8x10^{3b}$	$^{D}2.4x10^{3c}$	$^{D}1.7x10^{3d}$	$^{D}1.5x10^{3e}$
4	$^{C}7.8x10^{3a}$	$^{C}5.6x10^{3b}$	$^{C}4.2x10^{3c}$	$^{C}3.5x10^{3d}$	$^{C}3.6x10^{3d}$
8	$^{B}2.6x10^{5a}$	$^{B}1.4x10^{4b}$	$^{B}8.9x10^{3c}$	$^{B}6.5x10^{3d}$	$^{B}6.7x10^{3e}$
12	$^{A}3.2x10^{6a}$	$^{A}8.5x10^{4b}$	$^{A}4.6x10^{4c}$	$^{A}2.8x10^{4d}$	$^{A}2.6x10^{4c}$

T1: Control with chicken fat; T2: Sausage + Chicken fat + Red palm fat;
T3: Sausage + Red palm fat; T4: Sausage + Red palm fat + celery extract
T5: Sausage + Red palm fat + tomato extract
a-b: Means within a row with the different lower case letter are significantly different ($p<0.05$)
A-B: Means within a column with the different upper case letter are significantly different ($p<0.05$)

CONCLUSION

Red palm fat added to MDCM sausages to replace chicken fat exhibited antioxidative property. When blended with celery and tomato extracts, antioxidative and antimicrobial properties were significantly increased in MDCM sausages. It can be concluded that natural antioxidants such as carotenoids and tocopherols as well as plant extracts from celery and tomato-, are beneficial to reduce oxidation and improve the shelf life and quality of chicken sausages.

Acknowledgement – The project was funded by Universiti Kebangsaan Malaysia (UKM), Ministry of Science and Technology and the Environment (MOSTE) IRPA Grant, MPOB and Carotino Sdn. Bhd.

REFERENCES

1. Fernandez J., Perez-Alvarez J.A. and Fernandez-Lopez J.A. (1997) Thiobarbituric acid test for monitoring lipid oxidation in meat. *Food Chemistry* **59**(3): 345-353.
2. Addis P.B. and Warner G.J. (1991) The potential herbal aspects of lipid oxidation products in food. *In*: *Free radicals and food additives* (eds O.I. Aruoma and B. Halliwell) pp 77-119. Taylor & Francis, London.
3. Dawson L.E. and Gartner R. (1983). Lipid oxidation in mechanically deboned poultry. *Food Tech.* **37**(7): 112-116.
4. McNeill J., Kakuda Y. and Findlay C. (1988) Influence of carcass parts and food additives on the oxidative stability of frozen mechanically separated and hand-deboned chicken meat. *Poultry Sci.* **67**: 270-276
5. Sherwin E.R. (1990) Antioxidants. *In*: *Food Additives* (eds A.L. Branen *et al.*) pp 139-193. Marcel Dekker Inc., New York.
6. Pratt D.E. and Hudson B.J.F. (1990) Natural antioxidants not exploited commercially. *In*: *Food Antioxidants* (ed B.J.F. Hudson) pp 171-192. Elsevier Science Publishers Ltd., London.
7. Duthie G.G. and Brown K.M. (1999) Reducing the risk of cardiovascular disease. *In*: *Functional Foods, Desiger Foods, Pharmafoods and Nutraceuticals* (ed I. Goldberg) p 27. An Aspen Publications.
8. Di Mascio P., Kaiser S. and Sies H. (1989) Lycopene as the most efficient biological carotenoid singlet oxygen quencher. *Arch. Biochem. Biophys.* **274**: 532-538.
9. Tarladgis B.G., Watts B.M., Younathan M.T. and Dugan L.R. (1960) A distillation method for quantitative determination of malonaldehyde in rancid food. *J. Am. Oil Chem.* Soc. **80**: 37-44
10. AOAC (1984) Official methods of analysis. 14th ed. *Association of Official Analytical Chemist*, Washington, D.C.
11. Palozza P. and Krinsky N.I. (1992) α-Carotene and β-tocopherol are synergistic antioxidants. *Arch. Biochem. Biophys.* **297**: 184-187.
12. Babji A.S. (2001) Malaysian palm fat as animal fat analogue in processed meat product. *Proceeding of the 47th International Congress of Meat Science and Technology (ICoMST)* pp 268-269,Krakow, Poland.
13. Babji A.S. (2001) Physical and nutritional properties of frankfurter where chicken fat is substituted with red palm fat. *Proceeding of the 47th International Congress of Meat Science and Technology (ICoMST)* pp 270-271, Krakow, Poland.
14. Shahidi F. (1992) Prevention of lipid oxidation in muscle foods by nitrite and nitrite-free compositions. In: *Lipid Oxidation in Food* (ed J.S.A. Allen), *ACS Symposium Series 500*, pp 178-179 American Chemical Society, Washington DC.
15. Kim R.S. and Labella F.S. (1987) Comparison of analytical methods for monitoring autoxidation profiles of authentic lipids. *J. of Lipid Research* **28**: 1110-1117.
16. Gutteridge J.M.C. (1975) The use of standards for malondialdehyde. *Analytical Biochemistry*, **69**: 518-526.
17. Rossell J.B. (1994) Measurement of rancidity. *In*: *Rancidity in foods* (eds J.C. Ellen and Hamilton) pp 22-51, Applied Science Publisher, London.
18. Wang F.S., Jiang Y.N. and Lin C.W. (1995) Lipid and cholesterol oxidation in chinese-style sausage using vacuum and modified atmosphere packaging. *Meat Sci.* **40**: 93-101.
19. Crapiste G.H., Brevedan M.I.V. and Carelli A.A. (1999) Oxidation of sunflower oil during storage. *J. Am. Oil Chem. Soc.* **76**: 1437-1442.
20. Rhee K.S., Krahl L.M., Lucia L.M. and Acuff G.R. (1997) Antioxidative/antimicrobial effects and TBARS in aerobically refrigerated beef as related to microbial growth. *J. Food Sci.* **62**: 1205-1210.
21. Blickstard E. and Molin G. (1983) The microbial flora of smoked pork loin and frankfurter sausage stored in different gas atmosphere at 4°C. *J. Appl. Bacteriol.* **54**: 45-46.
22. Juvens B., Henis Y. and Jacoby B. (1972) Studies on the mechanism of the antimicrobial action of oleuropein. *J. Appl. Bacteriol.* **35**: 559-567.

Journal of Science and Technology in the tropics (2005) **1**: 109-115

Genetic engineering of silk banana (AAB) for tolerance to *Fusarium* wilt disease

S. Sreeramanan[1,2], M. Maziah[1], M. P. Abdullah[1], M. Sariah[3] and M. F. Nor'Aini[4]

[1] Department of Biochemistry, Faculty of Biotechnology and Biomolecular Sciences, Universiti Putra Malaysia, 43400 Serdang, Selangor Darul Ehsan, Malaysia

[2] Department of Biotechnology, Asian Institute of Medicine, Science and Technology (AIMST), Amanjaya, 08000, Sungai Petani, Kedah, Malaysia

[3] Department of Plant Protection , Faculty of Agriculture and [4] Department of Biology, Faculty of Science and Environmental Studies, Universiti Putra Malaysi

Abstract An effective method has been developed for the stable transformation and regeneration of silk banana (*Musa* spp. AAB group) cv 'Rastali' using microprojectile bombardment. Recent progress with advanced *in vitro* cultures of banana such as establishment of highly regenerable tiny single meristem buds opened the opportunity for the production of disease tolerant transgenic bananas. Chitinase and glucanase the important disease tolerant genes were successfully transformed into banana using microprojectile bombardment system together with *gfp* and *gusA* genes as reporter gene. Proliferating single buds were selected on geneticin G-418 to produce a number of putatively transformed bananas. Five different treatments using different chitinase and glucanase genes inserted singly or in combination were carried out. Molecular analyses such as polymerase chain reactions (PCR) and Southern blot was performed to confirm the integration and expression of the introduced genes in genome. The transgenic banana plantlets from each treatment inoculated with conidial suspension of fungal to evaluate the degree of tolerance and to investigate the effectiveness of the bioassay system as a potential tool for early screening. Differences chemical compound such as hydrogen peroxide (H_2O_2), and relevant enzyme activities such as phenylalanine ammonia lyase (PAL), chitinase, glucanase, peroxidase (PER) and polyphenol oxidase (PPO), were determined for each treatment including control plantlets. Evaluation of disease development in primarily and secondary infections showed that combination of the two transgenes gave substantially greater protection against the fungal than single-transgene introduction. Productive interactions between chitinase and glucanase transgenes *in planta* point to combinatorial expression of antifungal genes as an effective approach to enhanced tolerance to Fusarium wilt disease.

Keywords transgenic banana – chitinase – glucanase – *Fusarium* wilt tolerant

INTRODUCTION

Fusarium wilt disease causes severe damage in commercial plantations and represents a major constraint to banana production in Malaysia. Pisang Rastali (AAB) is a local dessert banana, which belongs to the AAB group and also known as Pisang Keling and Pisang Tali. Large-scale cultivation of this cultivar is difficult, as it is highly susceptible to *Fusarium oxysporum* f.sp. *cubense* race 1. Genetic engineering offers an alternative route to increase resistance to Fusarium wilt disease. Microprojectile bombardment was used for Pisang Rastali (AAB) transformation using tiny single meristem buds. Therefore, genetic engineering with the introduction of genes conferring resistance to fungal pathogens such as chitinase and β-1,3-glucanase is a useful complementary tool to overcome this problem.

Co-transformation is a potential tool to create multiple and durable resistance in banana [1]. Transgenic tomato plants expressing only a chitinase or a β-1,3-glucanase transgene were susceptible to *Fusarium oxysporum*, but plants expressing both genes had significantly higher resistance than the plants

Journal of Science and Technology in the Tropics (2005) 1: 109-115

expressing only chitinase or β-1,3-glucanase [2]. Similarly, Jach *et al.* [3] demonstrated that tobacco plants expressing a barley β-1,3-glucanase and a chitinase gene had a greatly enhanced resistance compared to plants expressing only one of these two enzymes. Bliffeld *et al.* [4] introduced barley seed class 11 chitinase gene (*Pr3*) driven by maize ubi promoter along with β-1,3-glucanase gene in Bobwhite cultivar of wheat using particle bombardment.

In this study, five different treatments using different chitinases and β-1,3-glucanase genes inserted singly or in combination were carried out. Multiple genes encoding either chitinases (RCC2 or *Chi*) or β-1,3-glucanase (Eg) and both was bombarded together with *gfp* gene (pGEM.Ubi-SgfpS65T) for early transient expression signal using an optimised physical and biological condition. For the analysis of transgene integration patterns, a polymerase chain reactions (PCR) and Southern blot hybridization techniques have been elaborated and evaluated. Transgenic plants with a transgene locus resulting from genomic integration of a single, perfect copy of delivered DNA are most desirable for banana improvement [5]. Finally, to assess practical applications of the developed transformation protocol for Fusarium wilt disease control, the chitinase and β-1,3-glucanase genes, was transferred into Pisang Rastali (AAB) and the transgenic banana produced were tested using an optimised fungal bioassay conditions.

MATERIALS AND METHODS

Target tissue

Corm slices of *in vitro* plantlets were cultured in MS, Murashige and Skoog, [6] medium supplemented with different concentrations of 6-Benzylaminopurine (BAP) to obtain multiple bud clumps [7]. Single buds (3 mm), excised from multiple bud clumps, were used for transformation studies.

Antibiotic selection agents

The effectiveness of kanamycin, geneticin G-418, neomycin, paromomycin, basta and hygromycin as selection agents to inhibit the growth of single buds derived from multiple bud clumps were evaluated. The concentration of selection agents tested was 0, 25, 50, 100, 150, 200, 250 and 300 mg/L in both solid and liquid medium. For basta and hygromycin, the experiment was further carried out at lower concentrations of 0, 5, 10, 15, 20 and 25 mg/L.

Physical and biological parameters of microprojectile bombardment

Optimisations of the physical and biological parameters were carried out based on GUS and GFP transient gene expressions. Optimisation of the physical parameters was carried out under the following conditions; rupture disc pressure; distance from stopping plate to target tissue; vacuum pressure; gold microcarrier size and number of bombardments per Petri dish. The biological parameters included the explant types, preculture treatment prior bombardment; DNA concentrations and various explants sizes. Introducing multiple genes encoding chitinases (pRCC2 and pMRC 1301) and β-1,3-glucanase (pROKLA-Eg) together with *gfp* gene (pGEM.Ubi-SgfpS65T) for early transient gene expression using an optimised physical and biological parameters as mentioned above.

Antibiotic selection of transformants

After bombardment, single buds were transferred to MS medium containing 10mg/L of BAP and were allowed to recover for two weeks in the absence of antibiotic selection. After this recovery period, explants were transferred to the same medium containing 50mg/L geneticin G-418 for two weeks. The survived explants were transferred back to the liquid medium containing 25mg/L of geneticin G-418 for additional two weeks. Liquid medium selection provides a better contact between the tissues and the antibiotic solution. The survived tissues were further selected in MS solid medium using geneticin G-418 at 25mg/L. The survived explants were maintained in hormone free medium for plant regeneration. The regenerated plantlets from each putatively independent transformed cell line were maintained under *in vitro* conditions for further confirmation.

Histochemical GUS staining and visualisation of GFP

Bombarded tissues were assayed for GUS expression according to Jefferson *et al.* [8]. A florescence microscope (Leica MZFL 111) equipped with GFP 2 filter set used to monitoring GFP expression of transformed tissues.

PCR and Southern blot hybridization analysis

Genomic DNA was extracted from putative transformants using an improved and modified CTAB

Table 1. Genes, primer, primer sequences and expected product length from PCR.

Gene	Primer	Sequence	Product length
gfp	Forward	5'-ATGAGTAAAGGAGAAGAACTTTTC- 3'	726 bp
(pGEM.Ubi1-SgfpS65T)	Reverse	5'-TTTGTATAGTTCATCCATGCCA- 3'	
gusA	Forward	5'-CGCCGATGCAGATATTCGTA- 3'	789bp
(pMRC1301)	Reverse	5'-ATTAATGCGTGGTCGTGCAC-3'	
Chitinase	Forward	5'-TGGATCCAGCGGCTCGTCGGTTG-3'	310 bp
(pBI333-EN4-RCC2)	Reverse	5'-GTATAATTGCGGGACTCTAAT-3'	
Chitinase	Forward	5'-TACAACTTCAACTACGGGCCG-3'	486 bp
(pMRC1301)	Reverse	5'-ACGACTCACTATAGGGCG-3'	
β-1,3 glucanase	Forward	5'-GATGTGATATCTCCACTGACGTAAG-3'	830 bp
(pROKla-Eg)	Reverse	5'-GTATAATTGCGGGACTCTAAT-3'	
npt II	Forward	5'-CCCCTCGGTATCCAATTAGAG-3'	900 bp
	Reverse	5'-CGGGGGGTGGCCGAAGAACTCCAC-3'	

method adopted from Pasakinskiene and Paplauskience [9]. PCR was done using the DNA Thermal Cycler 480 machine (Perkin-Elmer). RCC2 and *Chi* (Chitinases gene) , Eg (β-1,3 glucanase) and *npt II* genes were amplified using standard protocols [10].The following primers were used to amplify the transgenes and part of the regulatory sequences (Table 1).

PCR amplications were carried out in 100 µl reactions volume containing template DNA (500 ng genomic DNA or 60ng plasmid DNA), 200 ng of each primer (forward and reverse), 0.2 mM dNTP mix, 1.5 mM $MgCl_2$, 1X PCR buffer and 5 U Taq DNA polymerase (MBI Fermentas). Amplification for *gfp* and *gusA* genes were performed using the following conditions: 1 cycle of 94°C for 5 min; 30 cycles of 94°C (30 sec), 60°C (1 min) and 72°C (2 min); and 1 cycle of 72°C for 7 min. Amplification of chitinase gene (RCC2) fragments was performed for 35 cycles at 94°C for 1 minute, 55°C for 1 minute and 72°C for 2 minutes, for denaturing, annealing and primer extention, respectively. The conditions for amplification of chitinase gene (*Chi*) conducted were: 1 cycle of 95°C for 5 min; 35 cycles of 95°C (1 min), 58°C (1min) and 72°C (2 min); and 1 cycle of 72°C for 7 min. Amplification of β-1,3 glucanase gene (Eg) fragments was performed for 45 cycles at 94°C for 1 minute, 40°C for 2 minutes and 72°C for 3 minutes, for denaturing, annealing and primer extention, followed by 72°C for 7 minutes. Amplication of *nptII* gene fragments was performed for 35 cycles at 94°C for 1 minute, 62°C for 1 minute and 72°C for 2 minutes, for denaturing, annealing and primer extention, respectively. All amplified PCR products were checked on 1.2% agarose gel.

Southern blot analyses were carried out using a non-radioactive method was used to confirm stable integration of chitinase (RCC2 and *Chi*) and β-1,3 glucanase (Eg) transgenes in the host banana genome. DIG DNA Labeling and Detection Kit (Roche) were used in this study. DIG-labeled DNA probes are generated according to the method of random primed labeling which is based on the hybridization of random oligonucleotides to the DNA template [11].

Development of *Fusarium* bioassay method

Induction of sporulation and germination of *Fusarium oxysporum* f.sp. *cubense*, race 1 (VCGs 01217) were carried out for four weeks. For plant inoculation bioassay, untransformed Pisang Rastali (AAB) plantlets roots sections were cut at 3 cm from the root tips. The plants dipped into three different spore concentrations (10^4, 10^6 and 10^8 spores/ml) for one hour and were then transplanted in a plastic container (8cm x 8cm) with sterile perlite (Figs. 1,2). One ml of different spore concentrations was again inoculated near the root/stem regions for double confirmation. Each concentration of spores inoculated in four replicates and was repeated for three times except for testing transgenic bananas. The total spores obtained were diluted into three different spore concentrations ($2x10^4$, $2x10^6$ and $2x10^8$ spores/ml). The plantlets were watered using hormone and sucrose free MS liquid medium. Disease development and severity were monitored and measured over for a period of four weeks. The same protocol was applied for disease development in transgenic plantlets. Necrosis in new and old leaves tissue (yellowing) indicated Fusarium wilt symptoms occurred.

Journal of Science and Technology in the Tropics (2005) 1: 109-115

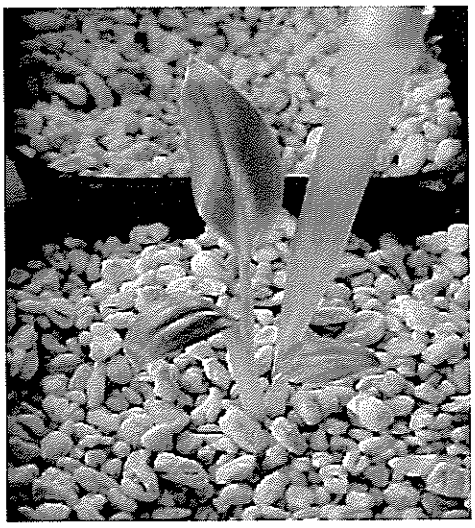

Figure 1. The assembly of the single banana plantlet with perlite for *Fusarium* bioassay assay. The pipette tip indicates the initial point where inoculum (one ml) was applied after the each single plantlet dipped for an hour in Fusarium spores suspension.

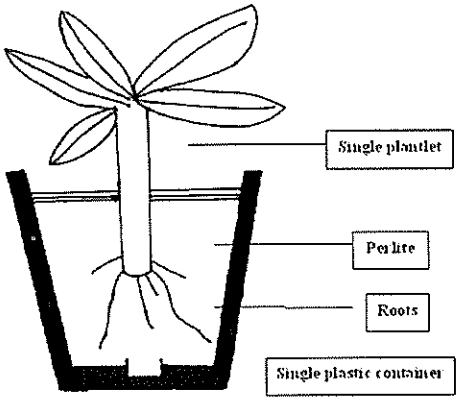

Figure 2. Systemic assembly of cross section the single banana plantlet onto perlite for *Fusarium* bioassay. The roots were challenged with different numbers of variable spores. Disease development was scored after 28 days of experiments.

Biochemical analyses

Hydrogen peroxide (H_20_2) compound and phenylalanine ammonia lyase (PAL) enzyme activities were carried out at 12 hours intervals for 72 hours, while other enzymes (peroxidase, polyphenol oxidase, chitinase and β-1,3-glucanase), activities were measured at four weeks after inoculation.

Hydrogen peroxide (H_20_2)

$H_2O_2$was assayed according to the method of Jiang *et al.* [12]. Hydrogen peroxide (H_2O_2) activity was expressed in nmol g^{-1} fresh weight.

Phenylalanine ammonia lyase (PAL) assay

PAL was assayed according to the method of Robert and Helmut [13]. PAL activity was expressed as changes in absorbance at 290 nm h^{-1} mg^{-1} protein.

Peroxidase activity assay

Peroxidase activity was assayed as described by Hammerschmidt *et al.* [14] and was expressed in unit/mg protein at 470nm. A change in 0.1 absorbance/minute/mg protein refers as one unit.

Polyphenol oxidase activity

Polyphenol oxidase activity was assayed as described by Mozzetti *et al.* [15] and was expressed in unit/mg protein at 410nm. A change in 0.1 absorbance/minute/mg protein refers as one unit.

Chitinase and β-1,3-glucanase assays

A modified method of Tonon *et al.* [16] was used to detect chitinase and β-1,3-glucanase activities. Chitinase activity was expressed as nkat/mg protein with N-acetylglucosamine as standard.β-1,3-glucanase activity was expressed as nkat/mg protein with glucose as standard.

RESULTS AND DISCUSSION

Of six antibiotic selection agents tested, hygromycin was the best selective agent and followed by basta. Both selection agents showed an earliest sign of toxicity in fast for inhibition response at low concentration level particular in liquid medium. However, geneticin G-418 was the preferable selection agent compared to kanamycin, neomycin and paramomycin which confers resistance to *npt II* gene. The use of alternating the solid and liquid medium appears to be more effective for selecting transformant tissues and possibility may minimise the occurrence of chimeras (non-transformed tissues). Main consideration was still on geneticin G-418 because all plasmids used in this study confers resistance to *npt II* gene.

For microprojectile bombardment system, it was found that optimised physical parameters could achieved by bombarding twice at 1100psi of helium pressure, 9mm distance from stopping plate to target tissues, 28mm Hg vacuum pressure and 1 μm of gold size based on GUS and GFP transient expressions. For biological parameters, single buds at 3mm, 1.5μg of gold per bombardment, three days preculture prior to bombardment and six days post bombardment were

found to be optimal conditions for Pisang Rastali (AAB).

For transformation using chitinase and β-1,3-glucanase genes, stable *gusA* and *gfp* genes in transformed single buds, multiple bud clumps, leaves and roots were successfully obtained (Fig. 3).

Integrative of the transgenes and stable of microprojectile bombardment system were assessed by PCR amplications of 726 bp of *gfp* gene, 789 bp of *gusA* gene, 310 bp of RCC2 (chitinase) gene, 486 bp of pMRC1301 (chitinase), 830 bp of pROKLA-Eg (β-1, 3-glucanase) and 900 bp of *npt11* gene (Fig. 4a-f). Genomic Southern blot hybridization confirmed the incorporation of the RCC2, pMRC1301 and pROKLA-Eg genes in host genome between one and four inserted copies (Fig. 5a-c).

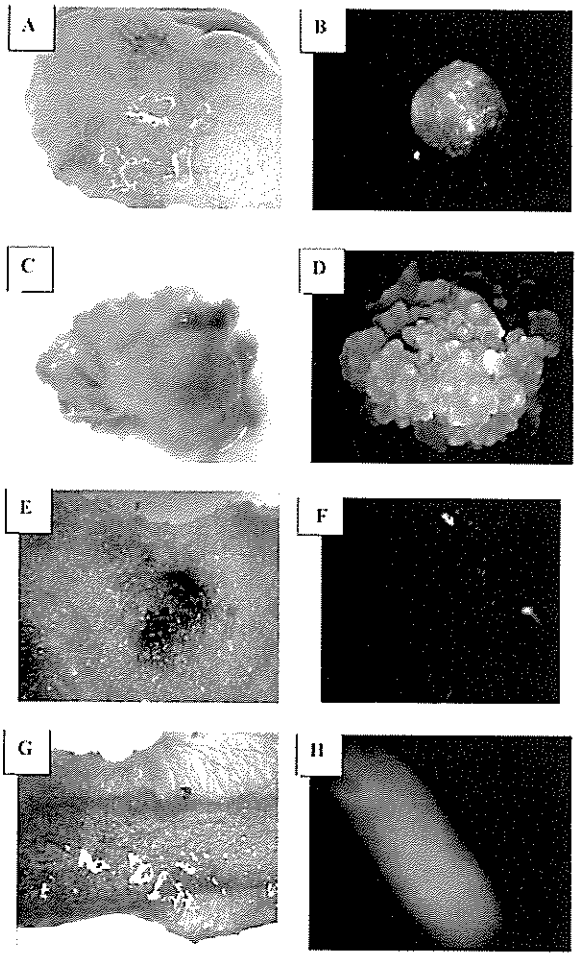

Figure 3. Visualisation of stable *gusA* (A, C, E and G) and *gfp* (B, D, F and H) genes expression in various tissues of Pisang Rastali (AAB). A and B: single buds; C and D: multiple bud clumps (Mbcs); E and F: leaves ; G and H: roots.

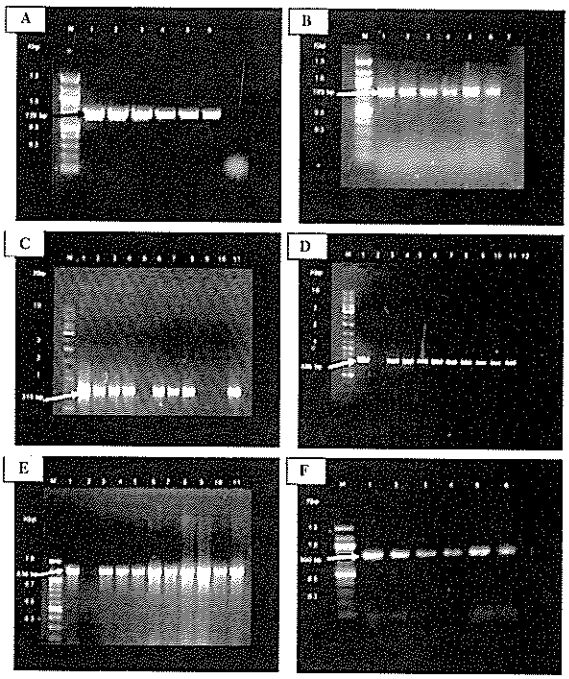

Figure 4. PCR analyses. Amplification PCR products of 726 bp of *gfp* gene (A), 789 bp of *gusA* gene (B), 310 bp of RCC2 (chitinase) gene (C), 486 bp of pMRC1301 (chitinase) gene (D), 830 bp of pROKLA-Eg (β-1,3 glucanase) gene (E) and 900 bp of *npt11* gene (F) in transgenic Pisang Rastali (AAB) plantlets selected on geneticin G-418.

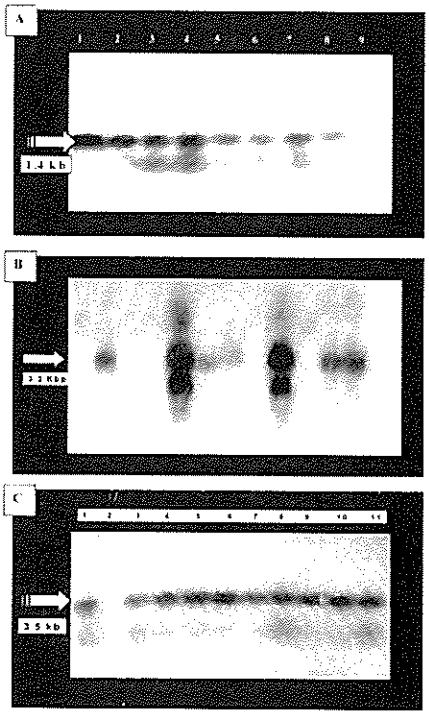

Figure 5 : Southern blot analyses. Integration patterns of the RCC2 (Chitinase) gene (A) pMRC1301(Chitinase) gene (B) and pROKLA-Eg (β-1,3 glucanase) gene (C) in transgenic Pisang Rastali (AAB) plantlets selected on geneticin G-418.

For *Fusarium* bioassay method, time course of *Fusarium oxysporum* f.sp. *cubense* (Race 1 ; VCGs 01217) spore production *in vitro* and the actual number of geminated spores determined. Highest spore production at 28 days with highest germination rate (62%) applied for bioassay testing of transgenic plantlets. The degree of resistance displayed by transgenic plantlets produced was correlated with hydrogen peroxide (H_20_2) and phenylalanine ammonia lyase (PAL) is the most sensitive compound and enzyme post to the *Fusarium* spore inoculations. The results showed that plantlets which contain chitinase and β-1,3-glucanase genes showing the highest chitinase, β-1,3-glucanase, peroxidase (PER) and poly-phenoloxidase (PPO) enzyme activities after four weeks compared to single inserted chitinase or β-1,3-glucanase gene. Progress of the disease symptoms caused by *Fusarium oxysporium* f.sp. *cubense* (race 1) on the leave of the transgenic Pisang Rastali (AAB) plantlets shown in Figure 6.

Transgenic tomato plants expressing only a chitinase transgene or a β-1,3-glucanase transgene were susceptible to *Fusarium oxysporum* f.sp. *lycopersici*, whereas plants expressing both genes had significantly higher resistance than the plants expressing only chitinase or β-1,3-glucanase [2]. However, we found that combination between RCC2 (Chitinase) and pROKla-EG (β-1,3-glucanase) genes found to be more effectives compared to combination with pMRC1301 (Chitinase) and pROKla-EG (β-1,3-glucanase) genes. In addition, several studies have been made on transgenic plants integrated with RCC2 chitinase gene possessed increased resistance to various fungal diseases [17,18]. Transgenic tobacco plants expressing a soybean β-1,3-glucan-elicitor releasing β-1,3 glucanase or the tobacco class II β-1,3 glucanase show reduced symptoms when infected with *Alternaria alternate* or the oomycetes *Phytophthora parasitica* var. *nicotiane* and *Peronospora tabacina* [19,20]. In addition, transgenic potato plants expressing soybean β-1,3-endoglucanase gene exhibit an increase in the activity of β-1,3-glucanase in transgenic plants [21].

The above transformation technology has a great potential for molecular improvement of banana especially to control *Fusarium* wilt disease.

Acknowledgements – The generous gifts of a RCC2 (rice chitinase) plasmid by Dr Yokoshiwa from National Institute of Agrobiological Resourses, Japan, pMRC1301 (rice chitinase) plasmid by Dr Ruslan Abdullah from Universiti Kebangsaan Malaysia, pROK1a-EG (soybean β-1, 3-glucanase) plasmid by Dr Yoji Takeuchi from Hokkaido University, Japan and pGEM.Ubi1-sgfps65T by Dr Adrian Elliott from CSIRO, Australia are gratefully acknowledged. This research was supported by the Ministry of Science, Technology and Environmental funded this research through IRPA PR Research Grant (01-02-04-0000-PR0010/04).

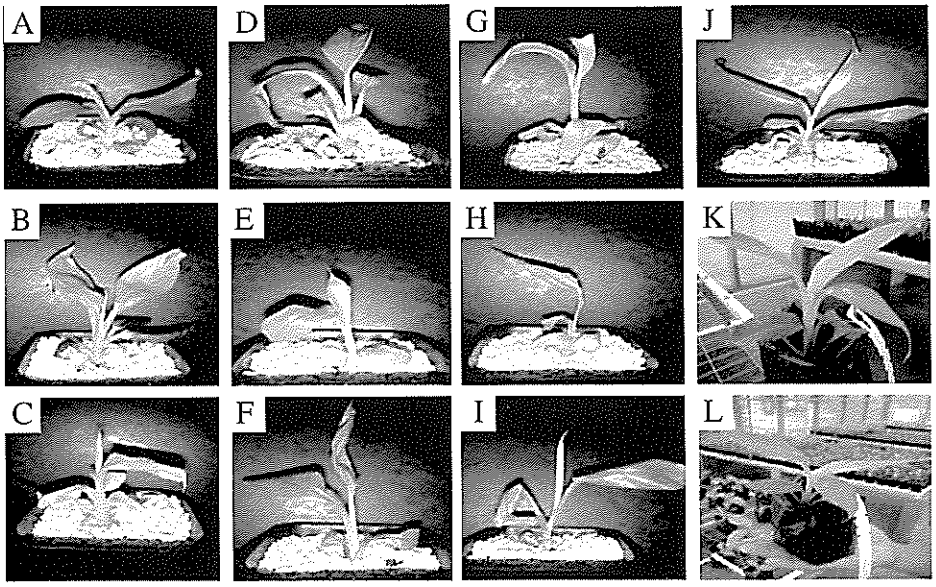

Figure 6. Progress of disease symptoms (secondary) caused by *Fusarium oxysporum* f.sp. *cubense* (Race1) on the leave of transgenic Pisang Rastali (AAB) plantlets (Particle bombardment-mediated transformation). (A) Control plantlet (No spore inoculated); (B) Control plantlet with (Spores were inoculated); (C) R2T1(19); (D) R3T1 (7); (E) R1T2 (11); (F) R3T2 (24); (G) R2T3 (Y10); (H) R2T3 (Y11); (I) R3T4 (7); (J) R2T5 (42); (K and J) Transgenic banana in the glasshouse.

REFERENCES

1. Remy S., Francois I., Cammue B.P.A., Swennen R. and Sagi L. (1998) Co-transformation as a potential tool to create multiple and durable resistance in banana (*Musa* spp.) *Acta Hort.* **461**: 361-365.
2. Jongedijk E., Tigelaar H., van Roekel J.S.C., Bres-Vloemans S.A., Dekker I., van den Elzen P.J.M., Cornelissen B.J.C. and Melchers L.S (1995). Synergistic activity of chitinases and β-1,3-glucanases enhances fungal resistance in transgenic tomato plants. *Euphytica.* **85**: 173-180.
3. Jach G., Gornhardt B., Mundy J., Logemann J., Pinsdorf E., Leah R., Schell J. and Mass C. (1995) Enhanced quantitative resistance against fungal disease by combinatorial expression of different barley antifungal proteins in transgenic tobacco. *Plant J.* **8**:97-109.
4. Bliffeld M., Mundy J., Potrykus I. and Futterer J. (1999) Genetic engineering of wheat for increased resistance to powdery mildew disease. *Theor Appl Genet.* **98**: 1079-1086.
5. Makarevitch I. Svitashev S.K. and Somers D.A. (2003) Complete sequence analysis of transgene loci from plants transformed via microprojectile bombardment. *Plant Mol. Biol.* **52**: 421-432.
6. Murashige T, and Skoog F. (1962). A revised medium for rapid growth and bioassays with tobacco tissue culture. *Physiol Plant* **.15:** 473-497.
7. Sreeramanan S., Marziah M. and Mohd Puad Abdullah (2002) Optimization of multiple buds production in Pisang Rastali (*Musa Sapientum* Cv Rastali). *In*: Proceedings of the 3 rd National Banana Seminar, Port Dickson , Negeri Sembilan, Malaysia. pp. 31.
8. Jefferson R.A. (1987) Assaying chimeric genes in plants: The GUS gene fusion system. *Plant. Mol .Bio. Rep.* **5**: 387-405.
9. Pasakinskiene I. and Paplauskiene V. (1999) Floral meristems as a source of enhanced yield and quality of DNA in grasses. *Plant Cell Rep.* **18**: 490-492.
10. Sambrook J., Fritsch E.F. and Maniatis T. (1989) Molecular cloning: a laboratory manual.Second edition. Cold Spring Harbor Laboratory Press, Cold Spring Harbor, New York, NY.
11. Holtke H.J., Ankenbauer W., Muhlegger K., Rein, R., Sagner, G., Seibl, R. and Walter T. (1995) The Digoxigenin (DIG) System for non-radioactive labeling and detection of nucleic acids-an overview. *Cell. Mol. Biol.* **41**(7): 883-905.
12. Jiang Z.Y., Woollard A.C. and Wolff S.P. (1990) Hydrogen peroxide production during experimental protein glycation. *FEBS Lett.* **268**(1): 69-71.
13. Robert E. and Helmut K. (1992). Isoflavonoid phytoalexins and their biosynthetic enzymes. *In*: Sarah J.G., McPherson D.J. and Bowles D.J. (eds.). Molecular Plant.
14. Hammerschmidt, R., Nuckleus, E.M. and Kuc J. (1982) Association of enhanced peroxidase activity with induced systemic resistance of cucumber to *Colletotrichum lagenarium. Physiol Plant Pathol.* **20**: 61-71
15. Mozzetti, C., Farraris, L., Tamietti, G. and Matta, A. (1995) Variation in enzyme activities in leaves and cell suspension as markers of incompatibility in different *Phytophthora* pepper- interaction. *Physiol. Mol. Plant Pathol.* **46**: 95-107.
16. Tonon C., Andreu A., Aued ME., Van Damme, M., Huarte, M. and Daleo G.R. (1998). Defense reactions in two potato cultivars following infection with two races of *Phytophthora infestans. Potato Res* **.41**:319-325.
17. Asao H., Nishizawa Y., Aria S., Sato T., Hirai M., Yoshida K., Shinmyo A. and Hibi. (1997) Enhanced resistance against a fungal pathogen *Sphaerotheca humuli* in transgenic strawberry expressing a rice chitinase gene. *Plant Biotechnol.* **14**:145-149.
18. Nishizawa Y.; Nishio Z, Nakazomo K, Soma M, Nakajima E. and Ugaki M. (1999) Enhanced resistance to rice blast (*Magnoporthe grisea*) in transgenic japonica rice by constitutive expression of rice chitinase. *Theor Appl Genet.* **99**:383-390.
19. Yoshikawa M., Tsuda, M. and Takeuchi, Y. (1993) Resistance to fungal diseases intransgenic tobacco plants expressing the phytoalexin elicitor-releasing factor β-1, 3-endoglucanse from soybean. *Naturwissenchaften.* **80**:417-420.
20. Lusso, M. and Kuc, J. (1996) The effect of sense and antisense epression of the *PR-N* gene for β-1,3-glucanase on disease resistance of tobacco to fungi and viruses. *Physiol. Mol. Plant. Pathol.* **49**:267-283.
21. Borkowska M., Krzymowska M., Talarczyk A., Awan M.F.M, Yakavleva L., Kleczkowsi K. and Wielgat B. (1998) Transgenic potato plants expressing soybean β-1,3-endoglucanase gene exhibit an increased resistance to *Phytohthora infestans. Z. Naturforsh.* **53**: 1012-1016.

Journal of Science and Technology in the Tropics (2005) **1**: 117-124

Inhibitory potential of *Quercus lusitanica* galls extract on the protein expressions of dengue virus type 2

S. Y. Muliawan[1,2], S. K. Lam[2], K. Sidik[1], N. Abdul Rahman[3], N. Khalid[4], O. H. Hashim[1] and R. Yusof[1]

[1] Department of Molecular Medicine and [2]Department of Medical Microbiology, Faculty of Medicine;
[3] Department of Chemistry, and [4]Institute of Biological Sciences, Faculty of Science, University of Malaya, 50603 Kuala Lumpur, Malaysia

Abstract In this study we report the *in vitro* inhibitory potential of crude galls extract of *Quercus lusitanica* on the replication of dengue virus type 2. The *in vitro* antiviral activity performed in C6 /36 cells showed inhibition in dose dependent manner. The crude galls extract of *Quercus lusitanica* at its maximum non-toxic concentration of 0.05 mg/ml completely inhibited 100 – 10,000 $TCID_{50}$ of virus as indicated by the absence of cytophatic effects. The inhibitory effect was further supported by the inhibition of plaque formation in cells infected by dengue virus type-2 following treatment by the *Quercus lusitanica* galls extract. We also described the development of two dimensional gel electrophoresis as a tool of differentiating cells infected by dengue virus type 2 by observing the changes in the level of NS1 protein as a biomarker. We have successfully shown by protein profiling in cells infected by dengue virus and treated with *Quercus lusitanica* galls extract, the expression of NS1 protein was reduced. Based on these findings the two dimensional gel electrophoresis could form the basis of useful additional test of dengue virus infection and screening of inhibitors towards dengue infection by using the protein expression of NS1 as a potentially good diagnostic marker.

Keywords dengue virus type 2 – *Quercus lusitanica* – proteomics

INTRODUCTION

Dengue is one of the most serious mosquito-borne viral diseases in humans. It occurs in tropical areas and accounts for up to 100 million cases of dengue fever (DF) [1-4], 500,000 cases of dengue hemorrhagic fever (DHF) and 25,000 deaths, with 2.5 billion people at risk [2]. Dengue virus is transmitted by mosquitoes of the genus *Aedes* and predominantly causes a debilitating illness known as dengue fever. Nevertheless, some patients with dengue viral infection may develop complications including dengue hemorrhagic fever (DHF) or dengue shock syndrome (DSS), especially when secondary infection of different serotypes occurs. DF and DHF are the most important medical arbovirus epidemics throughout the tropical and subtropical regions of the world [1].

Mosquito control programs are difficult to implement and maintain, making the development of new antiviral drugs and a safe vaccine imperative. The currently available synthetic antiviral drugs, such as zidovudine (AZT) mostly effective against Human Immunodeficiency Syndrome (AIDS), have limited therapeutic usefulness owing to high degree of toxicity towards target cells [5]. New antiviral agents from the plant origin can have easy acceptability being non-toxic and inexpensive. Several studies have been done to investigate whether commercially available plant extracts have inhibitory effect on certain diseases. In the present study, we investigated the effect of the galls extract of *Quercus lusitanica* against the replication of Dengue virus type-2 in C6/36 cell line. *Quercus lusitanica* often known as *Quercus infectoria*, is a small tree or a shrub from the Mediterranean area, mainly present in Greece, Asia Minor, Syria and Iran. The galls are produced when leaves of the *Quercus lusitanica* tree are penetrated by stinging wasps. The spontaneous chemical reaction caused by the penetration stimulates the leaves to produce a roundish hard ball called an oak gall. The galls of *Q. lusitanica* have a great

Journal of Science and Technology in the Tropics (2005) 1: 117-124

medicinal value and have pharmacologically been deciphered to be astringent, antidiabetic, antitremorine, local anaesthetic, antipyretic used over the centuries as antiparkinsonian [6-8].

In the present study, we report on the protective efficacy of this extract which was monitored by the inhibition of Dengue virus-2 growth as indicated by the relative absence/ reduction of cytopathic effects (CPE) in virus inhibition assay and also the inhibition of plaque formation. We also proceeded to determine the protein expression profile of dengue virus type 2 infected and uninfected cells and also dengue virus type 2 infected cells after treatment with *Q. lusitanica* extract through proteomics approach.

MATERIALS AND METHODS

Preparation of methanol extract of seed of *Quercus lusitanica*

One hundred grams of powdered form of *Q.lusitanica* seed extract were soaked in 800 mL methanol at room temperature overnight and then filtered. The residue was washed and extracted twice with additional methanol. The combined filtrate was concentrated *in vacuo*. Further dilutions were made with RPMI-1640 maintenance medium.

Cell line

C6/36 was obtained from Department of Medical Microbiology, Faculty of Medicine, University of Malaya, Malaysia and maintained by regular sub-culturing in RPMI-1640. Confluent monolayers of C6/36 were grown in Linbro- plate (24 wells) for *in-vitro* antiviral efficacy assay of *Q.lusitanica* extract.

Virus

Dengue virus type-2 (DEN-2) New Guinea C strain, obtained from Department of Medical Microbiology, Faculty of Medicine, University of Malaya, Malaysia was adapted in C6/36 cell culture and day old suckling mice for in-vitro test. The 20% mouse brain stock virus was titrated to determine the tissue culture infective dose 50% ($TCID_{50}$) for use in the in-vitro virus inhibition assay.

Determination of maximum non-toxic dose (MNTD)

Prior to screening of *Q.lusitanica* for the inhibitory potential, it was subjected to toxicity study in order to find out maximum dose which could be non-toxic to C6/36 cells in-vitro test, as in the method described by Schmidt [9]. Briefly, serial two-fold dilutions of the extracts were added to preformed cell monolayer of C6/36 cells in Linbro-plate along with suitable cell control for in-vitro MNTD determination. The inoculated cells were observed daily for the appearance of toxicity in cells.

Antiviral testing

In-vitro virus inhibition assay. In-vitro inhibitory potential of *Q.lusitanica* was evaluated in C6/36 cells by virus inhibition assay as described by John and Mukandan [10]. Briefly, serial two-fold dilutions of non-toxic doses of *Q.lusitanica* (0.003-0.2mg/ml) was prepared in RPMI-MM. Simultaneously, serial 10-fold dilutions (10^{-1} to 10^{-3}) of DEN-2 virus were also prepared separately. Fixed concentrations of extract were incubated on C6/36 cells for 2 hours at 37°C. After a predetermined period, the cells were challenged with the various dilutions of virus. If the compound possesses antiviral effects, the ability of the virus to infect and or replicate should be reduced. The plates were then incubated at 28°C and observed daily for development of cytopathic effects (CPE) up to day 4.

Determining the virus activity potential using a plaque assay. Tenfold serial dilutions of virus stock was prepared in L-15 2% foetal bovine serum. Pig spleen (PS) cells were resuspended in L-15 ($3x10^5$ cells/ml). Five hundred µl cells were added to each well of a 24 well Linbro-plate. One hundred µl of virus dilution were added to wells in duplicate. Two wells were kept as uninfected controls (cell control). The plates were gently shaken to mix the contents of wells. The cells were incubated at 37°C for 3-4 hours until adhered. The wells were then overlaid gently with 1.5% CMC agarose (0.5 ml). The wells were incubated at 37°C for the appropriate number of days (6 days). Cells were then stain with Naphthalene black on day 6. Plaques were counted and the titer of the virus calculated and recorded as the number of plaque forming units (PFU) per ml, of original 20% mouse brain suspension.

Preparation of overlay. The overlay medium was prepared mixing 50 ml of double-strength L-15 medium with an equal volume of 1.5%(w/v) carboxymethyl-cellulose in water. To this mixture was added 10 ml of tryptose-phosphate broth, 3 ml of fetal bovine serum, penicillin (100 units/ml), streptomycin (100µg/ml) and fungizone (2µg/ml).

Naphthalene Black staining method. After incubation for 6 days, the infected cultures were stained to demonstrate the presence of virus plaques. The overlay medium was poured off and the cells gently rinsed with normal saline solution. The wells were filled with 0.5 ml of Naphthalene black stain for 30 min. The stain was then discarded and the plate rinsed in tap water and air-dried. Then plaques were counted visually on the second day after their appearance when they were clearer and better defined.

Two-dimensional gel electrophoresis (2-DGE)

Sample preparation for 2-DGE. Monolayer C6/36 cells were disrupted by repeated fast freezing, three-times for 15 minutes. The cells were pelleted, spinning at 4°C, 2000 rpm, for 10 minutes. The pellet was washed with 1 ml cold-PBS (phosphate saline buffer) for two-times and spun as above. The pellet was resuspended with 1ml lysis buffer (8M Urea, 4% Triton X-100, 2% IPG-phor buffer 3-10), incubated for 2 hours at 4°C and spun as above. The supernatant was aliquoted and stored at -20°C.

Monolayer C6/36 cells was infected by DEN-2 virus stock, and incubated at 28°C. Daily monitoring was done for appearance of CPE up to day-4. Cells were processed with the same method as described above.

Serial dilution of *Q.lusitanica* extract (0.03-0.05mg/ml) were added to monolayer C6/36 cells. These were incubated for 2 hours at 37°C. After a predetermined time, DEN-2 stock was added, and incubated at 28°C (DV2-infected C6/36 cells were included as control). Daily monitoring was done for appearance of CPE up to day-4. Subsequent steps for processing the cells were the same as above.

Isoelectric focusing (IEF). Immobilized non-linear pH gradient (IPG) strips, pH 3-10 (Amersham Biosciences, Inc) were rehydrated overnight on rehydrated tray (Pharmacia Biotech). IEF was performed using a Multiphor II apparatus (Pharmacia Biotech) for a total of 11 kV-h at 20°C, 7 mA.

SDS-PAGE . Strips were equilibrated for 15 min. in 50mMTris-HCl, pH 8.8, 6M urea, 30% (v/v) glycerol, 1% (w/v)SDS, containing 0.1% (w/v) dithiothreitol followed by 15 min in the same buffer containing 0.45% (w/v) iodoacetamide and bromophenol blue. Equilibrated IPG strips were transferred onto 14 x 20 cm 10% homogenous polyacrylamide gels. Gels were prepared according to Laemmli system [11]. Strips were overlaid with 0.5% (w/v) agarose in running buffer. Gels were run in Hoeffer SE 600 at 40 mA/gel, at 16°C until the dye front run off 1 cm from the bottom of the gels. The gels were visualized by silver staining.

Immunoblotting. Immunoblotting was performed, in order to differentiate protein derived from DEN-2 virus or from C6/36 cells induced by DEN-2 virus. Briefly, the protein from the 2-DGE was transferred on to nitrocellulose membrane (0.45μm) as described by Rybicki and Purves, [12],using electroblotting (semi-dry unit, Novablot Kit) at a constant current of 0.8mA/cm^2 for 2 hours. Immunoblotting step was performed using hyperimmune anti rabbit sera against DEN-2 virus as primary antibody and as secondary antibody and immunodetection using amplified alkaline phosphatase goat anti-rabbit immunoblot assay kit.

N-terminal sequencing. Electroblotting was performed to transfer the protein samples from SDS gel to polyvinylidene fluoride (PVDF) membrane (Immobiline™, P transfer membrane, Millipore (0.45μM). Semi-dry system was chosen for transferring of proteins from SDS-PAGE on to PVDF membrane (0.45μm) as described by Rybicki and Purves [12]. Electroblotting (semi-dry unit, Novablot Kit) was performed at a constant 0.8mA/cm^2 for 2 hours. To visualize the total proteins and to assess the quality of transfer, the membrane was stained with coomassie brilliant blue R-250. Amino acid analysis was then performed on the protein spots of interest by N-terminal sequencing.

RESULTS

Cytotoxic studies to determine maximum non-toxic dose (MNTD) of *Quercus lusitanica* on C6/36 cells

The evaluation of the inhibitory potential of *Q.lusitanica* on DV-2 in an *in-vitro* system was preceded by cytotoxicity studies to find out the maximum non-toxic dose (MNTD) for virus inhibition assay. Serial dilutions of this extract were prepared from 0.016 to 1mg/ml. Figure 1, panel A shows the MNTD of various preparations of *Q.lusitanica* extract on C6/36 cells one day after treatment and the MNTD of this extract 4 days after treatment (Fig. 1, panel B). The MNTD of *Q.lusitanica* extract on C6/36 cells for further assay was based on the results of this extract for four days as this was the incubation time of infected C6/36 cells by

Malaysian Journal of Science and Technology in the Tropics (2005) **1**: 93

Editorial

The first issue of JOSTT has received an encouraging support from local and overseas readership. It is hoped that it will be accepted as the medium of communication for scientific research in tropical areas, which is being carried out all over the world and not only by researchers in the tropical countries. The tropics offer a wealth of opportunities for scientific findings. I would like to elaborate the case of tropical oils especially palm oil.

It is conventional thinking that saturated fatty acids in oils and fats are expected to raise blood cholesterols and thus contribute to cardiovascular diseases. In the anti-tropical oils campaign, palm oil has been highlighted as one of the culprits, as it contains about 50% saturated fatty acids. However, an article in Nutrition Reviews points out that palm oil in spite of its saturation level, does not behave like a saturated fat but more like an unsaturated fat. This conclusion has been inferred on the comparative data related to the thrombotic effects of various edible oils including palm oil. This view has been verified by numerous studies in humans. There have been at least two studies which demonstrate that palm olein (the liquid fraction of palm oil) is as good as virgin olive oil in the levels of LDL and HDL cholesterols but palm olein is better than olive oil in its anti-thrombotic effect as measured by the thromboxane-prostacyclin ratio.

We now have a contradiction: the past results on saturated fats and the current results on palm oil. Could it be that both results are valid and the explanation lies in the position of saturated fatty acids in the triglyceride molecules? The saturated fatty acids in animal fats are mainly in the second position of the triglyceride structure but in the case of palm oil, they are mainly in the 1 and 3 positions whilst the 2 position is occupied by an unsaturated fatty acid, particularly oleic acid. The relationship between position and lipidemic effect can be better understood in the context of the lipolysis of the triglyceride molecules in the digestive system and the absorption of the monoglycerides into the bloodstream. Further, the relative slow rates of absorption of the long chain fatty acids from the 1 and 3 positions result in inefficient resynthesis of the triglycerides, thus making palm oil, a structured lipid with unsaturated fatty acid in 2 position and saturated fatty acids in the 1 and 3 positions less fattening. Preliminary evidence has been obtained in a chicken model. When this line of investigation is firmly confirmed, we need to change our mindsets regarding our simplistic view of saturation and health effects.

Seeking for scientific truths is fascinating and this could be a magnificent obsession.

Academician Tan Sri Dr Augustine S.H. Ong
Chairman, Editorial Board

Journal of Science and Technology in the Tropics [2005] 1: 117-124

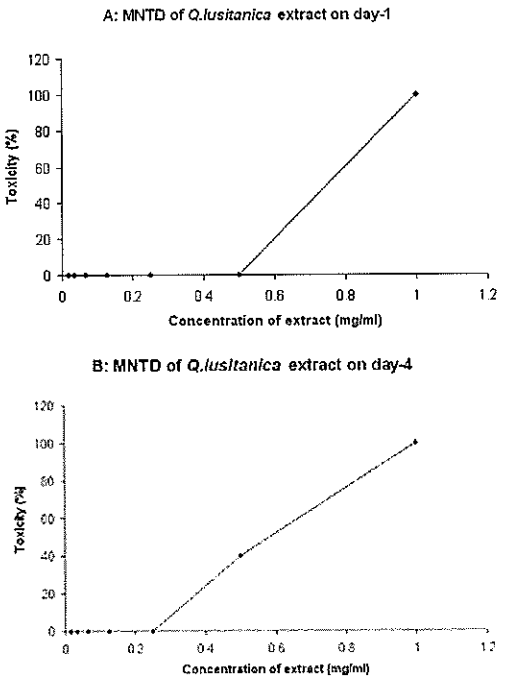

Figure 1. Relative toxicity and maximum non-toxic dose (MNTD) of various preparations of *Q. lusitanica* extract *in-vitro*. Panel A: MNTD of *Q.lusitanica* extract on day-1; Panel B: MNTD of *Q.lusitanica* extract on day- 4.

DV-2 for observation of cytopathic effect (CPE). The MNTD of *Q.lusitanica* extract was 0.25mg/ml. At higher concentrations, the monolayer decreased and cells started to shrink. *Q.lusitanica* extract concentrations below or equal to MNTD were therefore employed for subsequent antiviral screening.

Determination of inhibitory effect of *Q. lusitanica* on dengue virus type-2 in C6/36 cells

Prior to screening for the inhibitory potential of *Q.lusitanica* extracts on C6/36 cells, the 50% of tissue culture infective dose ($TCID_{50}$) was determined. The 50% end point titer was 10^{-4} dilution of dengue virus-2 stock (harvested from mice brain). Tenfold dilution of DV-2 stock from 10^{-1} to 10^{-8} were prepared. The maximum dilution of DV-2 that produced 100% cytopathic effects (CPEs) was determined and found to be 10^{-3} (10 $TCID_{50}$) and this value was employed as the highest dilution of virus that was used in the antiviral compound assay in-vitro.

To determine the effect of antiviral compounds against dengue virus-2 growth the criteria used was the presence or absence of CPE. The results showed that in-vitro *Q. lusitanica* extract inhibited dengue virus-2

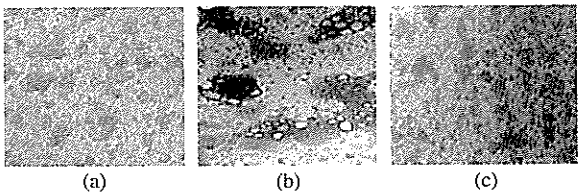

Figure 2. Virus inhibition assay showing the inhibition of cytopathic effects (CPE) of dengue virus type-2 in C6/36 cells by *Q.lusitanica*. (a) Healthy C6/36 cells. (b) CPE of dengue virus type-2 (1000$TCID_{50}$/ml). (c) Inhibition of CPE of dengue virus type-2 (1000$TCID_{50}$/ml) in C6/36 cells treated with *Q. lusitanica* (0.05mg/ml).

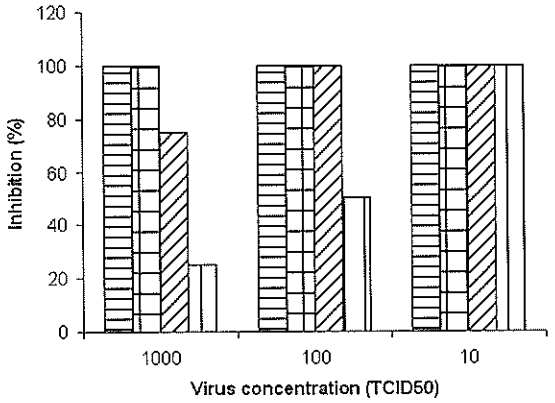

Figure 3. Inhibitory potential of various concentrations of *Q. lusitanica* extract on different concentrations of dengue virus type-2. * Concentrations of *Q. lusitanica* extract employed. ▤ 0.25mg/ml; ❑ 0.13mg/ml; ▨ 0.063mg/ml; ▢ 0.032mg/ml.

growth in C6/36 cells and greater inhibition of virus growth was noted with increasing doses, as depicted in Figure 2. The *Q. lusitanica* extract at its maximum concentration (0.25mg/ml) showed 100% inhibition on the growth across the whole range of virus concentrations employed in the present study as indicated by the absence of CPE (Fig. 3). The lower dose of *Q.lusitanica* (0.032mg/ml) gave 100% inhibition with 10 $TCID_{50}$ of virus but only 50% and 25% inhibition at 100 and 1,000 $TCID_{50}$ of virus, respectively.

Inhibition of viral replication (plaque formation)

From the *in vitro* inhibition assay, it was shown that *Q. lusitanica* extract protected cells infected with dengue virus type-2 at a concentration of 0.032 to 0.25mg/ml. To further evaluate *Q. lusitanica* as an antiviral compound at low concentration, the viral plaque assay was performed. Control cells were inoculated with a virus titer of 10^{-3} (10 $TCID_{50}$).

Figure 4 showed the differences between the uninfected monolayer of pig spleen cells (panel A) and dengue virus type 2-infected monolayer of pig spleen cells by dengue virus type-2 (panel B). Infected cells show cytopathic changes in a form of plaques.

Monolayers of pig spleen cells that were treated with 0.032 and 0.063mg/ml of *Q. lusitanica* extract were infected with 10 $TCID_{50}$ dilutions of dengue virus type-2. This was followed by overlaying with nutrient agar medium and then incubated for 6 days. For visualization, plaques were stained with naphthalene black. Plaques were counted on the second day after their appearance when they were clearer and better defined. The viral control at 10^{-3} dilution (10 $TCID_{50}$) of dengue virus type-2 gave a result of $13x10^4$ pfu/ml. The results also revealed that at 10^{-3} dilution of dengue virus type-2 treated with 0.032mg/ml of *Q. lusitanica* extract yielded $3.5x10^4$ pfu/ml (Fig. 4, panel C) while 0.063mg/ml *Q.lusitanica* extract gave $1.5x10^4$ pfu/ml (Fig. 4, panel D).

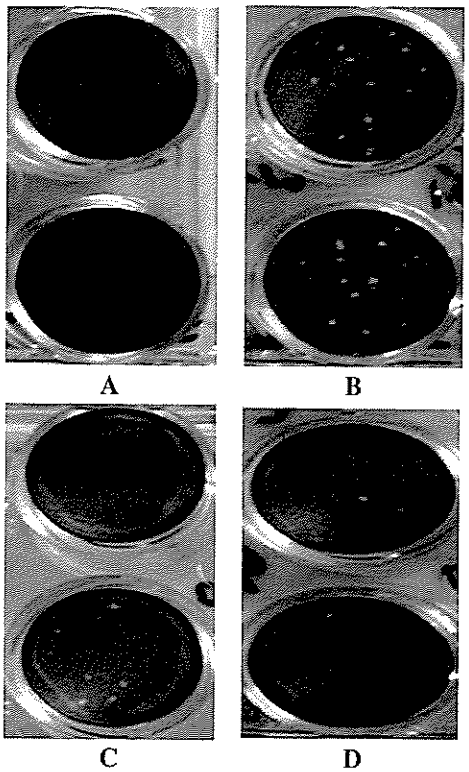

Figure 4. Plaque assay of DV-2 infected pig spleen cells treated with *Q. lusitanica* extract. Panel A: Uninfected pig spleen cells; Panel B: Pig spleen cells infected with dengue virus type-2 (10 $TCID_{50}$); Panel C: Pig spleen cells were treated with 0.032mg/ml *Q. lusitanica* extract prior infection with 10 $TCID_{50}$ dilution of DV-2; Panel D: Pig spleen cells were treated with 0.063mg/ml *Q. lusitanica* extract prior infection by 10 $TCID_{50}$ dilution of DV-2.

Two-dimensional gel electrophoresis (2-DGE)

Two-DGE is a sensitive and reproducible technique for differential expression analysis. Samples for 2-DGE were prepared from uninfected C6/36 cells, DV2-infected C6/36 cells, and DV2-infected C6/36 cells after treatment with *Q. lusitanica* seed extracts. Subsequent steps were isoelectric focusing which separates proteins according to their isoelectric points (pI) and followed by the second dimension separation based on their molecular weight.

Two-dimensional gel electrophoresis of infected sample by DV-2 and uninfected sample on C6/36 cells

To determine the differential protein expression between infected C6/36 cells by dengue virus type-2 and uninfected C6/36 cells, 2-DGE was performed on samples prepared. One hundred micrograms of sample from C6/36 cells infected by DV-2 (Fig. 5, panel A) and uninfected sample (Fig. 5, panel B) were loaded onto the dryStrip (pH 3-10, from left to right). The proteins were separated on isoelectric focusing unit for the first dimension. Then, the proteins were separated further by molecular weight on a 10% homogeneous polyacrylamide gel on the second dimension and were visualized by silver staining. When comparative

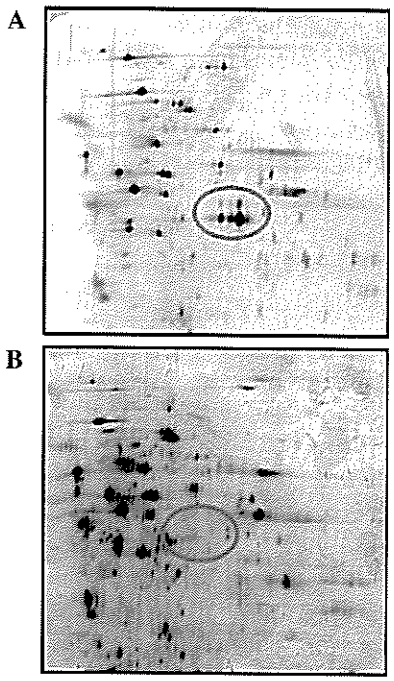

Figure 5. Proteins profile of C6/36 cells. Panel A: Protein sample of C6/36 cells which infected with dengue virus type-2; Panel B: Uninfected C6/36 cells.

Journal of Science and Technology in the Tropics (2005) 1: 117-124

analysis was made between 2-DGE protein profiles of C6/36 cells infected by DV-2 and uninfected C6/36 cells, it was noted that the protein spots of interest which migrated at the same molecular weight but with slight difference in pI was detected in cells infected with DV-2 but not detected in uninfected cells (Fig. 5, panel A).

Immunoblotting and immunodetection

Immunoblot was performed to investigate whether the protein spots that were present in infected C6/36 cells by DV-2 were derived from dengue virus type-2 protein or from cell culture induced by DV2. The proteins separated by 2-DGE were transferred by a semi-dry unit system to the nitrocellulose membrane (0.45μM), followed by immunodetection using hyperimmune rabbit antiserum against DV-2 as a primary antibody. Bound antibodies were detected with Amplified Alkaline Phosphatase Goat Anti Rabbit Blot Kit. The result showed the protein spots of interest were picked by antibody against dengue virus type-2 and were visualized as a purple colour.

Electroblotting for Edman degradation sequencing

To obtain further information of the identification of protein spots that were present in infected C6/36 cells by DV-2, this sample was run together with a molecular weight marker on two-dimensional gel electrophoresis (data not shown). The results showed the molecular weight of these proteins were about 50kDa.

The proteins on the gel were transferred by a semi-dry unit system onto a PVDF membrane (0.45μM), followed by identification by Edman degradation N-terminal sequencing. The result showed that the amino acid sequence to be DSGCVVSWKNK. Based on Swissprot databases, this sequence is homologous to position 2422-2454 of the nonstructural NS1 of dengue virus type-2 genome.

Two-dimensional gel electrophoresis after treatment with *Q. lusitanica* extract on C6/36 cells

From the *in-vitro* virus inhibitory assay, it was shown that *Q. lusitanica* extract has the ability to inhibit dengue virus type-2 growth at the concentration of 0.032 to 0.25mg/ml. To investigate the effect of inhibitory of *Q. lusitanica* against dengue virus type-2 on protein expression, two-dimensional gel electrophoresis was performed.

In this study, two-dimensional gel electrophoresis was performed on C6/36 cells that were treated with 0.05mg/ml of *Q. lusitanica* extract as a control (Fig. 6, panel A). When 2-DGE was performed on samples from C6/36 cells infected with DV-2, the four spots that were determined as NS1 earlier were seen (Fig. 6, panel A). Experiment was then performed where the C6/36 cells were first treated with low concentration (0.006mg/ml to 0.013mg/ml) (Fig. 6, panel B) and high concentration (0.025 to 0.1mg/ml) (Fig. 6, panel C) of *Q. lusitanica* extract followed by infection by DV-2. The results of the 2-DGE were visualized by silver staining and the results showed that as the concentration of *Q. lusitanica* extract was increased the expression of the NS1 protein was reduced and at a higher concentration of *Q. lusitanica* (0.1mg/ml) the NS1 protein was completely diminished (Fig. 6, panel C).

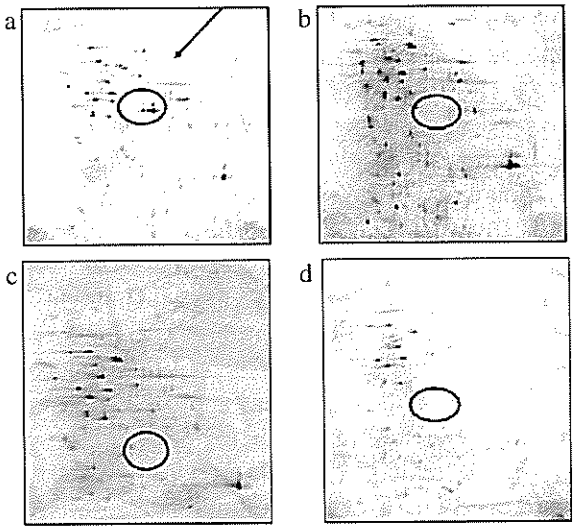

Figure 6. Two-dimensional gel electrophoresis (pH 3-10, from left to right on 10% homogeneous polyacrylamide gel). Protein expression of dengue virus type-2 in C6/36 cells with silver staining (a) Infected C6/36 cells. (b) Uninfected C6/36 cells. (c) Infected C6/36 cells treated with low concentration (0.006-0.013mg/ml) of *Q.lusitanica*. (d) Infected C6/36 cells treated with high concentration (0.025-0.05mg) of *Q. lusitanica*.

DISCUSSION

Dengue fever and dengue hemorrhagic fever are the most important medical arbovirus epidemics throughout the tropical and sub-tropical regions of the world. Mosquito control programs are difficult to implement and maintain thus making the development of new antiviral drug and a safe vaccine imperative. There are to date no specific antiviral therapies for dengue fever and many aspects of the mechanisms involved in antiviral activity remain to be explored.

The present study is undertaken to explore the *in vitro* inhibitory potential of *Q.lusitanica* on dengue virus type-2 replication. Prior to screening for inhibitory potential, the extract was subjected to toxicity study on the C6/36 cells where the maximum non-toxic dose was determined to be 0.25mg/ml.

The *Q. lusitanica* extract has been shown to also exhibit the protective effect from the dengue virus by inhibiting the virus growth in C6/36 cells as indicated by the absence of CPE in infected cells. This was further confirmed by the inhibition on the plaque formation in a dose dependent manner.

In Asian countries, the galls of *Q. lusitanica* have been used for centuries in oriental traditional medicines for treating inflammatory diseases [13]. Gargle of hot water extract of galls is very effective against inflamed tonsils, while direct application of boiled and bruish galls on skin effectively cures any swelling or inflammation [14]. In this study we have successfully shown that the galls of *Q. lusitanica* can also inhibit dengue virus growth *in vitro*.

In this study we have also explore the use of proteomic technology in determining the protein profiling of C6/36 cells in Dengue virus type 2 infected and non-infected cells and also in cells protected by the *Q. lusitanica* extract. Proteomics is widely accepted as a technology in the post genomic era to investigate global protein synthesis and gene expression [15]. By the very definition of proteomics, it is inevitable that complex protein mixtures will be encountered. Therefore methods must exist to resolve these protein mixtures into their individual components so that the proteins can be visualized, identified, and characterized by amino terminal sequencing and/mass spectrophotometer. In 2-DGE proteins are separated by two distinct properties. They are resolved according to their net charge in the first dimension and according to their molecular mass in the second dimension [16-19]. For visualization of the result from 2-DGE, silver staining can be used [20]. We have shown that in cells infected by dengue virus type-2 the protein profile indicated the presence of four distinct protein spots of almost the same molecular weight of about 50kDa but with slight difference in PI which is not present in uninfected cells. By N-terminal sequencing analysis, these proteins were identified as NS1 protein from Dengue virus type-2. The differences in pI could be due to the differences in glycosylation of the NS1 protein.

In cells treated with low concentration of *Q.lusitanica* (0.06 to 0.013 mg/ml) the appearance of the NS1 was reduced and on increasing the concentration of the plant extract from 0.025 to 0.05mg/ml, the NS1 proteins were completely diminished. This indicated that the NS1 protein is a good biomarker for determining growth inhibitor for Dengue virus.

The available data in this study does not permit us to discuss the mechanism of the inhibition on dengue virus type-2 but we could conclusively revealed the inhibitory effect of *Q. lusitanica* galls extract on dengue virus type-2 is by suppressing the virus replication or spread *in vitro*. The inhibition of the production of NS1 as seen by the protein profile could be attributed to a few factors such as inhibition of dengue virus entry into the cells, inhibition of NS1 production during polyprotein processing or inhibition of glycosylation of NS1 during posttranslational modification as NS1 is the only non-structural protein of the dengue virus that is glycosylated. Therefore, detailed in depth molecular study is required to elucidate the mechanism of inhibition.

REFERENCES

1. Halstead S.B. (1998) Pathogenesis of dengue: Challenges molecular biology. *Science* **239**: 476-481.
2. Monath T.P. (1994) Dengue: the risk to developed and developing countries. *Proc. Natl. Sci. USA* **91**: 2395-2400.
3. Gubler D. (1998) Dengue virus and dengue hemorrhagic fever. *Clin.Microbiol.Rev.* **11:** 480-496.
4. McBride W.J.H. and H.Bielefeldt-Ohmann (2000) Dengue viral infections; pathogenesis and epidemiology. *Microbes. Infect.* **2**: 1041-1050.
5. ParidaM.M., Upadhyay C, Pandya G, and Jana A.M. (2002) Inhibitory potential of neem (*Azadirachta indica Juss*) leaves on dengue virus type-2 replication. *J. Ethanopharmacology* **79**: 273-278.
6. Dar, M.S., Ikram M.and Fakouhi T. (1976) Pharmacology of *Quercus infectoria. Journal of Pharmaceutical Science* **65**: 1791-1794.
7. Dar M.S. and Ikram, M. (1979) Studies on *Quercus*

infectoria; isolation of syringic acid and determination of its central depressive activity. *Planta Medica* **35**: 156-161.

8. HwangJ.K., Kong T.W., Back N.I.and Pyun Y.R. (2000) Alpha-glycosidase inhibitory activity of hexagalloylglucose from the galls of *Quercus infectoria*. *Planta Medica*. **66**: 273-274.
9. Schmidt N.J. (1979) Cell Culture Technique for Diagnostic Virology in Diagnostic Procedures for Viral, Rickettsial and Chlamydial Infections. In: Lennette, E.H., Schmidt, N.J. (eds) *American Health Publications*, Washington, DC: 115-139.
10. John J.J and Mukandan P. (1978) Antiviral activity of tea. *Current Science* **47**: 159-160.
11. Laemmli U.K (1970) Cleavage of structural proteins during the assembly of the head of bacterio-phage T4. *Nature* **227**: 680-685.
12. Rybicki E.Pand Purves M. (1996) Enzyme-assisted immunoelectroblotting (IEB or Western Blotting). In: Coyne VE, James MD, Reid SJ, and Rybicki EP(eds). *Molecular BiologyTechniques Manual*, (3rd ed): 1-8
13. Galla B.P. (1911) Galls. *The British Pharmaceutical Codex*. Council of the Pharmaceutical Society of Great Britain.
14. Chopra R.N., NayarS.I. and Chopra I.C. (1956) Glossary of Indian Medicinal Plant. *Council of Scientific and Industrial Research*, India: p.208.
15. Cash P. (2000) Proteomics in medical microbiology. *Electrophoresis* **21**: 1187-1201.
16. Klose. J. (1975) Protein mapping by combined isoelectric focusing and electrophoresis of mouse tissues. A novel approach to testing for induced point mutations in mammals. *Human Genetic* **26**: 231-243.
17. O'Farrell P.H (1975) High resolution two-dimensional electrophoresis of proteins. *J. Biol. Chem.* **250**: 4007-4021.
18. Scheele G.A (1975) Two-dimensional gel analysis of soluble proteins. Characterization of guinea pig exocrine pancreatic proteins. *J. Biol. Chem.* **250**: 5375-5285.
19. Wirth P.J. (1995). Gel electrophoresis of proteins, two-dimensional polyacrylamide. In: Meyers R.A. (ed). *Molecular Biology and Biotechnology. A comprehensive Desk Reference*. Wiley-VCH, Canada: 343-345.
20. Shevchenco A, Wilm M, Vorm O, and Mann M. (1996) Mass Spectrometric sequencing of proteins from silver-stained polyacrylamide gels. *Anal.Chem.* **68**: 850-858.

Journal of Science and Technology in the Tropics (2005) **1**: 125-130

Dielectric properties and equivalent circuit modeling of hevea rubber latex at frequencies of 10^{-2} to 10^{6} Hz

J. Hassan, W. M. D. Wan Yusoff, K. Khalid and Z. Abbas
Department of Physics, Faculty of Science, Universiti Putra Malaysia,
43400 UPM Serdang, Selangor, Malaysia.
(e-mail: jumiah@fsas.upm.edu.my)

Received 15 July 2005; accepted 30 November 2005

Abstract Hevea rubber latex from latex concentrate of about 38% moisture and freshly tapped latex of about 49% moisture were frozen and its dielectric properties investigated in the frequency region of 10^{-2} to 10^{6} Hz using the Chelsea Dielectric Spectrometer. Measurements were made at selected moisture content over the temperature range of -20 to -60°C. The dielectric behaviour displayed three distinct responses in a parallel combination. These include the real part of the relative permittiv at high frequency $\varepsilon(\infty)$, loss peak response $\varepsilon(\omega)_{lp}$ and the dc conductivity σ which arise from polarisation effects. The total losses were ionic losses which appeared as conductivity losses and dipolar losses which appeared as loss peak responses. The conductivity losses were due to the ionic species found in latex while the loss peak response was due to the relaxation of the water molecules. The relaxation peak shifts towards the higher frequency region with increasing temperature and as water content in the latex decreases. This phenomenon could be ascribed to differences in the polarisation affecting the ions and protonic conduction in ice. Dielectric response model in the form of an equivalent circuit which best described the dielectric properties from the results obtained were also presented.

Keywords Hevea rubber latex – dielectric properties – polarization – conductivity losses – relaxation peak – equivalent circuit

INTRODUCTION

Natural rubber latex from hevea brasiliensis is visualised as a suspension of latex particles in an aqueous serum. Being a biological product, the composition of fresh latex varies between wide limits. Fresh latex consists of 55 - 80% water, 15 - 45% rubber hydrocarbon and approximately 2 - 4% non-rubber constituents [1,2]. The non-rubber constituents are made up of sugars, proteins, lipids, quebrachitol, carotenoids, mineral salts and many other nitrogenous substances. About 2 - 3% conducting phases arise from the non-rubber constituents. This composition varies widely according to season, weather, soil condition, clone and tapping system.

Under typical conditions, right after a tree has been tapped and during collection, latex became contaminated by bacteria and yeasts which produce large amount of acids that will coagulate the latex into clots of rubber and a clear serum with time. To prevent coagulation, the fresh latex are concentrated to a higher rubber content and preserved with 0.025% tetramethyl-thiuram disulphide (TMTD)/zinc oxide (ZnO) and 0.2 to 0.3% ammonia [3]. The present standard for latex concentrate has a dry rubber content of about 60% and 39% moisture.

The purpose of this study is to investigate the dielectric properties of hevea latex and its responses in the form of equivalent circuits in the low frequency region over a frequency range of 10^{-2} to 10^{6} Hz, and at five temperatures from -20 to -60°C. There appears to have been no extensive study done on the dielectric properties of latex in this region except by Laogun [4] in the frequency range of 0.1 to 100 MHz, however microwave dielectric properties of hevea latex has already been reported [5-7].

Journal of Science and Technology in the Tropics (2005) 1: 125-130

THEORY

The physical basis of the dielectric phenomena is that when a voltage is applied to a sample, it induces alignment of the dipoles present towards the direction of the field. This results in a change in the polarization P of the sample. In this paper, the sample is measured in a parallel plate capacitance cell with plate area A and distance between the plates d. Taking this into account, the linear rate of change of polarization with respect to the electric field, dP / dE, is the complex relative dielectric permittivity which can be expressed in terms of complex capacitance in the following form

$$C^*(\omega) = C'(\omega) - iC''(\omega) \quad (1a)$$

$$= \varepsilon_0 \frac{A}{d}\left[\chi'(\omega) + \varepsilon(\infty) - i\chi''(\omega)\right] - i\frac{G}{\omega} \quad (1b)$$

$$= \varepsilon_0 \frac{A}{d}\left[\varepsilon'(\omega) - i\varepsilon''(\omega)\right] - i\frac{G}{\omega} \quad (1c)$$

where ε_0 is the absolute permittivity of free space equivalent to 8.85×10^{-12} F/m, $\varepsilon(\infty)$ is the relative permittivity at high frequency, $\varepsilon^*(\omega) = \varepsilon'(\omega) - i\varepsilon''(\omega)$ is the complex relative permittivity, $\chi^*(\omega) = \chi'(\omega) - i\chi''(\omega)$ is the complex dielectric susceptibility of the polarizable entity, ω is the angular frequency and G is the conductance in mhos electrically in parallel with the dielectric response.

Equation (1) can also be expressed in term of its relative permittivity

$$\varepsilon^*(\omega) = \varepsilon_0\left[\varepsilon'(\omega) - i\varepsilon''(\omega)\right] - i\frac{\sigma}{\omega} \quad (2)$$

where $\varepsilon'(\omega)$ is the real relative permittivity or the dielectric constant, $\varepsilon''(\omega)$ is the dielectric loss factor and σ is the dc conductivity.

Based on Debye's model [8] on the interpretation of the dielectric response, it is assumed that the rotation of each dipole is associated with a relaxation time τ. However, recent work by Jonscher [9] has shown that this is inadequate to represent experimental observation. The relaxation of a dipole is considered dependent on the cooperative motions of the other dipoles and of the surrounding medium to form a cluster response, and with time an interaction develops between these clusters [10].

Equivalent Circuit Model

For bound dipolar behaviour the capacitances are in series given by

$$C_1^*(\omega) = C(0) - C(0)(i\omega/\omega_p)^n, \qquad \omega << \omega_p \quad (3a)$$

$$C_2^*(\omega) = C(0)(i\omega/\omega_p)^{n-1}, \qquad \omega >> \omega_p \quad (3b)$$

n and m are the correlation coefficients for intra-cluster and inter-cluster relaxation mechanisms respectively and they lie between zero and unity. n is a measure of the structural order of the cluster and as n approaches zero, the dipoles become decoupled from their surroundings. m is a measure of the extent to which one cluster can affect others environmentally. As m increases and approaching unity, the disturbance between clusters is spread homogeneously [10,11]. The values of m and n are experimentally determined from the slope of the curves.

Since, $\varepsilon^* = \varepsilon' - i\varepsilon''$, $\omega = 2\pi f$ and $C^* = \frac{\varepsilon^* A}{d}$, where A is the area of the plate and d is the distance between the plates, all of the above expressions can be rewritten in terms of ε' and ε''.

EXPERIMENTAL

The parameters being measured are the relative permittivity or the dielectric constant, ε' and the relative dielectric loss factor, ε'' and its variation with respect to temperature, frequency and moisture content. The capacitance method is employed for the dielectric measurements. About 3.5 ml of latex is poured into the lower plate and the upper plate is lowered until it just touched the latex. The thermocouple that registered the temperature is located right below the lower plate. After the sample had been placed between the plates, the whole system is isolated and enclosed in an oven which could be lifted easily. The temperature of the sample is lowered slowly by the circulation of liquid nitrogen through the outer part of the oven while the inner coil heats up to maintain the temperature if it goes beyond the required temperature. For the initial measurement at -20°C, the sample is maintain at this temperature for about 20 minutes to make sure that the sample is frozen before starting to vacuum. The whole system is vacuumed to remove excess moisture from forming ice crystals which could affect the measurement process. Dielectric measurements are then made at every 10 degrees interval after which the temperature is then lowered to -30°C. This requires another 20 minutes to stabilise the temperature before taking the next set of measurements. The same procedure is repeated for measurements at -40, -50, and -60°C.

For moisture content measurements, an empty petri dish is weighed to the nearest 1 mg using a digital balance (Scientech 5220). About 1.5 to 2.5 grams of the sample is poured into the dish and reweighed. The dish is then gently swirled to ensure that the latex covers the bottom and placed horizontally in the oven and heated at 70 ± 2°C. The sample is heated until it loses its whiteness and become transparent. It is then cooled in the dessicator for about 15 minutes, and weighed. The heating and cooling process are repeated for periods of 15 minutes until the loss in mass between successive weighing is less than 1 mg. Three sets of the same sample are dried for each experiment and the average result of the moisture content is recorded.

Latex concentrate with a moisture content of about 38% is supplied by the Rubber Research Institute of Malaysia while freshly tapped latex (RRIM 600 clone) with a moisture content of about 49% is obtained from the university research park.

RESULTS AND DISCUSSION

Frozen hevea latex shows a dielectric phenomenon which is almost similar to ice. Ice at temperatures 0°C to -80°C has its water molecules arranged in an orderly repetitive position with hexagonal symmetry. Ice is a good example of proton transfer where the protons have good mobilities about an order of magnitude higher than those of normal ionic conductors. Therefore, it is not a perfect insulator [12]. Figure 1 illustrates the dielectric spectrum of fresh latex and latex concentrate as compared to ice in the frequency range of 10^{-2} to 10^{6} Hz and at temperature -30°C. The relaxation peak is shifted to a higher value as water content in the latex decreases.

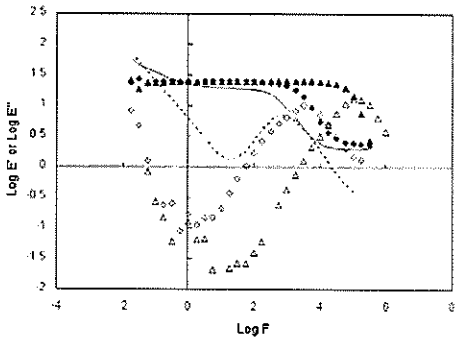

Figure 1. Dielectric properties of frozen hevea latex with respect to frequency at -30°C. – ε' (deionised water), ◆ ε' (fresh latex-49%), ▲ ε' (concentrated latex-38%), -- ε'' (deionised water), ◇ ε'' (fresh latex-49%) and △ ε'' (concentrated latex-38%).

Figures 2 and 4 present plots of hevea rubber latex in the log/log scale for temperatures -20 to -60°C at 10°C interval in the frequency region of 10^{-2} to 10^{6} Hz. In the five plots three distinct processes have been indicated. $\varepsilon(\infty)$ is the dielectric constant at high frequency, ε_{lp} is the loss peak, bound charge response or dipole relaxation mechanism based on Debye's model [8,10-11] and σ is the dc conductivity which results in polarization phenomena associated with the electrodes or electrode polarization [13]. This is similar to the equivalent circuit model for ice [12]. The curves through the data points had been fitted using the circuit model for the dielectric response shown schematically in Figures 6 and 7 and using the parameter values listed in Tables 1 and 2. Figures 3 and 5 also represent three distinct processes with two loss peak responses ε_{lp1} and ε_{lp2} and the dielectric constant at high frequency $\varepsilon(\infty)$. For latex concentrate, the dielectric constant is almost constant with values of 20 to 25 ($\varepsilon(0)$) in the region approximately below 10^{3} Hz before it decreases steeply and approached a value of 0.75 to 2.25 ($\varepsilon(\infty)$) at 10^{6} Hz and above and at temperatures -20 to -40°C.

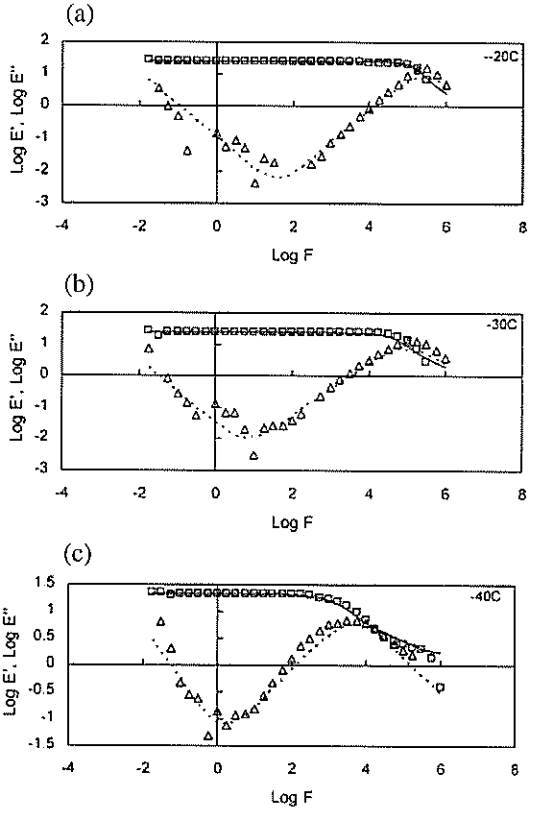

Figure 2. Schematic frequency response of latex concentrate exhibiting dc conduction and bound charge behaviour. □ ε' (experimental), – ε' (theory), △ ε'' (experimental) and -- ε'' (theory).

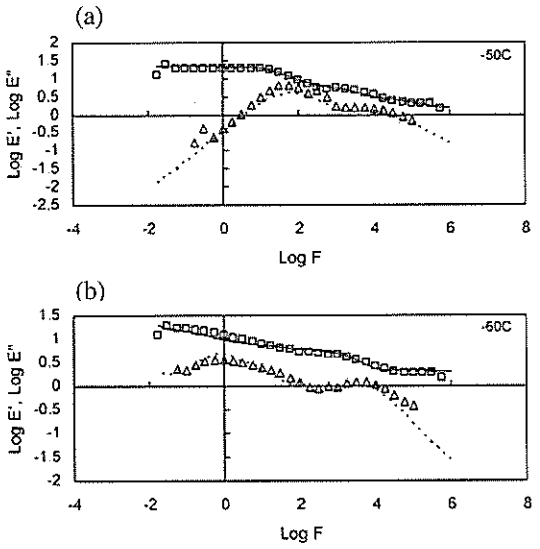

Figure 3. The frequency response demonstrates two bound charge behaviour. □ ε' (experimental), – ε' (theory), △ ε'' (experimental) and -- ε'' (theory).

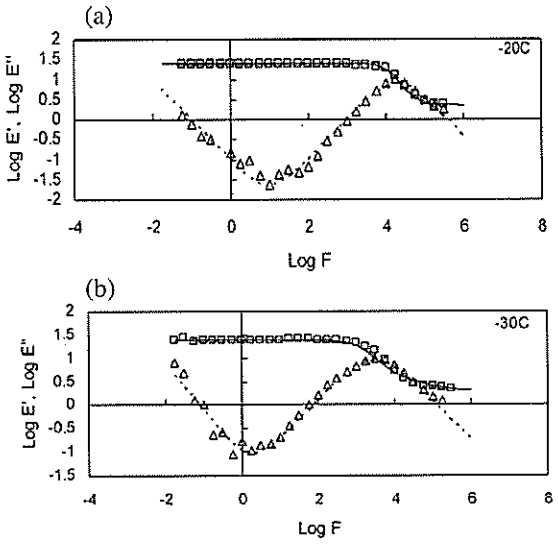

Figure 4. Schematic frequency response of fresh latex exhibiting dc conduction and bound charge behaviour. □ ε' (experimental), – ε' (theory), △ ε'' (experimental) and -- ε'' (theory).

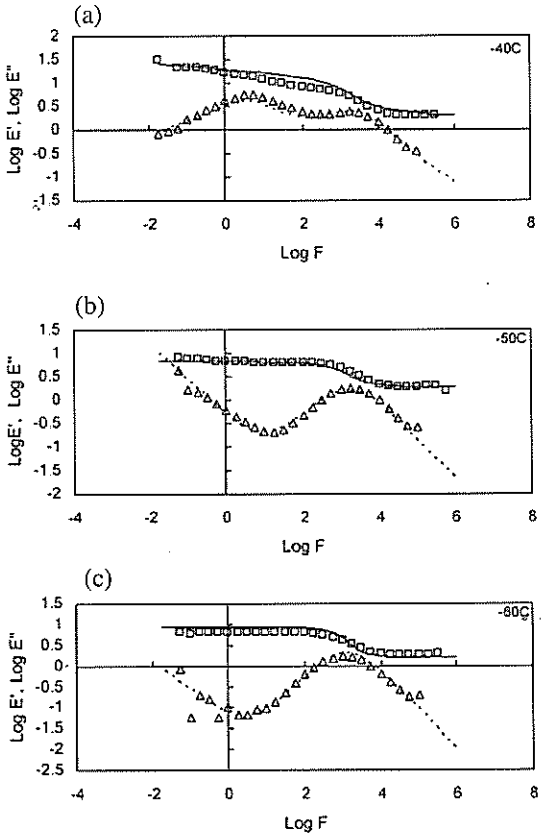

Figure 5. The frequency response demonstrates two bound charge behaviour. □ ε' (experimental), – ε' (theory), △ ε'' (experimental) and -- ε'' (theory).

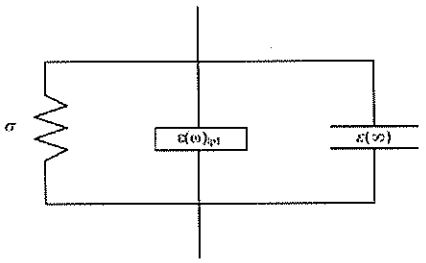

Figure 6. A dielectric circuit diagram (for figures 2(a-c)and 4(a-b)) showing a parallel combination of the dc conduction σ, the loss peak response $\varepsilon\ (\omega)_{lp1}$ for the bound charge behaviour and the response at high frequency $\varepsilon\ (\infty)$.

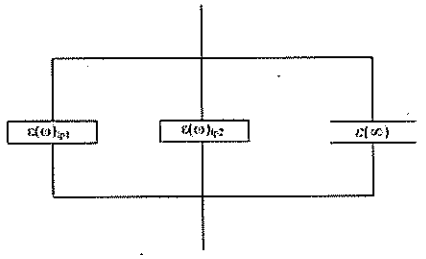

Figure 7. A dielectric circuit diagram (for figures 3 and 5) showing a parallel combination of two loss peaks $\varepsilon\ (\omega)_{lp1}$ and $\varepsilon(\omega)_{lp2}$ for the bound charge behaviour and the response at high frequency $\varepsilon\ (\infty)$.

For fresh latex, the dielectric constant is constant with a value of 23 ($\varepsilon(0)$) in the region approximately below 10^3 Hz before it decreases steeply and approached a constant value of about 2 ($\varepsilon(\infty)$) at 10^5Hz and above and at temperatures -20 to -30°C. The total losses are due to dipolar and ionic losses. The dipolar losses exhibit loss peaks at 0.36 and 0.125 MHz and 5.55 KHz for latex concentrate and at 27 and 4.18 KHz for fresh latex. Losses due to ionic conductivity or free charge carriers exhibit a dc conduction below 0.42, 0.35 and 0.32 Hz for latex concentrate and 0.5 and 0.33 Hz for fresh latex. The dipolar losses are in parallel with the dc conductivity. The dc conductivity appears as a slope of -1 and ε' is constant in this region. The ionic conductivity is due to the conducting phases found in latex.

However, at -50°C for latex concentrate and at -40°C for fresh latex, a transition appears in the form of two loss responses in parallel where the first loss response overrides the dc conductivity. The dielectric constant is constant at two different levels with a value of 15 ($\varepsilon(0)_1$) for the response and 5.55 ($\varepsilon(0)_2$) for the second for latex concentrate, while for fresh latex 20 ($\varepsilon(0)_1$) and 7 ($\varepsilon(0)_2$) respectively. The dielectric loss exhibits two loss peaks at 78.5 Hz and 10 KHz for latex concentrate and 2 Hz and 3 KHz for fresh latex. For latex concentrate at -60°C, the curves exhibit two loss responses with $\varepsilon(0)_1$ increasing slightly to 18 and $\varepsilon(0)_2$ decreasing slightly to 3.55. For fresh latex at -50 and -60°C, the curves exhibit two loss responses with $\varepsilon(0)_1$ with a value of 20 and $\varepsilon(0)_2$ decreasing slightly to 4.5. Even though the dielectric loss exhibits two loss peaks, only the second loss peak can be observed because the first loss peak shifts towards the lower frequency region beyond the scope of the tabulated data at 6 x 10^{-3} and 2.5 x 10^{-4} Hz respectively. Only the 'tail' end or one side of the slope can be seen. As temperature increases, the relaxation peak shifts towards the higher frequency region.

It has been reported that water naturally occurring in biological materials has some ionic content not including other ionic species found in the material and this conclusion is further supported by the values of the shape parameters n and m. Since both n and $1-m$

Table 1. Dielectric responses of latex concentrate (38%) at selected temperatures for frequencies 10^{-2} to 10^6 Hz.

Temperature (°C)	Response	Parameter
-20	Loss peak	$m_1 = 0.99$, $n_1 = 0.01$, $f_{p1} = 3.6\text{x}10^5$ Hz, $\varepsilon(0)_1 = 23$, $\varepsilon(\infty) = 2.25$
	DC conductivity	$\sigma = 0.95$ mho
-30	Loss peak	$m_1 = 0.98$, $n_1 = 0.2$, $f_{p1} = 1.25\text{x}10^5$ Hz, $\varepsilon(0)_1 = 25$, $\varepsilon(\infty) = 0.75$
	DC conductivity	$\sigma = 0.28$ mho
-40	Loss peak	$m_1 = 0.98$, $n_1 = 0.32$, $f_{p1} = 5.55\text{x}10^3$ Hz, $\varepsilon(0)_1 = 20$, $\varepsilon(\infty) = 1.45$
	DC conductivity	$\sigma = 0.77$ mho
-50	Loss peak	$m_1 = 0.9$, $n_1 = 0.2$, $f_{p1} = 7.85\text{x}10^1$ Hz, $\varepsilon(0)_1 = 15$
	Loss peak	$m_2 = 0.8$, $n_2 = 0.45$, $f_{p2} = 1\text{x}10^4$ Hz, $\varepsilon(0)_2 = 5.55$, $\varepsilon(\infty) = 1.25$
-60	Loss peak	$m_1 = 0.88$, $n_1 = 0.56$, $f_{p1} = 2.8\text{x}10^{-1}$ Hz, $\varepsilon(0)_1 = 18$
	Loss peak	$m_2 = 0.65$, $n_2 = 0.05$, $f_{p2} = 6.55\text{x}10^3$ Hz, $\varepsilon(0)_2 = 3.55$, $\varepsilon(\infty) = 2.05$

Table 2. Dielectric responses of fresh latex (49%) at selected temperatures for frequencies 10^{-2} to 10^6 Hz.

Temperature (°C)	Response	Parameter
-20	Loss peak	$m_1 = 0.99$, $n_1 = 0.03$, $f_{p1} = 2.7\text{x}10^4$ Hz, $\varepsilon(0)_1 = 23$, $\varepsilon(\infty) = 2.25$
	DC conductivity	$\sigma = 1.13$ mho
-30	Loss peak	$m_1 = 0.9$, $n_1 = 0.2$, $f_{p1} = 4.18\text{x}10^3$ Hz, $\varepsilon(0)_1 = 23$, $\varepsilon(\infty) = 2$
	DC conductivity	$\sigma = 0.66$ mho
-40	Loss peak	$m_1 = 0.9$, $n_1 = 0.65$, $f_{p1} = 2$ Hz, $\varepsilon(0)_1 = 20$,
	Loss peak	$m_2 = 0.8$, $n_2 = 0.13$, $f_{p2} = 3\text{x}10^3$ Hz, $\varepsilon(0)_2 = 7$, $\varepsilon(\infty) = 0.8$
-50	Loss peak	$m_1 = 0.7$, $n_1 = 0.35$, $f_{p1} = 6\text{x}10^{-3}$ Hz, $\varepsilon(0)_1 = 20$
	Loss peak	$m_2 = 0.8$, $n_2 = 0.1$, $f_{p2} = 3\text{x}10^3$ Hz, $\varepsilon(0)_2 = 5$, $\varepsilon(\infty) = 0.8$
-60	Loss peak	$m_1 = 0.7$, $n_1 = 0.35$, $f_{p1} = 2.5\text{x}10^{-4}$ Hz, $\varepsilon(0)_1 = 20$
	Loss peak	$m_2 = 0.8$, $n_2 = 0.07$, $f_{p2} = 1.9\text{x}10^3$ Hz, $\varepsilon(0)_2 = 4.5$, $\varepsilon(\infty) = 0.8$

are small (Tables 1 and 2), this indicate that the dipoles only distort their latex environment slightly and is only weakly inhomogeneous but the disturbance is spread almost homogeneously over the system[10] or the sample within the plates.

CONCLUSION

The low-frequency complex permittivity of hevea rubber latex has has been achieved through a series of measurements using the Dielectric Spectrometer in the frozen state and at different moisture content. The dielectric properties of hevea rubber latex depend on the frequency, temperature and moisture. The relaxation peak shifts towards the higher frequency region with increasing temperature and as water content in the latex decreases. This phenomenon could be due to the difference in the polarization affecting the ions and protonic conduction in ice.

The dielectric behaviour of hevea latex in the low frequency region display three distinct responses in a parallel combination. These include the dielectric constant at high frequency , the loss peak response and the conductivity σ. The total losses are ionic losses which appear as conductivity losses and dipolar losses which appear as loss peak responses. The conductivity is due to the conducting phases found in latex while the loss peak response is due to the relaxation of the water molecules. The small values for both and indicate that the water dipoles only distort their latex environment slightly and thus, the latex system is only weakly inhomogeneous.

Acknowledgements – This work was supported by the Universiti Putra Malaysia (UPM) research grant (50205-93-14). The authors wish to thank the technical staff, En. Roslim Mohd. of Applied Electromagnetic Laboratory, Department of Physics, for his invaluable help. The authors would also like to thank the Rubber Research Institute of Malaysia and the University Research Park of UPM for supplying the latex.

REFERENCES

1. Chin H.C. (1979) Methods for Measuring the Dry Rubber Content of Field Latex. *Training Manual on Analytical Chemistry*. Kuala Lumpur: Rubber Research Institute of Malaysia.
2. Chen S.F. (1979) Composition of Hevea Latex. *Training Manual on Analytical Chemistry*. Kuala Lumpur: Rubber Research Institute of Malaysia.
3. John C.K., Wong N.P., Chin H.C., Karim M.Z. and Ong C.T. (1982) LA-TZ Latex Concentrate. RRIM Technology Bulletin No. 6. Kuala Lumpur: Rubber Research Institute of Malaysia.
4. Laogun A.A. (1986) Beta Dielectric Dispersion in Natural Rubber Latex. *J. Appl. Polymer Sci.* **32**: 5085-5093.
5. Khalid K. and Wan Yusoff W.M.D. (1992) Dielectric Properties of Natural Rubber Latex at Frequencies from 200 MHz to 2500 MHz. *J. Nat. Rubb. Res.* **7**: 281-289.
6. Khalid K., Hassan J. and Wan Yusoff W.M.D. (1994) Dielectric Properties of Hevea Rubber Latex at Various Moisture Content. *J. Nat. Rubb. Res.* **9(3)**: 172-189.
7. Hassan J., Khalid K. and Wan Yusoff W.M.D. (1997) Microwave Dielectric Properties of Hevea Rubber Latex at Temperatures from -30°C to 50°C. *Pertanika J. Sci. & Tech.* **5**: 179-190.
8. Debye P. (1945) *Polar Molecule*. New York: Dover.
9. Jonscher A.K. (1983) *Dielectric Relaxation in Solids*. London: Chelsea.
10. Dissado L.A., Rowe R.C., Haidar A. and Hill R.M. (1987) The Characterization of Heterogeneous Gels by Means of a Dielectric Technique. *J. Colloid and Interface Science* **117**: 310-324.
11. Hill R.M. and Pickup C. (1985) Barrier Effects in Dispersive Media. *J. Material Sci.* **20**: 4431-4444.
12. Hobbs P.V. (1974) *Ice Physics*. Oxford: Clarendon Press.
13. Von Hippel A, Mykolajewycz R., Runck A.H. and Westphal W.B. (1971) *Technical Report 10* (Laboratory for Insulation Research) M.I.T.

Journal of Science and Technology in the Tropics (2005) **1**: 131-134

An information theoretic coding measure for hairpin RNAs

Goh Yong Kheng
Faculty of Information and Communication Technology, Universiti Tunku Abdul Rahman,
13 Jalan 13/6, 46200 Petaling Jaya, Selangor Darul Ehsan, Malaysia
(Email: gohyk@mail.utar.edu.my)

Received 29 September 2005; accepted 30 October 2005

Abstract Non-coding RNA (ncRNA) sequences are genetic sequences that do not produce proteins. Unlike protein coding gene, the statistical signals of ncRNA sequences are not obvious. Thus finding ncRNA sequences in a genetic sequence is difficult. This paper will report on a preliminary attempt to identify the hairpin RNAs in a genetic sequence. We present an algorithm based on Jensen-Shannon divergence to detect the potential hairpin RNA domain in a DNA sequence. The algorithm constructs a reverse-complementary copy of the DNA sequence, and compares the information entropy of two corresponding domains/segments from both sequences. The Jensen-Shannon divergence is minimal when the segment is cut at the borders of a potential hairpin RNA coding domain.

Keywords Bioinformatics – statistical mechanics – microRNA – information theory – Jensen-Shannon divergence

INTRODUCTION

Recent advancements in genetic engineering and bioinformatics have uncovered more and more evidences that contradict the conventional notions of genes. From the central dogma of molecular biology, genes encode proteins, and proteins perform every biological function. Gene is the main carrier of heredity. Every gene is transcribed into an intermediate messenger RNA. In turn messenger RNA is translated into protein. Protein, on the other hand, is believed to be the worker that performs or regulates every aspect of biological function. Although this central dogma of "one gene one protein" seems to be valid most of the time (at least for prokaryotes), more and more evidences [1-3] show that it is woefully incomplete for eukaryotes.

In eukaryotes genome, only very limited regions are protein coding sequences. For example, these protein-coding sequences account for less than 2% of human genome. Geneticists have long dismissed the other 98% of the non-coding sequences which they regard as junk. But the discoveries of RNA interference [4], pseudo-gene [5, 6], and anti-sense RNA [7] have brought up interests in these non-coding RNA sequences among the research communities.

There are various bioinformatics gene-finding tools [8] that allow searching for potential new protein coding genes with reasonable efficiency. However, non-coding RNA (ncRNA) gene-finding tools are still in its infancy. Rivas and Eddy [9] have developed an algorithm for detecting ncRNA by using a comparative sequence analysis and exploiting the property of conserved RNA secondary structure. This algorithm has been used successfully in the search of ncRNAs for *Saccharomyces cerevisiae* [10] and hyperthermophiles [11]. Note that the algorithm is a pair-Hidden Markov model that requires two homologous sequences as input.

We introduce an alternative ncRNA gene finding approach based on information theory. The presentation of this paper is organized as follows: Firstly, we will describe the theoretical background of the algorithm. Secondly, some results from simulations will be presented. Finally, we will summarize and discuss possible improvements to the algorithm.

Journal of Science and Technology in the Tropics (2005) 1: 131-134

ENTROPIC SEGMENTATION METHOD

Current methods for gene-finding, either coding or non-coding gene, often require prior knowledge of the biological system that is associated to the subject sequence. Most gene-finding algorithms either require prior training or need to perform the homologous sequence database search. These constraints causing the process of finding gene domains of a genome are highly dependent on the biological system being considered.

Bernaola-Galvan *et al.* [12] and Grosse [13] introduced an entropic segmentation method to identify the boundaries between coding and non-coding regions in DNA sequences. The principle of the method is based on calculating the Jensen-Shannon divergence of the partitions of DNA sequence by exploiting the nonuniform codon usage property of coding region. A DNA is first partitioned into two segments. For each segment, the compositional complexity is then calculated. By changing the size of the segments, the method identifies the borders of the coding and non-coding regions when the partition gives maximum compositional difference.

Bernaola-Galvan *et al.* used the Shannon entropy,

$$H(F) = -\sum_{i,j} f_{i,j} \log_2 f_{i,j}, \qquad (1)$$

as a measure for compositional complexity. The frequency vector $F = \{f_{i,j}\}$ is the set of the relative number of nucleotides $f_{i,j}$ of type $i \in \{A,T,C,G\}$ with phase $j \in \{0,1,2\}$. If the two segments of DNA sequences have lengths n_1 and n_2 with frequency vectors F_1 and F_2, then the compositional difference is given by the Jensen-Shannon divergence [14]

$$D(F_1,F_2) = 2(1n2)[NH(F) - n_1H(F_1) - n_2H(F_2)] \qquad (2)$$

where $N = n_1 + n_2$ is the total number of nucleotides of the original sequence and $NF = n_1F_1 + n_2F_2$. Bernaola-Galvan and colleagues have applied the technique to three bacteria genomes and obtained accurate location of borders [12].

EXTENSION TO ENTROPIC SEGMENTATION METHOD

The Bernaola-Galvan method, however, cannot extract accurate location for the borders of ncRNAs. This is due to the fact that ncRNA genes are intrinsically weak in statistical signals, as well as the nonuniform codon usage property of coding DNA which is not present in ncRNA. We will present an extension to the entropic segmentation method to find the borders of hairpin RNAs.

Hairpin RNAs are small RNAs that fold back on themselves. Suppose a DNA sequence containing hairpin RNA could be divided into 5 domains: J_1 L H R J_2 [Fig. 1]. The left arm, L of the hairpin RNA can be transformed into the right arm, R of the hairpin RNA by the following operations

$$R = \hat{R}\hat{C}[L] \qquad (3)$$

Here the operator $\hat{C}$ represents the complementary operation, i.e. {A→T, T→A, C→G, G→C}, and the operator $\hat{R}$ represents the operation of reversing a sequence Sq .

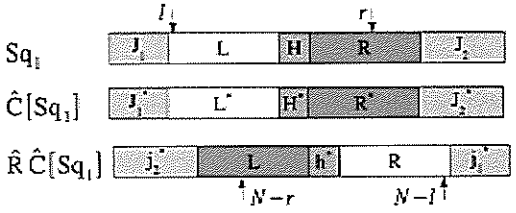

Figure 1. Schematic diagram of a DNA sequence undergoing complementary operation and reverse operation. Note that after the operations, the left arm of the input sequence becomes identical to the right arm of the input sequence, $R = \hat{R}\hat{C}[L]$.

Our extension to the entropic segmentation method is based on comparing the compositional complexity of a segment of the DNA sequence with the corresponding segment in the complementary-reserved sequence.

From the input sequence Sq_1, we generate the complementary-reversed sequence $Sq_2 = \hat{R}\hat{C}[Sq_1]$. A moving window, which is specified by left pointer l and right pointer r, is used to define the potential hairpin RNA segment Sg_1 on the input sequence. The corresponding segment Sg_1 and Sg_2 is, on the other hand, defined by a moving window with left pointer $N - r$ and right pointer $N - l$. Then the compositional difference between Sg_1 and Sg_2 will be calculated.

The Shannon entropy can be used as the compositional complexity measure for the segments. However, the frequency vector component $f_{i,j}$ defined above is based on the type and the phase of the nucleotides, and it is not suitable for RNA study for

reasons mentioned earlier. Instead, we redefine the frequency vector component f_α as the relative number of the lateral neighboring nucleotide links. Now, if we only consider the nearest neighbor links, the frequency vector $F = \{f_\alpha\}$ has 4 x 4 components, i.e.$\alpha \in \{X-Y\}, X,Y \in \{A,T,C,G\}$. If we include the next nearest neighbor, then F has 4 x 4 x 4 components.

The compositional difference for Sg_1 and Sg_2 is given by Eq. (2) as in the Bernaola-Galvan method. However, this time our aim is to find a window that minimizes the Jensen-Shannon divergence. This is because if the moving window on Sq_1 hits a hairpin RNA gene, then in theory Sg_1 and Sg_2 are almost identical except in the central region of the segments where nucleotides do not complement each other (the "head" of the hairpin).

SIMULATIONS AND RESULTS

We have applied and tested the new approach with randomly generated hairpin RNA data. Figure 2 and Figure 3 show some of the results obtained from a sequence where the number of nucleotides for J_1, L, H, R, J_2 are 50 bps, 100 bps, 50 bps, 100 bps and 50 bps correspondingly. Figure 2 shows that the result for the nearest neighbor links scheme and Figure 3 is for the next nearest neighbor links scheme. Both nearest neighbor and next nearest neighbor schemes show that the minimal value of D occurring near the right pointer position is close to 300, which agrees with our generated sequence.

DISCUSSION AND CONCLUSION

We have extended the entropic segmentation method is this paper such that it is able to detect the hairpin RNA genes in a DNA sequence. Our initial trials show promising results where the boundaries of RNA gene are correctly located. Although we could identify the possible boundaries for the RNA gene, but the boundaries are not as clear cut as in finding the boundaries of the coding and non-coding regions in [12]. In some simulations, sometimes we could have the case where the method fails to spot the RNA gene boundaries, due to the weak statistical signals of RNA or the very short RNA gene. However the method is very flexible and promising, as the method could be easily modified, either by including a longer nucleotide link or devising a better contrast function to replace Jensen-Shannon divergence.

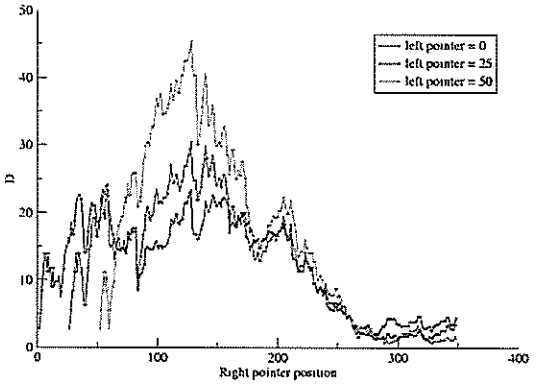

Figure 2. Jensen-Shannon divergence, D against right pointer position, r, for the nearest neighbor scheme. Each curve represents different fixed values of left pointer position, l. (Black solid line corresponds to $l = 0$, gray solid line corresponds to $l = 25$ and light gray solid line corresponds to $l = 50$)

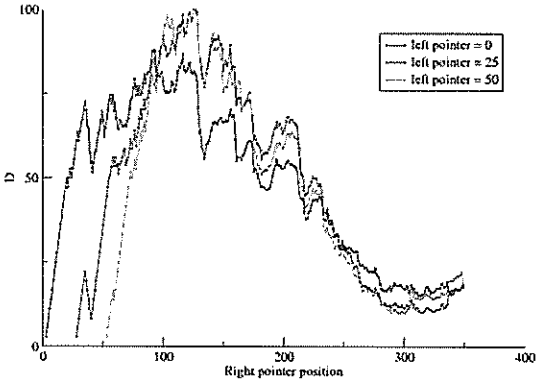

Figure 3. Jensen-Shannon divergence, D against right pointer position, r, for the next nearest neighbor scheme. Each curve represents different fixed values of left pointer position, l. (Black solid line corresponds to $l = 0$, gray solid line corresponds to $l = 25$, and light gray solid line corresponds to $l = 50$)

REFERENCES

1. Mattick J. S. (2003) Challenging the Dogma: The Hidden Layer of Non-Protein-Coding RNAs In Complex Organisms. *BioEssays: news and reviews in molecular, cellular and developmental biology* **25:** 930-939.
2. Gibbs W. W. (2003) The Unseen Genome: Gems among the Junk. *Scientific American* **289(5):** 26-33.
3. Eddy S. R. (2001) Non-Coding RNA Genes and the Modern RNA World. *Nature Reviews Genetics* **2(12):** 919-929.
4. Palatnik J. F., Allen E., Wu X., Schommer C., Schwab R., Carrington J. C., and Weigel D. (2003) Control of Leaf Morphogenesis by microRNAs *Nature* **425:** 257-263.
5. Hirotsune S., Yoshida N., Chen A., Garret L., Sugiyama F., Takahashi H., Yagami K., Wynshaw-Boris A., and Yoshiki A. (2003) An Expressed Pseudogene Regulates the Messenger-RNA Stability of its Homologous Coding Gene. *Nature* **423:** 91-96.
6. Yano Y., Saito R., Yoshida N., Yoshiki A., Wynshaw-Boris A., Tomita M., and Hirotsune S. (2004) A New Role for Expressed Pseudogenes as ncRNA: Regulation of mRNA Stability of its Homologous Coding Gene. *Journal of Molecular Medicine* **82 (7):** 414-422.
7. Yelin R., Dahary D., Sorek R., Levanon E. Y., Goldstein O., Shoshan A., Diber A., Biton S., Tamir Y., Khosravi R., Nemzer S., Pinner E., Walach S., Bernstein J., Savitsky K., and Rotman G. (2003) Widespread occurrence of antisense transcription in the human genome. *Nature Biotechnology* **21(4):** 379-386.
8. Burge C. B. and Karlin S. (1998) Finding the Genes in Genomic DNA. *Current Opinion in Structural Biology* **8:** 346-354.
9. Rivas E. and Eddy S. R. (2001) Noncoding RNA gene detection using comparative sequence analysis. *BMC Bioinformatics* **2:** 8.
10. McCutcheon J. P. and Eddy S. (2003) Computational Identification of non-coding RNAs in *Saccharomyces cerevisiae* by comparative genomics. *Nucleic Acids Research* **31(14):** 4119-4128.
11. Klein R. J., Misulovin Z. and Eddy S. R. (2002) Noncoding RNA Genes Identified in AT-Rich Hyperthermophiles. *Proceeding of the National Academy of Science USA* **99:** 7542-7547.
12. Bernaola-Galvan P., Grosse I., Carpena P., Oliver J. L., Roman-Roldan R., and Stanley H. E. (2000) Finding Borders between Coding and Noncoding DNA Regions by an Entropic Segmentation Method. *Physical Review Letters* **85(6):** 1342-1345.
13. Grosse I., Bernaola-Galvan P., Carpena P., Roman-Roldan R., Oliver J., and Stanly H. E. (2002) Analysis of symbolic sequence using the Jensen-Shannon divergence. *Physical Review E* **65:** 041905.
14. Casas M., Lamberti P. W., Plastino A., and Plastino A. R. (2004) Jensen-Shannon divergence, Fisher information, and Wootters' hypothesis. eprint *arXiv:quant-ph/0407147.*

Journal of Science and Technology in the Tropics (2005) 1: 135-140

Occurrence of trihalomethanes in drinking water tainted by peat swamp runoff in Sarawak

Sim Siong Fong and Murtedza Mohamed
Faculty of Resource Science & Technology, Universiti Malaysia Sarawak,
94300 Kota Samarahan, Sarawak, Malaysia

Received 15 July 2005; accepted 27 October 2005

Abstract Streams in peat swamp forests are important sources of potable water supply in Sarawak. However, the high content of humic substances in peat tainted water can potentially result in the formation of the carcinogenic trihalomethanes (THM) when the water is subjected to chlorination. This study was carried out to determine the level of THM in drinking water and to assess the effects of dissolved organic carbons (DOC), chlorine and DOC removal efficiency of water treatment plants (WTP) on the formation of THM. Water samples from four WTP and one consumer outlet were collected. The levels of THM were determined using liquid-liquid extraction method with n-pentane as the solvent. The chloroform concentrations detected were between 5 and 115 µg/L, with elevated concentrations being consistently attributed by two WTP processing peat water. The results clearly indicated that upon treatment with chlorine, water tainted by peat swamp leachate contained a higher quantity of THM compared to water from non-peat water sources. This was attributed to the higher contents of DOC, particularly the humic substances (THM precursor constitutents) in the former. Thus, WTP processing raw water sources containing high concentrations of DOC would have difficulty complying with the maximum allowable chloroform contaminant level of 30µg/L.

Keywords peat swamp – chlorine – trihalomethanes – drinking water

INTRODUCTION

The 1.67 million ha of peatland in Sarawak occur predominantly in the populated coastal flood plain of the State. As such the 'tropical black water' (TBW) from the peat area has been one the important sources of household water supply to the coastal region of Sarawak. About 45 water catchment in peat areas have been serving as the sources of raw water to supply the settlements and townships residing around the peatland of the coastal zone. The daily volume of raw peat water extracted from these catchment areas is approximately 7,700 Megalitres, serving about 140,000 coastal population [1].

Dissolved organic materials found in TBW have a great potential to react with chlorine in drinking water distribution system, and lead to the formation of trihalomethanes (THM) [2]. The THM formed are chloroform ($CHCl_3$), dichlorobromomethane ($CHCl_2Br$), chlorodibromo-methane ($CHClBr_2$) and bromoform ($CHBr_3$). Epidemiological studies have suggested a possible link between chlorination and chlorination by-products and excess risk of bladder and rectal cancer [3]. The concern of the national health authorities has resulted in recommendations or regulations of the maximum levels of disinfection by-products in drinking water. The USEPA has set limits on acceptable total trihalomethanes (TTHM) and chloroform concentrations in finished drinking water at 100 µg/L and 30 µg/L, respectively [4]. In Malaysia, the National Drinking Water Standard [5] sets the permissible limit of chloroform in drinking water at 30 µg/L although this has later been revised upward to 200 µg/L in accordance with the WHO Guidelines (1993) [6].

This paper presents the findings of a study carried

Journal of Science and Technology in the Tropics (2005) 1: 135-140

out to determine the level of THM in drinking water produced from peat swamp source waters, and from non-peat source at several water treatment plants (WTP) in Sarawak. The formation of THM is also discussed in relation to the DOC level in the raw water, the amount of residual chlorine remained in the treatment and distribution system, and the efficiency of the treatment plants in removing DOC from the raw water.

MATERIALS AND METHODS

Water treatment process

All the four water WTP studied, namely the Batu Kitang, Asa Jaya, Bau and Bako WTP, employ the following general sequence of treatment processes: Raw water → Dosing chamber → Flocculation → Sedimentation → Filtration → Chlorination, prior to distribution. Generic chemicals employed are alum (coagulant), polyelectrolyte (coagulant aid) and soda ash (to precipitate acidic dissolved organics). After sedimentation and filtration processes, calcium hypochlorite (1%) would be charged into the filtered water to produce an average distribution of free chlorine residual of 1.5 - 2.0 ppm for disinfection purpose. Soda ash was finally added at the clear well for post treatment pH adjustment. Samples of tap water from Universiti Malaysia Sarawak (UNIMAS), which is directly connected with the distribution system, was chosen for this study. It is one of the locations receiving water supply from Batu Kitang WTP.

Water sampling

A total of 234 THM analyses were performed on the raw, filtered and treated water samples, collected once a month for six consecutive months from the four earlier mentioned WTP. Raw water samples was collected directly from the source prior to treatment; filtered water was semi-treated water which had gone through the designed treatment except chlorination, and treated water was the water which had run through the complete treatment processes. Triplicate samples were collected for each sampling point. Samples were collected in the glass bottle sealed with Teflon lined screw caps. Fresh water supply was collected from the tap after allowing the water to run for 3 minutes after which the bottles were filled just to overflow to prevent any headspace. 2.5 mg/L of the dechlorination agent, sodium thiophosphate, was added to each sample. The samples were stored at 4 °C and analysed within 24 hours.

Analytical methods

THM in drinking water were determined by liquid-liquid extraction method with n-pentane as the solvent [7]. Water samples (10 ml) were pipetted with glass syringe into silicate extraction tubes containing 1.0 g of sodium chloride. Pentane (2 ml) was introduced into the extraction tubes and shaken vigorously. The solution was allowed to stand until the organic and aqueous phases separated. 1 µl of the pentane extract was injected into a Hewlett Packard 5890 Series II Plus gas chromatograph equipped with Ni^{23} electron capture detector. Quantification of THM was performed using the external standards peak area calibration method. Dissolved organic carbon (DOC) analysis was performed using a TOC analyzer. The water samples were filtered through 0.45 µm membrane prior to analysis. The humic substances in the water samples were measured on a spectrophotometer at 260 nm without pH adjustment.

Material recovery

Recoveries of the THM were examined by spiking 100 ml of distilled water with freshly prepared standards to give a final concentration of 100 µg/L. Four replicates were carried out for the measurement of recoveries using the same analytical methods. The mean percentage recoveries of standard aqueous solution of chloroform ($CHCl_3$), bromodichloromethane ($CHBrCl_2$), dibromochloromethane ($CHBr_2Cl$) and bromoform ($CHBr_3$) amounted to 90.24%, 94.94%, 99.10% and 99.00%, respectively.

RESULTS AND DISCUSSION

Level of THM in treated water

In the present study, a total of 234 THM analyses were performed. The average concentration of THM in the raw water, filtered water and treated water samples are presented in Table 1. Notably, chloroform represents the major component of the total trihalomethanes (TTHM) in drinking water, followed by other brominated species.

Chloroform was detected in trace amount in all of the raw water and filtered water samples, suggesting the natural occurrence of halogenated organic compounds in the environment. According to Asplund, 1992 [8], there is a vast majority of halogenated compounds being stored in soils and fresh water sediments. These compounds are produced by more

Table 1. Average level of THM in raw water, filtered water and treated water.

Treatment plant	Water sample	$CHCl_3$ (mg/L)	$CHBrCl_2$ (mg/L)	$CHBr_2Cl$ (mg/L)	$CHBr_3$ (mg/L)
Batu Kitang	Raw water	1.59	nd	nd	nd
	Filtered water	3.99	nd	nd	nd
	Treated water	17.40	0.50	nd	nd
Bako	Raw water	1.49	nd	nd	nd
	Filtered water	2.07	nd	nd	nd
	Treated water	54.55	nd	0.39	nd
Bau	Raw water	1.92	nd	nd	nd
	Filtered water	2.18	nd	nd	nd
	Treated water	18.73	1.51	1.02	4.98
Asa jaya	Raw water	3.00	nd	nd	nd
	Filtered water	2.93	nd	nd	nd
	Treated water	80.24	5.64	1.53	2.78
Unimas	Treated water	22.50	0.41	nd	nd

than 1000 species of fungi, lichens and marine bacteria. In addition, non-marine bacteria, higher plants and vertebrates are also generating halometabolites. The natural production of halogenated compounds can be enhanced under acidic condition. As such, it can be expected that chloroform occurs in detectable quantity in peatland environment.

It was evident that the levels of chloroform detected in treated water samples from the Asa Jaya (58-115µg/L) and Bako (37-85 µg/L) WTP were much higher compared to those of Bau (5-30 µg/L) and Batu Kitang (10-28 µg/L) WTP. Both the Asa Jaya and Bako WTP are sourcing water from the peat swamp runoff and the formation of THM in the treated water was the result of chlorine disinfection process employed at these two WTP. The presence of DOC (such as humic substances) in the raw water sourced by these two WTP could have served as the precursors of THM formed during treatment, and also thereafter due to further reactions between the remaining DOC and free chlorine residual present in the water reticulation system.

Chloramination method involving the use of chlorine and ammonia has been proven to have a low potential of forming THM as they are more stable than chlorine. Among the four WTP studied, only the Batu Kitang WTP uses chloramination at the chlorination stage. Obviously, this method results in the generation of less chloroform, which was well under the permitted maximum contaminant level of 30 µg/L.

Unimas is one of the furthest locations receiving water supply from the Batu Kitang WTP. It was expected that THM in the tap water at Unimas would be much higher as the residual chlorine continue to halogenate the remaining DOC along the distance. Consumers towards the end of the distribution system are likely to receive water with higher THM level than consumers at the beginning of the distribution system [9]. However, the chloroform level in the tap water of Unimas (8-31µg/L) was similar to that in the treated water collected from Batu Kitang WTP (10-28 µg/L). This observation suggested that chloramination is a more effective way in reducing the formation of THM in drinking water.

Brominated THM were not always detected. The formation of brominated THM could only be expected during saline water intrusion as there would be an increase in the normally absent bromide ion in the raw water. It was noted in a study of the Sacramentosan River delta in the United States [10]. During drought season and low river flow conditions, sea water intrusion from the San Francisco Bay had resulted in higher bromide ion levels in water coming from the delta. This had led to an increase in the TTHM as well as a shift to more brominated species. A similar scenario was observed in the analysis of THM in drinking water obtained from Batu Kitang Treatment Plant, Kuching during the drought period in 1997. It was found that the brominated THM, which were normally absent, were detected probably due to saline intrusion [11]. Besides, method of extraction could also lead to detection of brominated species. According to the USEPA Method 551, sodium chloride was added to increase the extraction efficiency but its high bromide impurity may react with residual chlorine and natural organic matter causes higher brominated THM levels [12].

Journal of Science and Technology in the Tropics (2005) 1: 135-140

Evaluation of the toxicity of TTHM

Evaluation of the toxicity of TTHM is crucial in determining if the treated water is safe for drinking. Asplund, [8] suggested a fractional approach of evaluating the toxicity of TTHM as follows:

$$C_{Bromoform}/GV_{Bromoform} + C_{DBCM}/GV_{DBCM} + C_{BDCM}/GV_{BDCM} + C_{Chloroform}/GV_{Chloroform} < 1$$

where C = Concentration (mg/L),
DBCM = Dibromochloromethane,
GV = Guildeline value,
BDCM = Bromodichloromethane.

The computed ratio should not exceed 1 for safe drinking water. For the present study the results obtained were all below the limit of one (Table 2).

Table 2. Fractional approach of total trihalomethanes.

	$C/GV_{Chloroform}$	C/GV_{DBCM}	C/GV_{BDCM}	$C/GV_{Bromoform}$	sum of ratio
Asa Jaya	0.401	0.056	0.025	0.028	0.511
Bako	0.273	0.004	0.000	0.000	0.277
Bau	0.094	0.015	0.017	0.050	0.176
Batu Kitang	0.401	0.056	0.025	0.028	0.511
Unimas	0.113	0.004	0.000	0.000	0.117

Effect of DOC

The rate and extent of THM formation increases as precursor content increases (usually measured as total organic carbon). Traditionally water treatment plants are designed and operated to maximise removal of DOC through the use of coagulation-flocculation-sedimentation and filtration processes. The system does not remove all the humic material in the source water. To investigate the THM formation potential, the average DOC content of filtered water was used to correlate with the chloroform level in treated water (Figure 1).

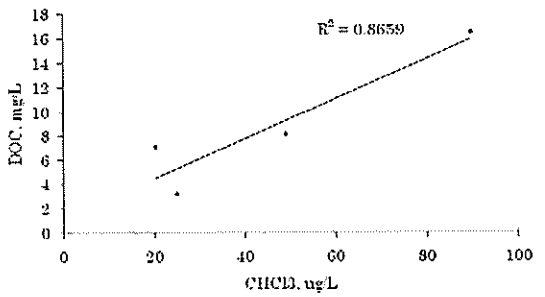

Figure 1. Correlation of chloroform formation with the DOC content.

The results obtained exhibited a good correlation between the DOC in the raw water and the chloroform level in the treated water.

Nevertheless it was suggested that the potential for one water system to form THM should not be compared to another on the basis of DOC level [13]. Instead, these workers suggested the use of UV absorbance at 260 nm (E_{260}) which is sensitive to coloured natural organic materials that are referred to as humic substances. They are the major precursor of THM formation.

A study similar to this, carried out on drinking water samples from Selangor, Kuala Lumpur, West Pahang and Negeri Sembilan reported 48% cases of 'non-compliance' (i.e. the chloroform levels were in excess of 30 µg/L) [14]. Chloroform concentrations of up to 227 µg/L had been reported for samples obtained from Negeri Sembilan. This elevated level of chloroform was attributed to high total organic carbon contents in the raw water.

Effect of residual chlorine concentration

The formation of THM increases as the residual chlorine increase. In 1994, the maximum residual disinfectant goals for chlorine, chloramines and chlorine dioxide in treated water in the USA were regulated at 4 mg/L, 4 mg/L and 0.8 mg/L, respectively [15]. In Malaysia, the National Guidelines issued by the Ministry of Health requires that water utilities maintain a minimum level of disinfectant of not less than 0.2 mg/L for free chlorine residual. Figure 2 illustrates the level of residual chlorine and chloroform in treated water of the four treatment plants. It was observed that the water treatment plants utilising peat swamp runoff i.e. Asa Jaya and Bako WTP showed a high level of chloroform with low concentration of residual chlorine. The free chlorine residual at both treatment plants could be slightly too low for achieving adequate level of disinfection. This

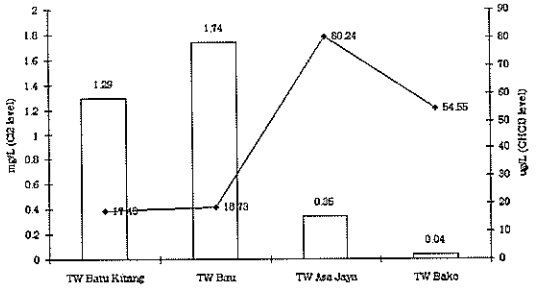

Figure 2. Level of residual chlorine and chloroform in treated water samples from the four WTP.
◆ chloroform; box, free chlorine.

finding suggests that water tainted from peat swamp leachate could exert a greater demand of residual chlorine. Conversely, the condition at Batu Kitang and Bau WTP was better with chloroform level remained comfortably below the maximum permissible level.

Removal efficiency

The efficiency of WTP in removing dissolved organic material is extremely important in minimising the formation of THM. It is common for WTP to produce treated water with high residual DOC due to the lack of on-site expertise in water treatment to determine adequate coagulant dosage and appropriate pH for the coagulation process [13, 16]. In this study the DOC removal efficiency of each treatment plant was determined based on UV absorbance and correlation was established between the level of chloroform and the DOC removal efficiency The DOC removal efficiency by coagulation-sedimentation-filtration was expressed using the following equation.

$$R\ (\%) = [(E_{raw} - E_{treated})/E_{raw}] \times 100\%$$

where R is removal efficiency, E_{raw} is the absorbance of raw water, and $E_{treated}$ is the absorbance of water after coagulation-sedimentation-filtration processes at 260 nm.

The results obtained (Figure 3) indicated similar performance for all of the treatment plants. However, there was a great variation in the formation of chloroform in the treated drinking water. The Asa Jaya WTP with the highest DOC removal efficiency failed to reduce the formation of chloroform. The process may have successfully removed the high molecular weight DOC but failed to filter those low molecular weight

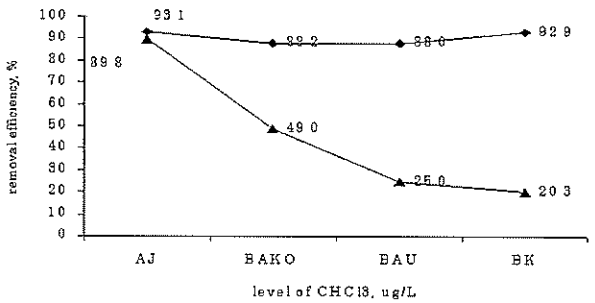

Figure 3. Relationship between DOC removal efficiency and chloroform formation. ▲ chloroform; ◆ % removal (E).

DOC which is the major precursor of THM formation ($E_{treated}$ Asa Jaya: 0.059; $E_{treated}$ Bako: 0.122; $E_{treated}$ Batu Kitang: 0.013; $E_{treated}$ Bau: 0.023).

CONCLUSION

An important conclusion from this work was that treatment plants with raw water sources having high concentration of dissolved organic materials may not be able to meet the maximum allowable chloroform contaminant level of 30 µg/L. The difficulty was very likely due to the nature of dissolved organic present. Therefore, additional treatment such as treatment with activated carbon and aeration process may be required for THM to remain below this maximum allowable level.

Acknowledgements – The authors gratefully acknowledge the research funding extended by Universiti Malaysia Sarawak and cooperation rendered by the water works personnel of the four selected WTP.

REFERENCES

1. Mohamad Sabari Shakeran. (2003) *Water catchment and supply. In* Chew D. and Hua S.A. (eds). Integrated Peatland Management for Sustainable Development. Sarawak Development Institute. Kuching, Sarawak.
2. Morris J.C. and Baum B. (1978) Precursors and mechanisms of haloform formation in the chlorination of water supplies. *In* Jolley R.L. (ed) *Water Chlorination: Chemistry, Environmental Impact and Health Effects.* **2.** Lewis Publisher, Chelsea. Pp. 29-48.
3. Morris R.D., Audet A.M., Angelillo I.F., Chalmers T.C. & Musteller, F. (1992) Chlorination, chlorination by-products and cancer: A meta-analysis. *Amer. J. Public Health* 82: 955-963.
4. USEPA (1998) *National primary drinking water regulations.* Control of Trihalomethanes in drinking water. USEPA, Washington.
5. MOH (Ministry of Health, Malaysia) (1990) *Piawaian Air Minum Malaysia.* Kementerian Kesihatan Malaysia, Kuala Lumpur.
6. MOH (Ministry of Health, Malaysia) (2001) *National*

Journal of Science and Technology in the Tropics (2005) 1: 95-101

A low cost and simple to operate human calorimeter for the measurement of daily energy expenditure in the developing countries

M. S. Razali[1] and M. N. Ismail[2]

[1] Faculty of Sports Science & Recreation, Universiti Teknologi Mara, Shah Alam, Selangor, Malaysia

[2] Department of Nutrition & Dietetics, Faculty of Allied Health Sciences, Universiti Kebangsaan Malaysia, 50300 Kuala Lumpur, Malaysia

Received 19 September 2005; accepted 30 November 2005

Abstract Measurements of daily energy expenditure are necessary to assess energy requirements, and to determine the effects of physiological, pathological and environmental conditions on energy expenditure and work efficiency. A room measuring 3.05 m x 2.08 m x 2.90 m (18.40 m^3) was converted into an open-circuit indirect calorimeter. Air was drawn out of the calorimeter and analyzed for differences in oxygen concentration between room air and baseline (outside air) using Servomex Xentra 4100 Gas Purity Analyzer. The volume of the calorimeter – determined by using two different gases, oxygen 99.8% and oxygen-free nitrogen (OFN) – produced a mean value of 18,112±993 L. Permeability tests were carried out to ascertain that there was little or no diffusion or leakage of gases in the calorimeter during the experiments. The accuracy of the calorimeter, assessed by a series of tests using burning butane gas, produced a range of –1.2% to +1.8%; the measured value was 98.77±0.21% of that obtained by theoretical calculation. The energy expenditure was calculated based on Weir formula and computed using an on-line datalogger. Repeatability studies carried out on normal and obese subjects showed a 4.3% within subject day-to-day coefficients of variations (CV) on 24-h EE measurements. We conclude that the calorimeter is reliable and suitable for measurements of total daily energy expenditure (TDEE).The design is novel in its cost of construction and simple to operate without sacrificing accuracy. It could also be reproduced economically without difficulty in the developing countries.

Keywords low-cost human calorimeter – energy expenditure – developing countries

INTRODUCTION

The minimum physiological need for energy is certainly variable and the necessity to estimate energy requirements from data based on energy expenditure has repeatedly been emphasized [1]. Numerous techniques, both calorimetric and non-calorimetric, have been used for assessing energy expenditure. Non-calorimetric techniques such as heart-rate recording and time and motion studies are known to interfere with life style and prone to large errors. In contrast, direct calorimeters, which were popular at the turn of the century, are highly accurate for long-term measurements of energy expenditure. The era of human calorimeter began with the ingenious construction of the Atwater calorimeter 100 years ago [2]. Unfortunately, financial constraint was a major factor for researchers to construct either direct or indirect human calorimetry even in the affluent countries. This is because a human calorimeter with a high level of accuracy and large enough to live in comfortably needs very high cost of construction, maintenance and operation.

Nevertheless, successful construction of previously reported room calorimeters [3-6] in the developed countries for the measurement of 24 h energy expenditure has inspired us to construct our own. Of particular interest, is the reported 10-13% lower basal metabolic rate (BMR) among adult Malaysians [7] when compared to the FAO/WHO/UNU [8] equations but only differed by 3% when compared with Henry and Rees equations for populations living in the tropics [9].

Drinking Water Standrad Guidelines. Engineering Services Divison, Ministry of Health Malaysia, Kuala Lumpur.

7. Mehran M.F., Slifker R.A. and Cooper W.J. (1984) A simplified liquid-liquid extraction method for analysis of trihalomethanes in drinking water. *J. Chromatogr Sci.* 22: 241-243.
8. Asplund G.A. (1992) *On the origin of Organohalogens found in the environment.* Dissertation, Linkoping Studies in Art and Science, Sweden.
9. World Health Organization. (1993) *Guidelines for Drinking- Water Quality* 1: 95.
10. Xie Y. and Reckhow, D.A. (1996) Correspondence to identification of halogenated compounds in chlorinated seawater and drinking water produced off shore using n-Pentane extraction and open-loop stripping technique. *Environ Sci Technol.* 30: 720.
11. Wong S.S. (1997) *Disinfection by-products (DBPs) in water treatment & Trihalomethanes (THM) Standard.* Reports, Kuching Water Board, Sarawak.
12. Asplund G.A. (1991) Organohalogens in nature: More widespread than previously assumed. *Environ. Sci. Tech.* 25: 1347-1350.
13. Tambo N. and Kamei T. (1989) Evaluation of extent of humic substances removal by coagulation. *In* Suffet I.H. & MacCarthy P. (eds) *Aquatic humic substances - Influence on fate and treatment of pollutants,* p.455-462. American Chemical Society, Washington.
14. Yew C.H. (2002) *Kajian Penjanaan, Teknik Analisis dan Pemodelan Trihalometana dalam Air Minum.* PhD Thesis. Universiti Kebangsaan Malaysia, Bangi.
15. Dennett K.E., Amirtharajah A., Studstill A., Moran T.F. and Gould J.P. (1995) Humic Substances Removal and Minimization of Trihalomethanes by Ferric Chloride Coagulation. *AWWA Research Foundation*, Order Number: 90665.
16. Trussell A.R., Cromor J.L., Umphres M.D., Kelly P.E. and Moncur, J.M. (1979) A survey of twelve drinking waters from various parts of the world. *In* Jolly R.Z., Brungs W.A., Combing, R.S. & Jacobs V.A. *Water Chlorination Environmental Impact and Health Effects,* ed. p. 39. Ann Arbor Science, Michigan

Journal of Science and Technology in the Tropics (2005) **1**: 141-146

Pertinent statistical techniques for the reporting of annual concentration of total suspended particles in ambient air

G. Redzwan[1] and S. Sinyaw[2]
[1] Faculty of Science, University of Malaya, 50603 Kuala Lumpur, Malaysia
[2] Environmental Studies Division, Malaysian Meteorological Service
46667 Petaling Jaya, Selangor D.E., Malaysia
(Email: ghufran@um.edu.my)

Received 26 October 2005; accepted 29 November 2005

ABSTRACT This paper attempts to include data quality assessment which has been proposed by US-EPA. It has been pointed out that the reporting of the specific parameter based on its average concentration should be validated prior to the reporting. The averaging value could be calculated either by an arithmetic mean or a geometric mean. Based on the arithmetic mean, the daily average for total suspended particles (TSP) in 2004 at Petaling Jaya was at the concentration of 67.9 $\pm$ 24 mg.m^{-3}. Subsequent statistical analysis by probability graph suggested that geometric mean might not be suitable to be used.This was concurred by obtaining the value of geometric mean, which gave the average of TSP concentration at 63.7 $\pm$ 1.4 mg.m^{-3}. Relatively low value for the standard geometric deviation deems to show that the data was homogenous and the deviation values did not fall in the typical probability range. Therefore, arithmetic mean of TSP average should be used for the reporting of ambient air quality.

Keywords Air quality – Malaysia – Petaling Jaya – total suspended particles – data quality assessment

INTRODUCTION

Episodes of haze are becoming a typical incidence in Malaysia. The occurrence would be elongated as long as the activity of open burning could not be curbed either locally or regionally. In 2005, haze episode has reached to the declaration of emergency in some of the affected areas. The declaration was done based on the results of the on-line data monitoring of the ambient air quality. All parameters which are used for the calculation of air pollution index (API) are uploaded hourly to a centralised data collection. Once the API reading has been established, it will be relayed to the office of Department of Environment (DOE) for further notification.

In Malaysia, API has been used synonymously with the description of ambient air quality. Parameters which are used for the determination of API, namely as particulate matter-10 micron (PM_{10}), nitrogen dioxides (NO_2), sulfur dioxides (SO_2), carbon monoxide (CO), ozone (O_3) are being collected by continuous air quality monitoring stations or known as CAQMS [1]. Since 1998, there are 51 CAQMS available in major towns and cities. These stations have become one of the significant accomplishments in Malaysia, in order to accomplish collective means of ways to manage the air quality. This service is maintained by a private limited company as the concessionaire serving as environmental data provider to DOE.

Statistical analysis is one of the common tools that could be used for the reporting of ambient air quality. This pertinent statistical approach has been considered useful for assessing the quality of ambient air sampling data [2]. Besides providing online data by CAQM, another objective of having such stations is to provide background data for specific locations and areas. Provision of background air quality data could assist towards the development of environmental standard for

air quality, instead of depending solely on the emission standard as being gazetted in Environmental Quality Acts, 1974. Up till now, environmental standard for air quality is yet available to be used.

Proper use of statistics and statistical techniques are important to establish criteria for air quality and the development of data collection designs. The statistical approach is an initial step for the conduct of data quality assessment (DQA) and data quality objectives (DQO) [2]. Both of DQA and DQO will lead to the development of a quantitative and qualitative framework for the configuration of environmental monitoring and assessment of ambient air quality. Although monitoring of TSP has been excluded as one of the health index indicators, but TSP is still relevant for the atmospheric study. It represents various types of particles including both of primary and secondary particles with various sizes from various sources [3]. TSP could contain combustion-generated particles, photo-chemically produced particles, salt particles and soil-like particles [4]. Analysis on the composition of TSP particles could identify the source and type of air pollutants presence in the ambient air.

This paper attempts the pertinent statistical techniques for the expression of the annual average of TSP concentration in Petaling Jaya. The reporting of parameters to describe air quality have to be determined its validity. Those parameters could be reported either by arithmetic mean or geometric mean. It is aimed that this study will initiate the process of DQA and DQO to take place for the framework of environmental reporting for air pollutants as to achieve a more effective air quality management in Malaysia.

MATERIALS AND METHODS

Data Collection

Two standard high volume samplers were used to collect daily reading for the concentration of TSP for the ambient air quality reporting in 2004. They are collected on a fibreglass filter paper and weighted with an analytical balance (four decimal points accuracy). Sampling points for the parameter is located 20 meters above the ground, which is placed on the roof of an administrative building in Petaling Jaya, Selangor.

Statistical Techniques

Common statistical techniques for environmental monitoring and reporting were adapted from Wheater and Cook [5]. The techniques were data frequency table, histogram and cumulative frequency curve. From these set of analysed data, further statistical analysis was carried out for data distribution, probability graph, normal and log normal distribution curves, arithmetic mean and geometric mean, and standard deviation and standard geometric deviation. Each step of the statistical analysis would lead to the recognition for their usefulness in DQA and DQO.

RESULTS AND DISCUSSION

Overall data collection

One year of daily data for TSP concentration had been collected and they are shown in Figure 1. As indicated in the figure, the overall data is usually hard to be interpreted. Fluctuations of TSP concentration in 2004 ranged from 20 $mg.m^{-3}$ to 140 $mg.m^{-3}$. Such fluctuations would not provide much information for the extraction of useful data about ambient air quality. Averaging the whole data gives the average concentration of TSP at 67.9 $\pm$ 24 $mg.m^{-3}$. However, this value is yet to be accepted without further statistical analysis as part of the practise in DQA [2]. Table 1 shows the monthly average for the concentration of TSP in the same duration of time. The monthly averaging has shown that TSP concentration ranges from 51 to 89 $mg.m^{-3}$. The available data neither represents the background data nor baseline data.

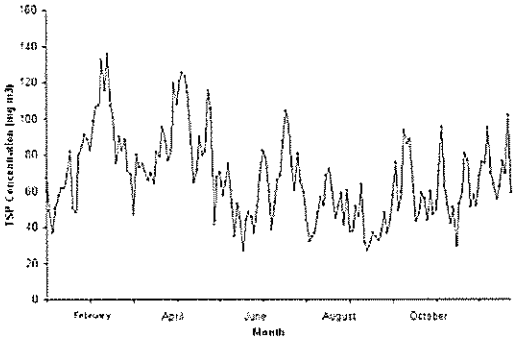

Figure 1. Daily Concentration of TSP in 2004.

Table 1. Monthly average for the concentration of TSP in 2004.

Month	Average ($mg.m^{-3}$)	Standard Deviation
January	56.5	± 15.6
February	67.7	± 17.8
March	61.5	± 17.3
April	68.8	± 16.6
May	70.2	± 27.0
June	88.7	± 38.0
July	59.8	± 14.6
August	84.2	± 21.5
September	79.3	± 28.3
October	60.4	± 18.4
November	50.8	± 17.5
December	63.1	± 16.2

This range of monthly average was calculated according to the arithmetic mean, which is represented by Eq. (1). In such cases, geometric mean will provide more meaningful statistical analysis for ambient air monitoring [6]. Geometric mean can be calculated by Eq. (2). Nevertheless geometric mean is often used for data whose causes behave exponentially rather than linearly. In order to determine such causes, graphical techniques of summarising such data should be considered, which would be explained in the following sections.

$$\bar{X} = \frac{X_1 + X_2 + X_3 .... + X_n}{n} = \frac{\Sigma X_i}{n} \qquad (1)$$

$$\bar{X}_z = \sqrt[n]{X_1 . X_2 . X_3 ..... X_n} \qquad (2)$$

$\bar{X}$ = arithmetic mean, $\bar{X}_z$ = geometric mean,
X_i = i^{th} measurement,
n = total number of observations

Frequency table

Frequency table is often used to summarise the data. The preparation was done by dividing a data set into selected class intervals, then counting and inserting the number of frequency of occurrence. In this study, the obtained data range was within 20 - 140 $mg.m^{-3}$. An interval class with 20 units in length was adopted and gave nine classes of interval. This amount of interval class is sufficient to run a statistical analysis for the data [2].

Counting the number for the frequency of occurrence in each interval gave the frequency table, which is shown in Table 2. Based on the observation of frequency table, concentration of TSP appears to be clustered between 40-100 $mg.m^{-3}$. In fact, based on the relative frequency, 81% of the data are located in this interval. This observation shows that the annual daily average for TSP in the whole year around with the concentration of 67.9 $mg.m^{-3}$. It was calculated with Eq .(1) with n = 366; could not conform the purpose of environmental reporting, which is to indicate the ambient air quality.

Table 2. Frequency table for concentration of TSP during 2004.

Class interval ($mg.m^{-3}$)	Frequency of occurrence	Relative frequency
0 - 20	0	0.00
20 - 40	32	0.09
40 - 60	130	0.36
60 - 80	109	0.30
80 - 100	53	0.15
100 - 120	23	0.06
120 - 140	9	0.03
140 - 160	3	0.01
160 - 180	0	0.00

Histogram

Constructing a histogram would be useful for statistical purposes as it could give probabilistic based on the scale of abscissa and its association with interval's portion of the total area of interval. This can be achieved by drawing a histogram of frequency distribution curve as shown in Figure 2.

Figure 2 could assist to determine the probability of occurrence for each range of TSP concentration to occur. However, this must be referred with the similar weather condition at specific location. If similar

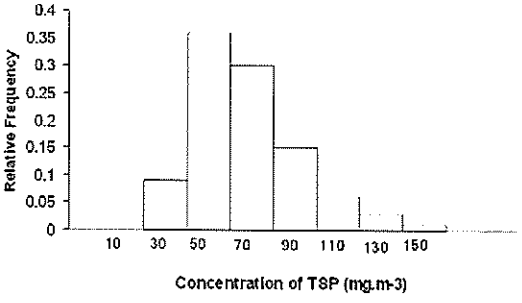

Figure 2. Frequency of TSP concentration in 2004.

meteorological condition for the 2004 has to occur in future, then the figure could give the probabilistic of TSP to occur, i.e. based on Figure 2, less than five percent chances that TSP concentration will occur at the range of 140 – 150 mg.m^{-3} subjected to similar meteorological condition to 2004.

Cumulative frequency curve

Based on the frequency table and histogram in Table 2 and Figure 2, apparent method of estimation could be constructed are shown in the following Table 3 and Figure 3. The cumulative frequency table could read the probability values based on the number of observations less than a given value. For example, to find the probability of TSP concentration to occur which is less than 100 mg.m^{-3}; the closest answer would be at the probability of 95%. Alternatively, the probability could be read up to the curve at the point of x-axis = 100, gives an across value of 0.90 at y-axis. It could be used the other way around, for the probability of certain event of TSP concentration could take place, i.e. there would be 35% chances for Petaling Jaya to receive TSP lower than 36 mg.m^{-3}.

Table 3. Cumulative frequency table for TSP in 2004.

TSP Concentration (mg.m^{-3})	Cumulative frequency	Relative cumulative frequency
Under 20	0	0
Under 40	32	0.09
Under 60	162	0.45
Under 80	271	0.75
Under 100	324	0.90
Under 120	333	0.96
Under 140	336	0.99
Under 160	336	1.00

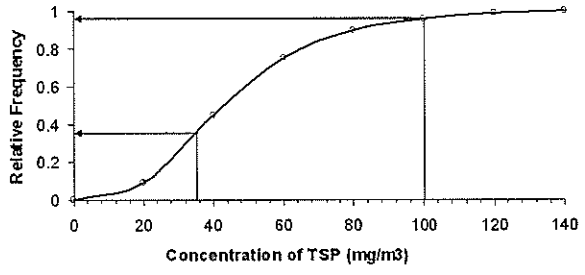

Figure 3. Cumulative frequency distribution curve of TSP in 2004.

Data distribution

The histogram in Figure 2 represents the distribution of overall data in 2004. Further statistical analysis by plotting the relative frequency against the concentration of TSP as shown in Figure 4 enable the determination of data distribution characteristics referring to central location, dispersion and skewness.

As shown in Figure 4, the determination whether the TSP distribution curve could be considered as normal distribution curve is obscured. The central location has been shifted to the left, and it is also slightly skewed to the left. Thus, it is desirable to transform the data in some way so that a symmetrical curve resembling the normal curve results, as the current data could not be considered as normally distributed. One of the ways to derive a symmetrical distribution from a skewed distribution is by transforming the existing data in terms of logarithms. The transformed data would go through the same statistical analysis, which is by setting the interval class and listing in the form of frequency of occurrence. This transformation by logarithm and other statistical work for the frequency analysis are shown in Table 4.

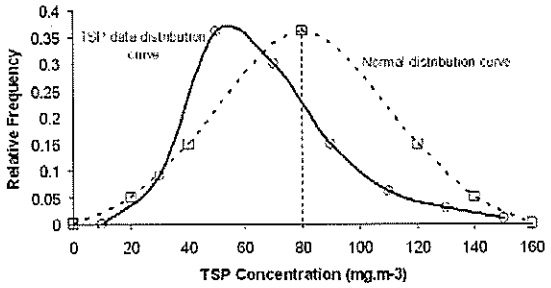

Figure 4. Comparison of relative frequency distribution curve for TSP concentration in 2004 to normal distribution curve.

Table 4. Logarithmic frequency table for TSP concentration in 2004.

Class interval	Frequency of occurrence	Cumulative frequency	Relative cumulative frequency
1.4-1.5	8	8	0.022
1.5-1.6	24	32	0.089
1.6-1.7	62	94	0.261
1.7-1.8	90	184	0.511
1.8-1.9	87	271	0.753
1.9-2.0	56	327	0.908
2.0-2.1	25	352	0.978
2.1-2.2	7	359	0.997
2.2-2.3	1	360	1.000

Probability graph

Probability graph method uses the analysis of cumulative frequency. This is a rough test that can be used to determine whether the arithmetic or logarithmic scale best approximates a normal distribution. Figure 5 shows the plot for cumulative distribution curve of both non-transformed data and transformed data. The plot shows that logarithmic scale yields better fit, as it is more nearly a straight line compared to ordinary scale. However, the probability graph still could not suggest that the central tendency for daily concentration of TSP in 2004 should be represented by a geometric mean, rather than an arithmetic mean. If it should be represented by geometric mean, the probability graph should give a linear graph for the transformed data [5]. Therefore the analysis was further carried out with the calculation of geometric mean. Eq. (3) gives the value for the geometric mean for the concentration of TSP at 63.7 mg.m^{-3}. Eq. (3) is the simplification of Eq. (2). Meanwhile, the standard geometric deviation can be can calculated with Eq. (4) and gives a homogenous standard deviation, equivalent to 1.4 mg.m^{-3}. Based on the standard geometric deviation, the value does not represent the overall TSP data distribution. Figure 4 shows a typical 68.27% of data points should lie within the range of average $\pm$ standard deviation. Therefore standard arithmetic deviation is acceptable compared to standard geometric deviation. The given value for standard geometric deviation does not represent the typical range of probability for standard deviation.

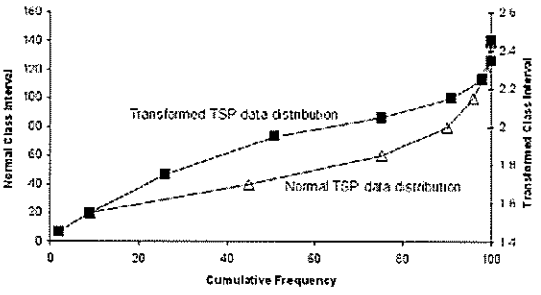

Figure 5. Cumulative distribution curve for normal data against transformed data TSP concentration in 2004.

$$Log_{10}\bar{X} = \frac{1}{n}\Sigma Log_{10}X_i \qquad (3)$$

$$s_g = anti\log\left[\frac{\Sigma(\log X_i)^2 - \frac{(\Sigma \log X_i)^2}{n}}{n-1}\right]^{1/2} \qquad (4)$$

s_g = standard geometric deviation, X_i = i^{th} *measurement*, n = total number of sample.

CONCLUSION

Calculation of the average for annual TSP concentration based on the arithmetic mean should be further analysed with statistical analysis. This is to fulfill data quality assessment prior to the reporting of the ambient air quality monitoring. This study has shown that TSP concentration in 2004 at Petaling Jaya has given a wide range of data distribution and some of the data were clustered at several concentrations. Data distribution ranging from 20 to 140 mg.m^{-3} and clustered at the range of 50 to 90 mg.m^{-3}. These groups of clustered data show similar range of the monthly average, which were also between 50 and 90 mg.m^{-3}. TSP data distribution indicates that they are not normally distributed. However, the probability graph method falls short to show that a geometric mean is more appropriate to represent the measurement of central tendency for the data. Further statistical analysis with the calculation of geometric mean, gives an average for TSP concentration in 2004 of 63.7 $\pm$ 1.4 mg.m^{-3} whereas the arithmetic mean gives an average of 67.9 $\pm$ 24 mg.m^{-3}. Relatively low value for the standard geometric deviation deems to show that the data was homogenous and the deviation values did not fall in the typical probability range. Therefore, the arithmetic mean should be used to report the annual average of TSP concentration, instead of geometric mean. Range of TSP concentration can be predicted if similar meteorological condition has to occur based on the histogram of frequency. Apparent method of estimations could be carried out with the cumulative frequency data.

Acknowledgment – This work has been adapted from the recommendation of US-EPA 1998 [2] for data quality management.

REFERENCES

1. DOE (Department of Environment) (2004) *Malaysia Environmental Quality Report 2003*, Kuala Lumpur, Malaysia: pp. 6–64.
2. US-EPA (1998) *Guidance for Data Quality Management, Practical Methods of Data Analysis.* EPA QA/G-9, EPA/600/R-96/084. Environmental Protection Agency, United States of America.
3. US-EPA (1997) *National ambient air quality standards for particulate matter—final rule*. Federal Register 62, pp. 38652–38752.
4. Wilson W.E., Chow J.C., Claiborn C., Fusheng W., Engelbrecht J. and Watson J.G. (2002) Monitoring of particulate matter outdoors. *Chemosphere* **49**: 1009–1043.
5. Wheater C.P. and Cook P.A. (2000) *Using Statistics to Understand the Environment*. Routledge (Taylor and Francis Group), London, UK: pp. 25–49.
6. Quiterio S.L., da Silva C.R.S., Arbilla G. and Escaleira V. (2004) Metals in airborne particulate matter in the industrial district of Santa Cruz, Rio de Janeiro, in an annual period. *Atmospheric Environment* **38**: 321–331

Journal of Science and Technology in the Tropics (2005) **1**: 147-155

A micro-scale wastewater treatment system for domestic effluents

Law Puong Ling, Oon Yin Wee and Ngu Lock Hei
Department of Civil Engineering, Universiti Malaysia Sarawak, 94300 Kota Samarahan
(e-mail: puonglaw@feng.unimas.my)

Received 7 July 2005; 17 November 2005

ABSTRACT A micro-scale wastewater treatment system consists of (1) a mixed flow (vertical flow alternated with cross flow) filter, and (2) a *Pistia stratiotes*-based free surface water (FSW) wetland (FSW) system filled with *Pistia stratiotes* operating in series was recently developed. Field tests were carried out to determine the efficiencies of the system in removal of organic matters such as biochemical oxygen demand (BOD), ammonia-nitrogen (NH_3-N), suspended solids (SS), and nutrients such as nitrogen (N), phosphorous (P), and potassium (K) from wastewaters. From this study, it was found that the mixed flow filter was capable of reducing approximately 33.2% in BOD, 59.9% in NH_3-N, 51.6% in N, 14.7% in P, 20.1% in K, 24.4% in turbidity level; and the *Pistia stratiotes*-based FSW wetland system was capable of removing approximately 30.8% in BOD, 30.3% in NH_3-N, 40.9% in N, 42.2% in P, 53.2% in K, and 29.7% in reduction in turbidity level. When the mixed flow filter and *Pistia stratiotes*-based FSW wetland system operated in series, the removal efficiencies of the system were approximately 64.1% for BOD, 90.2% for NH_3-N, 92.5% for N, 56.9% for P, 73.3% for K, and 54.1% for turbidity. Experimental data also showed that daily uptake rates or removal rates (mg/kg-day) of organics and nutrients by per kilogram of dry *Pistia stratiotes* were approximately 1,460 mg for BOD, 942 mg for NH_3-N, 1,134 mg for N, 1,361 mg for P, and 5,884 mg for K.

Keywords Micro-scale – performance tests – *Pistia stratiotes* – organics – nutrients

INTRODUCTION

Aerobic wastewater treatment system utilizes microorganisms for removal of suspended and dissolved organic matters from wastewaters, and the nutrients in a free surface water (FWS) wetland could be assimilated by floating aquatic plants such as Pistia stratiotes and Eichhornia Crassipes growing on it [1]. The traditional trickling filter consists of a bed of a highly permeable medium to which microorganisms are attached and through which wastewater is percolated or trickled. The filter media usually consist of either rock or a variety of plastic packing materials. Rock filter beds are usually circular, and wastewaters are distributed over the top of the bed by a rotary distributor [2]. As wastewater trickles downwards over the slime layer, organic matters and dissolved oxygen are extracted, metabolic end products such as carbon dioxide are released, and organic content would decrease to the point where microorganisms in the lower zone are in a state of starvation (Fig. 1). Thus, majority of BOD is extracted from the wastewater after passing through the filter media [2].

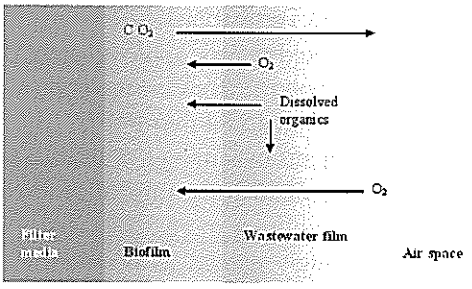

Figure 1. Biological activity of attached-growth biological microorganism [2].

These bacterial populations would carry out nitrification process sequentially and oxidize ammonium growing on the slime layer to nitrate with intermediate formation of nitrite carried out by *nitrosomanas* and *nitrobacter*. The two steps in nitrification process and their equations are as follows [2]:

(1) Ammonia is oxidized to nitrite (NO_2^-) by *Nitrosomanas* bacteria.

$$2\,NH_4^+ + 3\,O_2 \rightarrow 2\,NO_2^- + 4\,H^+ + 2\,H_2O \quad (1)$$

(2) The nitrite is converted to nitrate (NO_3^-) by *Nitrobacter* bacteria.

$$2\,NO_2^- + O_2 \rightarrow 2\,NO_3^- \quad (2)$$

Recently, rock trickling filters are continuously being upgraded and rehabilitated with plastic sheet media and synthetic media to replace the use of stone. As compared to rock, plastic sheet media has 2 to 3 times higher in specific surface area that provides proportionally more area for biomass attachment [3,4]. Thus, void volume would be substantially increased that improves ventilation and hydraulic loading capacity. At present, primary types of plastic flow media widely used include cross flow media, vertical flow media and mixed flow media. In cross flow media design, down-flowing liquid is split at each cross point creating more redistribution points, and its major drawbacks are its inferior bio-solids flushing action and biomass fouling problem. Vertical flow media has vertical channels with cross flow at module interface by making use of its limited inner surface area of the channels that results in low specific surface area available for biomass attachment and low organic loading. Commercially available mixed media takes advantage of its uniformity in distribution of wastewater over the surface of the filter by alternating cross flow and vertical flow media layers [5]. Additionally, mixed media filter reduces excessive biomass build up of shearing materials from vertical layers. This medium type and arrangement could provide approximately 16% more surface area per volume from the recommended plastic cross flow media of 15.84 m^2/m^3 [6].

Floating aquatic plants hyacinth grow profusely in the tropics and the use of such floating vegetation as one of the functional units in municipal wastewater treatment has increasingly gained its potential [1,7]. For instance, duckweed-based wastewater treatment has been implemented by the city of San Diego, USA to produce a treated effluent attaining quality standards that would be expected from advanced secondary treatment processes [1]. Floating aquatic plants could potentially be used in both tertiary treatment systems for the removal of nutrients, and in integrated secondary and tertiary treatment systems for removal of both organics and nutrients [1,5]. Floating aquatic plant-based system is a free surface water (FSW) wetland system typically formed by shallow channels or basins where the water surface is open to the atmosphere and a suitable medium exists to support the growth of emergent or submerged aquatic plants [2,5]. Wastewater treatment takes place as the hyacinth assimilate nutrients from the effluents [1]. Recently, two floating aquatic "macrophyte" plants have been used in wastewater treatment including *Eichhornia crassipes* (a type of water hyacinth) and *Lemnacea spirodella* (duckweed) [5]. As the influents move along the system, organics are biodegraded either aerobically or anaerobically. Nutrients are reduced through a variety of biological, physical and chemical processes [1,7]. It is believed that two major mechanisms for ammonia reduction in floating aquatic plant systems are bacterial nitrification and plant uptake [8].

SYSTEM DESIGN AND DEVELOPMENT

This research involves the development and field tests of a two-stage micro-scale wastewater treatment system for small volume domestic wastewaters loaded with SS, BOD, NH_3-N, and nutrients. As illustrated in Figure 2, the system consists of (1) a plastic medium mixed flow trickling filter, and (2) *Pista stratiotes*-based FWS wetland system operating in series.

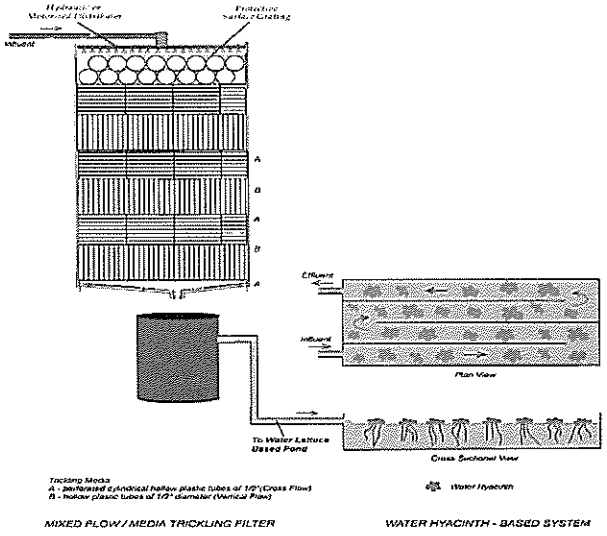

Figure 2. Schematic diagram of waste-water treatment system consisting of (a) a mixed flow filter, and (b) *Pistia stratiotes*-based FSW system operating in series.

Mixed flow trickling filter

In this research, a micro-scale trickling filter was designed and developed from conventional design with the differences in its filter medium design characteristics and media arrangements. As shown in Figure 3, the major components of the system consists of (1) circular tower for filter medium storage, (2) hydraulic nozzle distributor equipped with high pressure hydraulic pump, and (3) filter medium consists of hollow perforated plastic tubes arranged in alternating cross and vertical parallel manners. The first layer of the filter makes up of 40 mm diameter spherical plastic (Fig. 4a,b) to achieve better uniformity of water distribution for the following layer of plastic tube medium. The hollow tubular structure as filter medium enables the usage of the inner surface area of the hollow tubes and thus providing higher specific surface area. Additionally, the alternating vertical and cross flows would raise the void spaces to increase the biological growth for waste treatment (Fig. 5a,b). The details of specific surface area and percent void space for filter fill or selected media are shown in Table 1.

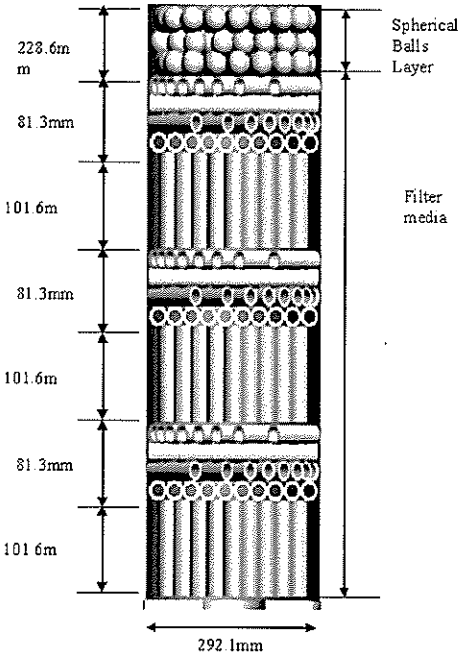

Figure 3. Mixed flow trickling filter filled with plastic medium.

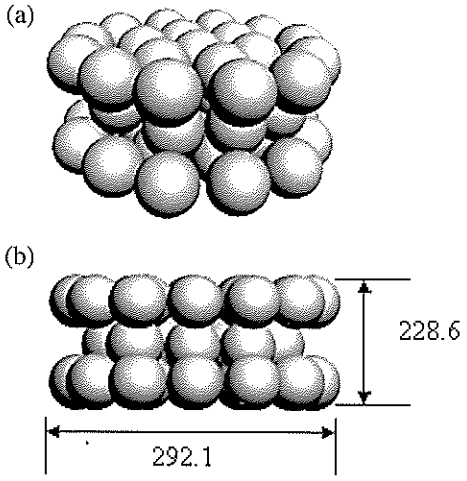

Figure 4. Top layer of trickling filter. (a) perspective view; (b) side view.

Table 1. Specific surface area vs percent void space.

Volume	0.05 m^3 (1.84 ft^3)
Specific surface area	190.08 m^2/m^3 (57.50 ft^2/ft^3)
Void space, %	55.60

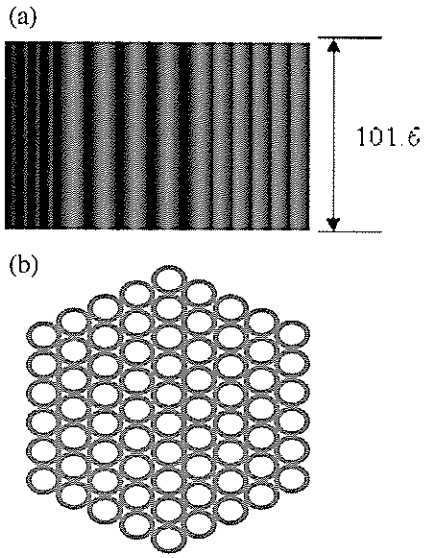

Figure 5. Filter vertical flow media. (a) side view; (b) top view.

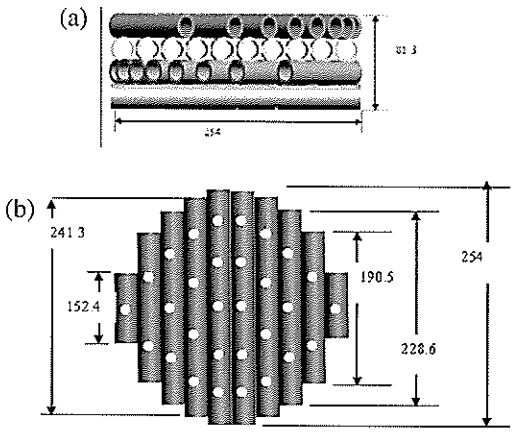

Figure 6. Filter cross flow media. (a) side view; (b) top view.

We describe here a simple, inexpensive and easy-to-operate human calorimeter that is operational in the nutrition laboratory at Universiti Kebangsaan Malaysia.

DESIGN AND METHODS

An ordinary room (3.09 m long x 2.00 m wide x 2.99 m high) with a glass window (65 cm x 75 cm) located on the third floor of the Nutrition laboratory was converted into an open-circuit indirect calorimeter (Fig. 1). The walls and the ceiling are made of concrete brick

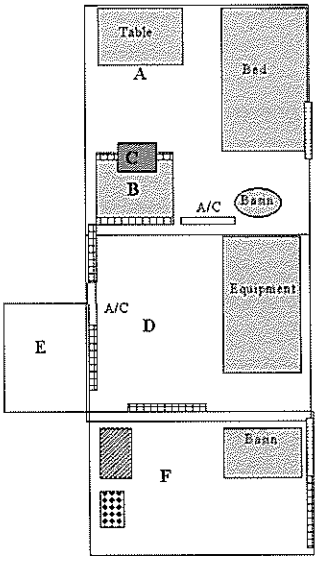

Figure 1. Calorimeter Unit, Universiti Kebangsaan Malaysia, Kuala Lumpur, Malaysia. A = Calorimeter chamber; B = Twin door "air-lock"; C = Food hatch; D = Equipment room; E = Toilet; F = Kitchen; A/C = Air conditioning unit; ▦ = Door; ▭ = Window; ▨ = Refrigerator; ▦ = Microwave oven.

coated with plaster, and the floor is made of cement and covered with polyvinyl chloride (PVC) carpet. The putty-sealed and tinted glass window is located as such to give the subject an outside view of a playing field. Two 37 mm-thick wooden doors were built to create an air-lock twin door system. Both doors were made air tight with draught-excluder rubber tape. The inner door was fitted with a double window hatch (41 cm wide x 30 cm long x 21 cm high) to allow food and drinks to be passed into and out of the calorimeter. Only one of the hatch windows is opened at any one time, hence a negligible volume of air can pass into or out of the chamber. The room is furnished with a table, a resting arm-chair, a bed, a wash basin with direct water supply, a telephone, a television, a video tape player, and a radio cassette player. There is enough space for a bicycle ergometer and an exercise box for step tests. The construction of the calorimeter and its calibration and standardization tests were replicated with some modifications from previous successful operational calorimeters [3,4]. A schematic representation of the calorimeter is shown in Figure 2.

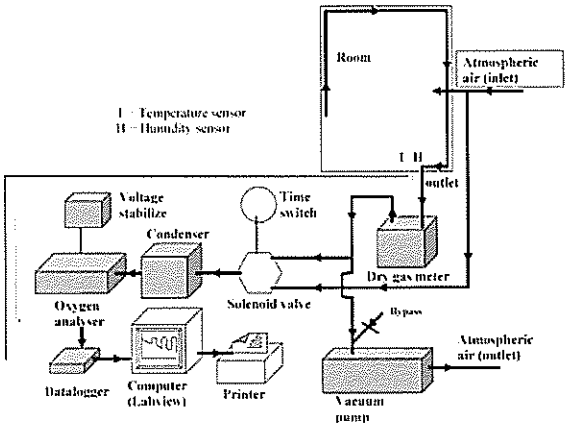

Figure 2. A schematic representation of room converted into a calorimeter for measuring daily energy expenditure in humans.

Ventilation

The room is ventilated by drawing out air from the calorimeter. Three levels of PVC pipes (internal diameter 2 cm) with small holes (2 mm) at 15 cm apart, are placed around the walls at the upper, center and floor level of the chamber. The pipes are then linked to a single exit point drilled through the chamber wall into the equipment room. The chamber is sufficiently sealed to ensure that air leaves only through the single outlet. By means of a voltage-controlled RV3 Rotary Vane Pump (Edwards High Vacuum International, UK) with maximum capacity of 120 L/min, air is continuously drawn out of the chamber. The negative pressure thus generated allows outside atmospheric air to enter the chamber through a small one-way valve inlet in the wall thus replacing the volume of air being drawn out. The system operates on the open-circuit principle.

The volume of air drawn from the calorimeter (exhaust air) is continuously measured by a dry gas meter (Harvard Apparatus, UK) before being expelled into an open space outside the building. All the necessary precautions are taken to ensure that the composition of the ambient air surrounding the

The filter medium tubes measure 24.13 mm on outer diameter, and 21.59 mm on inner diameter are alternatively placed in a plastic circular basin of 292.1 mm in diameter and 777.24 mm in height as illustrated in Figure 5a and Figure 5b. As shown in Figure 6a and Figure 6b, the cross flow perforated tubes are arranged in four sub-layers at 45° between each other to enhance oxygen transfer and wetting rates inside the filter. The perforated holes in cross flow media layer tubes are approximately 7.62 mm in diameter at approximately 65 mm apart on top and bottom of the tubes. For the vertical flow media layers, each layer consists of 121 units of 101.60 mm vertical tubes.

This system is equipped with a fixed nozzle distributor controlled by a valve to permit a desired flow rate at approximately 185 liters/day (L/day). Flow is applied to the trickling filter through a hydraulic pump before distributed by the nozzle. Because of the hydraulic gradient factor, a 6-metre pressure head hydraulic pump is selected for this purpose to provide uniform distribution of wastewater on top of trickling filter. The under drain collects the filtrate and solids, and serves as a source of air for the microorganisms to maintain aerobic conditions in the filter. Sufficient air is being provided to the filter medium by natural draft and wind forces through numerous of ventilation ports located at the bottom of the filter. Effluents from the filter are channeled to a clarifier whereby solid particles would be settled out before overflowing to the *Pistia stratiotes*-based FSW wetland system.

Pistia stratiotes-based FSW wetland system

The *Pistia stratiotes*-based FSW wetland system consists of a plastic basin with approximately 250 liters in volume (length = 1220 mm, width = 910 mm, and depth = 230 mm as illustrated in Figure 7a. The basin is partitioned into four compartments to enhance the uniformity flow throughout the basin (Fig. 7b) and two holes are provided for influents from trickling filter and final effluents (Fig. 7c). Operational parameters such as surface overflow rate (SOR), detention time (DT), and horizontal velocity (V_h) are shown in Table 2.

The proposed *Pistia stratiotes*-based FSW wetland system is filled with a type of floating tropical aquatic plant called "*Pistia stratiotes*" (Fig. 8). *Pistia stratiotes* is characterized by numerous number of suspended roots of over one foot long (>30cm), and the above water portion consisting of leaves are traditionally used as animal feeds frequently practiced by local farmers in the tropics. *Pistia stratiotes* is a free-floating aquatic

Table 2. *Pistia stratiotes*-based system: SOR, DT, V_h.

Surface overflow rate (SOR)	165.70 liters/day.m^2 (15.4 L/day.ft^2)
Detention time (DT)	24 hours (1.0 day)
Horizontal velocity (V_h)	5.15(10^{-2}) m/hr (0.17 ft/hr)

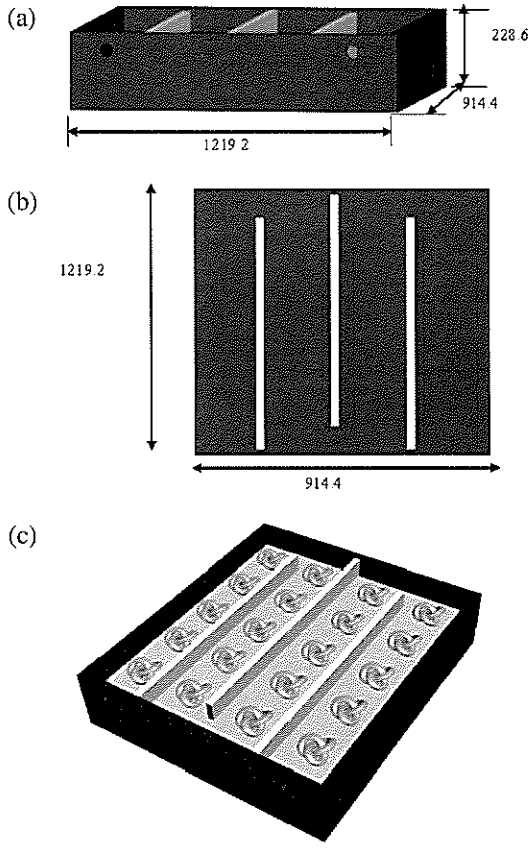

Figure 7. *Pistia-stratiotes*-based system. (a) basin dimensions; (b) top view; (c) basin filled with *Pistia stratiotes*.

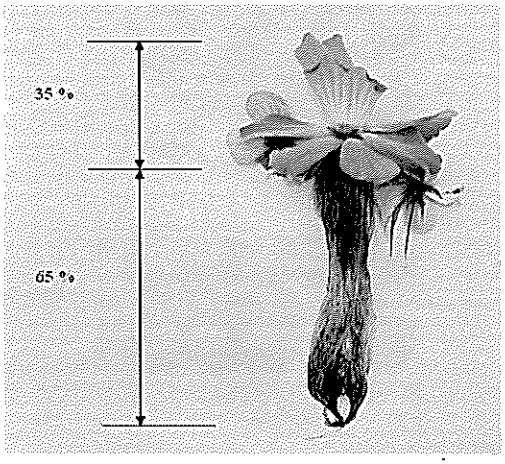

Figure 8. *Pistia stratiotes* and leave-to-root ratio.

plant commonly used as an ornamental plant in water gardens. This tropical plant produces attractive rosettes of bright green, wedged shaped, overlapping, deeply veined velvety leaves that grow up to 10 inches (25.4 cm) long and 4 inches (10.16 cm) wide. This species of floating aquatic plant grows well outdoors all year-around in the tropics with water pH between 6.2 and 7.2 [9,10]. *Pistia stratiotes*, because of it floating capabilities, is believed to have filtration capability for ponds with high nitrogen and phosphate levels. This type of water plant grows vegetatively by production of daughter plants that allows intertwining of the plants, thereby forming large contiguous mats of floating vegetation [9,10]. These mats are one of the most important growth characteristics contributing to the removal of nutrients from wastewaters. Details on system design outlining the dimensions, settling basin and *Pistia stratiotes*-based system are summarized in Table 3.

Table 3. Dimensions of trickling filter, settling basin and *Pistia stratiotes*-based system.

Circular trickling filter			
(a) Storage basin			
	Flow rate	=	185 L/day
	Diameter	=	292.10 mm
	Height	=	777.20 mm
	Volume	=	52.10 liters
(b) Spherical balls	Diameter	=	40 mm
	Number of units	=	85
(c) Cylindrical tubes			
(i) Cross flow			
· Solid surface			
	Tube internal diameter	=	21.59 mm
	Tube external diameter	=	24.13 mm
	Length of tube	=	15.24 - 25.40 mm
	Number of sub-layers	=	4
	Number of layers	=	3
· Hole			
	Internal diameter	=	7.62 mm
	External diameter	=	7.62 mm
	Number of units / layer	=	30
	Number of sub-layers	=	4
	Number of layers	=	3
(ii)Vertical Flow			
·Solid surface			
	Tube internal diameter	=	21.59 mm
	Tube external diameter	=	24.13 mm
	Length of tube	=	101.60 mm
	Number of units		121
	Number of layers	=	3
***Pistia stratiotes*-based (FWS) wetland system**			
a) Tank/Basin			
	Flow Rate	=	185 L/day
	Length	=	1219.20 mm
	Width	=	914.40 mm
	Height	=	228.60 mm
	Water level	=	190.50 mm
	Soil bed level	=	25.40 mm
	Actual water level	=	165.10 mm
	Volume	=	250 liters
b) Plant	*Pistia stratiotes*	=	1.69 kg

MATERIALS AND EXPERIMENTAL PROCEDURE

Influent wastewater source

Figure 9 schematically illustrates experimental setup details, process flow and wastewater sampling points. In this study, raw wastewater samples were collected from one of the facultative ponds at Universiti Malaysia Sarawak (UNIMAS) campus. The pond water contains a mixture of septic tank effluents and wastewaters generated from food courts, pantries, laboratories, and storm waters that contain a relatively high amount of BOD, NH_3-N, SS, N, P, and K.

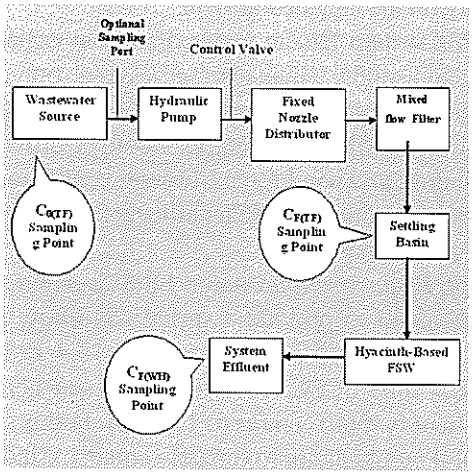

Figure 9. Schematic diagram of process flow and water sampling points.

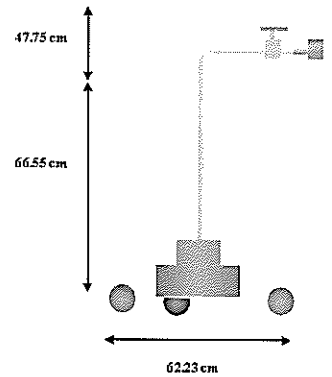

Figure 10. Hydraulic pump details.

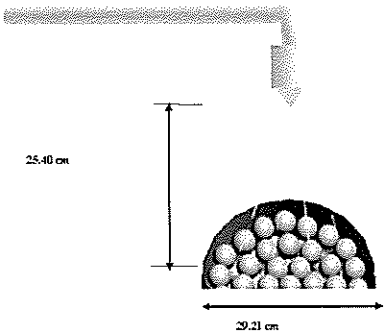

Figure 11. Fixed nozzle distributor.

Raw wastewaters were pumped to the mixed flow filter by a hydraulic pump (Fig. 10) and applied onto the top layer of the filter by a fixed nozzle distributor (Fig. 11). Because of the hydraulic gradient factor, a 6-metre pressure head submersible hydraulic pump was chosen for this experimental work. Flow rate through the fixed nozzle distributor was controlled by a valve to permit a desired flow at approximately 185 liters/day (L/day) so as to minimize the impact of shear velocity on the attached growth.

This system has an under drain that collects the filtrate and solids, which also serves as a source of air for the microorganisms to maintain aerobic conditions in the filter. Sufficient air supply would be provided by natural draft and wind forces through ventilation ports at the bottom of the filter. Filter effluents were gravitated to the settling basin.

The *Pistia stratiotes*-based FSW wetland system was designed to provide a surface overflow rate of approximately 167.70 liters/day.m^2 (15.4 L/day.ft^2), detention time of 24 hours (1.0 day), and horizontal velocity of 5.15(10^{-3}) m/hr (0.17 ft/hr). In this study, a total of 47 units of approximately equally sized *Pistia stratiotes* were used with the total plant mass of 1.69 kg. This FSW wetland system was placed outdoor sheltered by a transparent plastic sheet (Fig. 12). *Pistia stratiotes* is characterized by having high number of suspended roots of over one foot long and longer roots are believed to have higher uptake capacity.

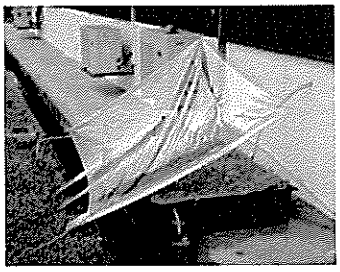

Figure 12. *Pistia stratiotes*-based FSW wetland system.

Sampling and analysis

In this study, raw wastewater samples abbreviated as $C_{o(TF)}$ (trickling filter influent) were collected at location prior to influent to the filter. A valve is located between the hydraulic pump and nozzle distributor to regulate flow rate and to provide uniform spray onto the top layer of the filter. The wastewaters would trickle down from the top layer to the bottom by gravitation and collected in the settling basin. Samples were collected from the settling tank and abbreviated as $C_{F(TF)}$ (filter effluent). Filter effluents ($C_{F(TF)}$) were then channeled to the hyacinth-based FSW wetland system as influent. Samples were then collected from the effluent of the *Pistia stratiotes*-based FSW wetland system abbreviated as $C_{F(WH)}$. Temperatures, pH values, and turbidity at the sampling points were also monitored regularly and recorded throughout this experimental period. The experimental work of this research study was carried out for a period of 30 days. Trail run period extended from 2nd to 10th of February 2005 to make sure that stabilized conditions were attained. Actual sampling and analysis started on 11th February 2005 and ended on 2nd March 2005, and a total of 9 batches of data were collected at the individual points and analyzed. Samples drawn at individual points as $C_{o(TF)}$, $C_{F(TF)}$ and $C_{F(WH)}$ (Figure 9) were then analyzed at Environmental Engineering Laboratory, Department of Civil Engineering, Univeristi Malaysia Sarawak (UNIMAS). Some of the major analysis equipments and methods used in this study included HACH DR/4000 Spectrophotometer (8038, 8075, 8048 and 8237; 2), Hanna Dissolved Oxygen (DO) meter (APHA 5210B), Atomic Absorption (AA) Spectrophotometer (APHA 3500 KB).

RESULTS AND DISCUSSION

Figure 13 illustrates the BOD removal efficiencies of the mixed flow filter and *Pistia stratiotes*-based FSW wetland system by observing the amount of reduction in BOD levels during the experimental period. As shown, the filter demonstrated a very consistent removal rate (%) regardless of influent concentrations with an average removal efficiency of approximately 33.2%. Similarly, the *Pistia stratiotes*-based FSW wetland system recorded a consistent removal rate with an average of approximately 30.8%. It is shown that the performances of the two components of the system were quite close with a deviation of approximately 2.4%. The combined BOD removal rate of the two

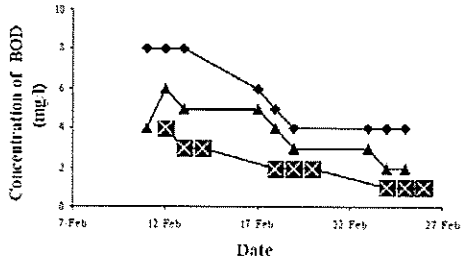

Figure 13. $C_{0(TF)}$, $C_{F(TF)}$ and $C_{F(WH)}$ BOD levels vs time. ♦ influent of trickling filter; ▲ effluent of trickling filter/influent of *Pistia stratiotes* system; ■ effluent of *Pistia stratiotes* system.

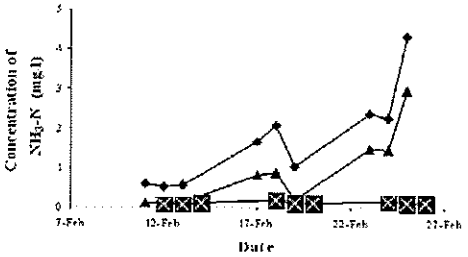

Figure 14. $C_{0(TF)}$, $C_{F(TF)}$ and $C_{F(WH)}$ ammoniacal nitrogen levels vs time. ♦ influent of trickling filter; ▲ effluent of trickling filter/influent of *Pistia stratiotes* system; ■ effluent of *Pistia stratipotes* system.

components, i.e., the mixed flow filter and *Pistia stratiotes*-based system operated in series was approximately 64.0%.

Figure 14 shows the observed removal efficiencies of NH_3-N by trickling filter and *Pistia stratiotes*-based FSW wetland system from wastewaters during the study period. The average NH_3-N removal efficiency achieved by the filter recorded 59.9% and the reduction rate (mg/L) was rather consistent throughout the experimental period regardless of influent NH_3-N levels. As shown in Figure 6, *Pistia stratiotes*-based FSW wetland system demonstrated a similar consistent achievable effluent level to less than 2mg/L regardless of the influent NH_3-N levels, which indicates that *Pistia stratiotes* has an extremely high uptake capacity of NH_3-N. As observed, it was demonstrated that NH_3-N levels would substantially be reduced by both the mixed flow filter and *Pistia stratiotes*-based system. When the mixed flow filter and *Pistia stratiotes*-based system were to operate in series, the overall achievable removal efficiency of the system could be as high as 90.2%.

Plots of total nitrogen (N) measured at the influents and effluents of the filter and hyacinth-based system with respect to time are illustrated in Figure 15. The average amount of reduction in total nitrogen recorded between $C_{0(TF)}$ and $C_{F(TF)}$ was approximately 51.6% by mixed flow filter, and between $C_{F(TF)}$ and $C_{F(WH)}$ indicated a 40.9% reduction by *Pistia stratiotes*-based system. When the filter and *Pistia stratiotes*-based system were to operate in series, the overall average total nitrogen removal efficiency could be as high as 92.5%. When expressed in amount of N removed from per liter (mg/L) of wastewater, the mixed flow filter attained an average of 0.88 mg/L while the *Pistia stratiotes*-based system achieved approximately 0.95 mg/L. An analysis of the plots in Figure 14 and Figure 15 show that the patterns of total nitrogen reduction in the wastewater samples observed were similar to NH_3-N. This could be due to the direct relationship of NH_3-N and total nitrogen because NH_3-N molecules are formed by the nitrogen atoms after combining with hydrogen atoms to achieve stabilization. In the nitrogen cycle, the NH_3-N would be transformed to nitrite and nitrate or backward through nitrification or denitrification processes. Thus, a reduction in NH_3-N would give a lower total nitrogen level.

Figure 16 shows the differences in phosphorous (P) levels between $C_{0(TF)}$ and $C_{F(TF)}$, and between $C_{F(TF)}$ and $C_{F(WH)}$. The amount of P reduced by the mixed filter was approximately 14.7%, while the *Pistia stratiotes*-based FSW wetland system achieved 42.2%. This indicates that the removal of P by *Pistia stratiotes*-based system was 27.5% higher that the mixed flow filter.

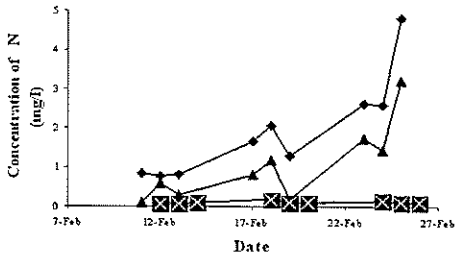

Figure 15. $C_{0(TF)}$, $C_{F(TF)}$ and $C_{F(WH)}$ total nitrogen levels vs time. ♦ influent of trickling water; ▲ effluent of trickling filter/influent of *Pistia stratiotes* system; ■ effluent of *Pistia stratiotes* system.

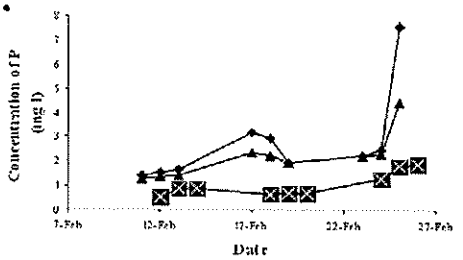

Figure 16. $C_{0(TF)}$, $C_{F(TF)}$ and $C_{F(WH)}$ total phosphorus levels vs time. ♦ influent of trickling water; ▲ effluent of trickling filter/influent of *Pistia stratiotes* system; ■ effluent of *Pistia stratiotes* system.

When the performances are expressed in mg/L of P reduced in the wastewaters, the observed data collected during experimental period demonstrated that, the filter could achieve an average of 0.6 mg/L reduction of P while the *Pistia stratiotes*-based FSW system achieved an average of 1.14 mg/L. When the filter and *Pistia stratiotes*-based system operated in series, the combined overall achievable removal efficiency of the system was approximately 56.9%.

In this experimental work, the potassium (K) levels in the raw wastewater influents of the trickling filter recorded were in the range of 3.14 and 18.86 mg/L. As illustrated in Figure 17, the trickling filter was capable of removing an average of approximately 20.1% and *Pistia stratiotes*-based FSW wetland system attained an average of 53.2% of K from wastewaters, which indicates that the K uptake rate of *Prista stratiotes* is approximately 33.1% higher than the mixed flow filter. It was also demonstrated that when the filter and *Pistia stratiotes*-based FSW wetland system were to operate in series, the combined overall system removal efficiency system could achieve approximately 73.3%.

In this study, effluent turbidity levels are measured in Nephelometry Turbidity Unit (NTU) for all water samples collected. The turbidity readings showed a decreasing trend as the wastewater moved through the

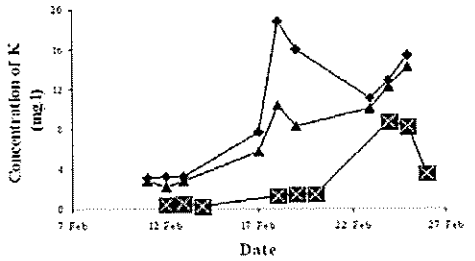

Figure 17. $C_{0(TF)}$, $C_{F(TF)}$ and $C_{F(WH)}$ total potassium levels vs time. ♦ influent of trickling water; ▲ effluent of trickling filter/influent of *Pistia stratiotes* system; ■ effluent of *Pistia stratiotes* system.

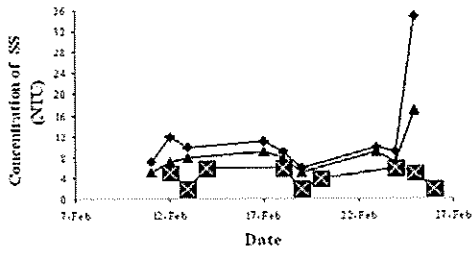

Figure 18. $C_{0(TF)}$, $C_{F(TF)}$ and $C_{F(WH)}$ turbidity levels vs time. ♦ influent of trickling water; ▲ effluent of trickling filter/influent of *Pistia stratiotes* system; ■ effluent of *Pistia stratiotes* system.

treatment system. In Figure 18, it is shown that the *Pistia stratiotes*-based FSW wetland system was capable of bringing down the average turbidity level to about 4 NTU, while the trickling filter was capable of reducing average turbidity level to approximately 8 NTU. The average reduction in turbidity levels were approximately 24.4% achieved by the mixed flow trickling filter, 29.7% by *Pistia stratiotes*-based system, and 54.1% when the filter and *Pistia stratiotes*-based system operated in series.

As shown in Table 4, the observed average removal efficiencies of trickling filter were 33.2% for BOD, 59.9% for ammoniacal nitrogen, 51.6% for total nitrogen, 14.7% for phosphorus, 20.1% for potassium, and 24.4% reduction on turbidity levels. The *Pistia stratiotes*-based FSW wetland system demonstrated to be capable of removing an average of 30.8% of BOD, 30.3% of ammoniacal-nitrogen, 40.9% of nitrogen, 42.2% of phosphorus, 53.2% of potassium, and 29.7% reduction on turbidity levels.

It is found that *Pistia stratiotes*-based FSW wetland system was relatively more efficient than trickling filter in terms of phosphorus and potassium removal, while the trickling filter was relatively more efficient in BOD and total nitrogen removal. When filter and *Pistia stratiotes*-based system were to operate in series, the removal efficiencies (Table 4) were 64.1% for BOD, 90.2% for ammoniacal nitrogen, 92.5% for total nitrogen, 56.9 for phosphorous, 73.3% for potassium, and 54.1% reduction on turbidity levels.

In this research, *Pistia stratiotes* mass increment versus nutrient uptake rates by the hyacinth was studied. Measured field tests data showed that daily uptake rate of organics and nutrients expressed in mg/kg-day, i.e., mg of organics and nutrients removed by one kg of

Table 4. Overall removal efficiencies (%) when trickling filter and *Pistia stratiotes*-based system operated in series.

Parameter	Removal efficiency (%)		
	Trickling filter	*Pistia stratiotes*-based system	Trickling filter & *Pistia stratiotes* - based system operating in series
Biochemical oxygen demand	33.2	30.8	64.0
Ammoniacal nitrogen	59.9	30.3	90.2
Nitrogen	51.6	40.9	92.5
Phosphorus	14.7	42.2	56.9
Potassium	20.1	53.2	73.3
Turbidity	24.4	29.7	54.1

Pistia stratiotes per day were approximately 1,460 mg for BOD, 942 mg for NH_3-N, 1,134 mg for N, 1,361 mg for P, and 5,884 mg for K.

CONCLUSIONS

A two-stage treatment system consisting of a mixed flow filter and *Pistia stratiotes*-based FSW wetland was developed and field tests were carried out to determine system efficiencies in removal of organic matters and nutrients. It is concluded that the removal efficiencies achieved by the mixed flow filter were approximately 33.2% for BOD, 59.9% for NH_3-N, 51.6% for N, 14.7% for P, 20.1% for K, and 24.4% reduction in turbidity level, whilst the *Pistia stratiotes*-based FSW system achieved 30.8% for BOD, 30.3% for NH_3-N, 40.9% for N, 42.2% for P, 53.2% for K, and 29.7%, reduction in turbidity level. The combined overall system removal efficiencies (i.e., mixed flow filter and *Pistia stratiotes*-based system operating in series) were approximately 64.1% for BOD, 90.2% for NH_3-N, 92.5% for N, 56.9% for P, 73.3% for K, and 54.1% reduction on turbidity levels. It is also concluded that daily uptake or removal rates (mg/kg-day) of organics and nutrients by one kg of *Pistia stratiotes* per day were approximately 1,460 mg for BOD, 942 mg for NH_3-N, 1,134 mg for N, 1,361 mg for P, and 5,884 mg for K.

REFERENCES

1. Brix H. and Schierup H. (1989) The use of aquatic Macrophytes in water-pollution control. Ambio, 18(2), 100-107.
2. Tchobangoglous G and Burton F.L. (1991) Wastewater Engineering: Treatment, Disposal, and Reuse, Third Edition. Metcalf & Eddy, Inc., USA.
3. United States Environmental Protection Agency (USEPA), Sept 2000. Wastewater Technology Fact Sheet Trickling Filters, EPA 832-F-00-014, Office of Water, Washington, D.C.
4. United States Environmental Protection Agency (USEPA), Sept 2000. Wastewater Technology Fact Sheet Trickling Filter Nitrification, EPA 832-F-00-015, Office of Water, Washington, D.C.
5. Middlebrooks E.J. (1995) Upgrading pond effluents: An overview. Water, Science & Technology, 31(12), 353-368.
6. Brentwood Industries (2004) Brentwood AccuPac Cross Flow media. Available at URL: http://www.brentw.com/water/crossflow_main.html —> June 2004
7. Mandi L. (1994) Marrakesh wastewater purification experiment using vascular aquatic plants Eichhornia Crassipes and Lemna Gibba. Water, Science & Technology, 29(4), 283-287.
8. Hauser J. R. (1984) Use of wastewater aquatic treatment system for ammonia control and effluent polishing. Research Journal of the Water Pollution Control Federation, 56(3), 219-225.
9. Kumar P. and Garde R.J. (1989) Potentials of water hyacinth for sewage treatment. Research Journal of the Water Pollution Control Federation, 61 (11/12), 1702-1706.
10. Mars R. (2004) Greywater Treatment with Macrophytes, Greywater Reuse Systems. Washington: Midland Business Centre.

Journal of Science and Technology in the Tropics (2005) **1**: 157-163

The commensurately modulated bis(aquachlorotriphenyltin·1, 10-phenanthroline) crystal structure

A. David Rae[1], Kenneth J. Haller[2] and Ng Seik Weng[3]
[1]Research School of Chemistry, Australian National University, Canberra ACT 0200, Australia
[2]School of Chemistry, Suranaree University of Technology, Nakhon Ratchasima 30000, Thailand
[3]Department of Chemistry, University of Malaya, 50603 Kuala Lumpur, Malaysia

Received 31 January 2005; accepted 16 June 2005

Abstract Bis(aquachlorotriphenyltin.1,10-phenanthroline) [$P2_1/n$, a = 21.1053(5), b = 12.2347(3), c = 51.772(2) Å, β = 101.525(2)°; Z = 10] has a diffraction pattern dominated by a set of strong reflections with $2h + l = 5N$. Average intensities for reflections with $2h + l = 5N$, $5N \pm 1$ and $5N \pm 2$ are in the ratio 1.000 : 0.157 : 0.075, the differences between categories being more pronounced at lower θ angles. The structure is a commensurate displacive modulation of an idealized parent structure of $P2_1/c$ symmetry whose unit cell is one-fifth the volume of the $P2_1/n$ cell, the cell axes being given by $a_o = (2a + c)/5$, $b_o = -b$, $c_o = (3a - c)/5$ [*i.e.*, a_o = 11.9814(3), b_o = 12.2347(3), c_o = 17.8875(4) Å; β = 92.418(2)°]. The choice of a global phase for the modulation waves was an essential part of the structure determination as it distinguished between pseudo homometric structure solutions. The structure was refined to R = 0.039 for 3666 reflections.

Keywords Bis(aquachlorotriphenyltin.1,10-phenanthroline) – commensurately modulated – crystal structure

INTRODUCTION

The nature of the hydrogen-bonding interactions in the hydrated complex of triphenyltin chloride with 1,10-phenanthroline, which is the first example of a triorganotin entity that binds indirectly, through the coordinated water molecule, to the potentially bidentate 1,10-phenanthroline heterocycle, is of interest to the understanding of how triorganotin cations bind to nucleic acids. The dimeric complex (Scheme 1) was described in the monoclinic $P2_1/c$ space group [a = 11.9602(7), b = 12.2196(7), c = 17.854(1) Å; β = 92.409(6)°]; the crystal structure could only be refined to R = 0.128, the large discrepancies between observed and calculated structure factors being attributed to "twinning" [1]. The isolation of this complex has led to studies on the 1,10-phenanthroline complexes of other triaryltin halides [2,3]and carboxylates [4-6] as well as on the triphenyltin complexes with other bidentate *N*-heterocycles [7-10]. The differing types of hydrogen bonds found in these 'outer-sphere coordination' complexes prompted a re-investigation of the parent complex, but we could not find the $P2_1/c$ cell although we were able to find a $P2_1/n$ cell that was five times as large and whose b-axis was identical to that of the reported cell. This observation was reproduced using crystals prepared in separate syntheses and using different diffractometers. *SHELXS*-97 [11] gave an initial solution for this 13,000 Å^3 cell, but the refinement of the model with *SHELXL*-97 [11] required an excessive number of constraints and was later found to be incorrect as to its choice of global phase. We have refined the modulated structure by using the constrained refinement program *RAELS*00 [12], and we discuss here the implications of its commensurate nature.

Journal of Science and Technology in the Tropics (2005) 1: 157-163

EXPERIMENTAL

Synthesis and measurements

The colorless complex was obtained by reacting equimolar quantities of triphenyltin chloride and 1,10-phenanthroline. The reagents were heated in ethanol until they dissolved completely. Slow cooling of the filtered solution afforded large colorless crystals. The crystals are stable in air for several years. The room-temperature diffraction measurements on a cubic specimen were performed on a Nonius KappaCCD area-detector diffractometer ($\lambda = 0.71073$ Å) in the 2.01 to 27.50° θ-range. The 326,049 intensities were corrected for absorption effects [13]. The raw intensities were reduced by *DENZO-SCALEPACK* [14] for solution by *SHELXS*-97 [11]. Crystallographic data (excluding structure factors) have been deposited with the Cambridge Crystallographic Data Centre as supplementary publication no. CCDC 168882. *Crystal data*: $C_{60}H_{50}Cl_2N_4O_2Sn_2$, monoclinic, $P2_1/n$, a = 21.1053(5), b = 12.2347(3), c = 51.772(2) Å, β = 101.525(2)°; Z = 10.

Refinements

The program *RAELS*00 that was used for refinement allows the use of refinable local coordinates relative to refinable orthonormal axial systems and the use of refinable *TLS* rigid-body thermal-motion parameters [15]. The 1,10-phenathroline molecules and the C_6H_5 groups attached to Sn were constrained to have identical local planar geometry of *mm*2 symmetry. The Sn-O distances were all constrained to be equal. The axial systems of the C_6H_5 groups were restrained to approach coplanarity with the Sn atoms; the Sn-C-C angles were constrained to be equal. The Sn, Cl and O atoms were given individual atom anisotropic temperature parameters. The 1,10-phenathroline molecules and C_6H_5 groups were each refined using separate 15-parameter *TLX* models, and 12-parameter *TL* models centered on the appropriate Sn atom, respectively. This permitted 524 degrees of freedom to describe meaningfully the 175 non-H atoms in the asymmetric unit from the refinement of 12317 reflections [out of 29,670 independent reflections obeying the $I > 3\sigma(I)$ cutoff] to obtain the final statistics (Table 1). H-atoms other than the water-H atoms were recalculated in sensible geometric positions after each refinement cycle and given thermal parameters determined by rigid parameters describing the atoms to which they were attached. There were no degrees of freedom advantages

Table 1. Statistics for the refinements on F for the commensurate structure of $[(C_6H_5)_3SnCl{\cdot}H_2O{\cdot}C_{12}H_8N_2]_2$.

Class*	No. of reflns.	$R(F)$	$R(F^2)$	wR	Gof**
$m = 0$	3666	0.039	0.057	0.063	1.48
$m = \pm 1$	4785	0.068	0.098	0.091	1.75
$m = \pm 2$	3866	0.078	0.119	0.089	1.53
All m	12317	0.057	0.068	0.081	1.60
Others	17353	0.458	0.626	0.500	1.60

* The reflections that were calculated but not included in refinement had $I < 3\sigma(I)$.

** Weighting scheme $w = [\mathrm{var}(|F_{obs}|) + (0.03\,|F_{obs}|)^2]^{-1}$.

Table 2. Atomic coordinates and equivalent isotropic temperature factors for $[(C_6H_5)_3SnCl{\cdot}H_2O{\cdot}C_{12}H_8N_2]_2$.*

Atom	*X*	*y*	*z*	U_{eq}
Sn1*a*	0.69461(2)	0.55834(4)	0.51650(1)	0.0516(1)
Cl1*a*	0.8148(1)	0.5757(2)	0.5232(1)	0.064(1)
O1*a*	0.5813(1)	0.5112(2)	0.5061(1)	0.072(1)
C21*a*	0.6872(1)	0.5623(2)	0.4753(1)	0.053(2)
C22*a*	0.6634(2)	0.6534(3)	0.4608(1)	0.077(3)
C23*a*	0.6589(3)	0.6566(4)	0.4336(1)	0.090(3)
C24*a*	0.6780(2)	0.5687(4)	0.4208(1)	0.089(3)
C25*a*	0.7016(3)	0.4776(4)	0.4348(1)	0.123(4)
C26*a*	0.7062(3)	0.4745(3)	0.4619(1)	0.100(3)
C31*a*	0.7008(1)	0.4190(3)	0.5411(1)	0.052(2)
C32*a*	0.7350(2)	0.3273(3)	0.5364(1)	0.068(2)
C33*a*	0.7390(2)	0.2361(3)	0.5526(1)	0.086(3)
C34*a*	0.7089(2)	0.2357(4)	0.5737(1)	0.085(3)
C35*a*	0.6748(2)	0.3255(4)	0.5788(1)	0.080(3)
C36*a*	0.6708(2)	0.4167(3)	0.5625(1)	0.065(2)
C41*a*	0.6760(1)	0.7083(3)	0.5346(1)	0.058(3)
C42*a*	0.7238(2)	0.7863(3)	0.5414(1)	0.069(2)
C43*a*	0.7118(3)	0.8839(3)	0.5532(1)	0.087(2)
C44*a*	0.6518(3)	0.9045(4)	0.5584(1)	0.104(4)
C45*a*	0.6038(2)	0.8285(4)	0.5518(1)	0.118(4)
C46*a*	0.6158(2)	0.7310(4)	0.5400(1)	0.089(2)
N1*a*	0.4941(1)	0.5082(3)	0.5510(1)	0.061(1)
C2*a*	0.4834(2)	0.6004(3)	0.5629(1)	0.080(2)
C3*a*	0.4781(2)	0.6044(4)	0.5897(1)	0.095(2)
C4*a*	0.4843(2)	0.5098(4)	0.6037(1)	0.087(2)
C5*a*	0.5024(2)	0.3105(4)	0.6058(1)	0.076(2)
C6*a*	0.5131(2)	0.2179(3)	0.5939(1)	0.075(2)
C7*a*	0.5294(2)	0.1214(3)	0.5539(1)	0.084(2)
C8*a*	0.5339(2)	0.1242(4)	0.5280(1)	0.094(2)
C9*a*	0.5269(2)	0.2257(4)	0.5148(1)	0.082(2)
N10*a*	0.5162(1)	0.3182(3)	0.5266(1)	0.062(2)
C11*a*	0.5002(1)	0.4143(3)	0.5651(1)	0.053(1)
C12*a*	0.5118(1)	0.3149(3)	0.5523(1)	0.053(2)
C13*a*	0.4955(1)	0.4123(4)	0.5919(1)	0.065(1)
C14*a*	0.5183(1)	0.2163(3)	0.5668(1)	0.064(1)
Sn1*b*	0.30137(2)	0.57217(4)	0.31400(1)	0.0493(1)
Cl1*b*	0.4213(1)	0.5921(2)	0.3203(1)	0.067(1)
O1*b*	0.1866(1)	0.5373(2)	0.3030(1)	0.059(1)
C21*b*	0.2877(1)	0.5702(2)	0.2725(1)	0.059(3)
C22*b*	0.2724(3)	0.6645(3)	0.2579(1)	0.110(3)
C23*b*	0.2635(3)	0.6634(4)	0.2305(1)	0.135(4)
C24*b*	0.2698(2)	0.5680(5)	0.2175(1)	0.099(4)
C25*b*	0.2848(3)	0.4736(4)	0.2316(1)	0.101(3)
C26*b*	0.2937(2)	0.4747(3)	0.2589(1)	0.087(3)
C31*b*	0.3076(1)	0.4312(3)	0.3381(1)	0.051(2)
C32*b*	0.2709(2)	0.3393(3)	0.3300(1)	0.066(2)
C33*b*	0.2753(2)	0.2469(3)	0.3458(1)	0.075(3)
C34*b*	0.3164(2)	0.2454(4)	0.3699(1)	0.092(3)
C35*b*	0.3532(3)	0.3354(4)	0.3783(1)	0.139(4)
C36*b*	0.3488(2)	0.4278(3)	0.3624(1)	0.108(4)
C41*b*	0.2849(1)	0.7241(2)	0.3319(1)	0.053(3)
C42*b*	0.3327(2)	0.7728(3)	0.3505(1)	0.064(2)
C43*b*	0.3220(2)	0.8712(3)	0.3623(1)	0.081(3)
C44*b*	0.2633(2)	0.9219(3)	0.3556(1)	0.087(4)
C45*b*	0.2152(2)	0.8753(3)	0.3373(1)	0.084(3)
C46*b*	0.2260(2)	0.7769(3)	0.3255(1)	0.066(2)
N1*b*	0.1211(1)	0.5194(3)	0.3455(1)	0.057(1)
C2*b*	0.1334(2)	0.6171(3)	0.3566(1)	0.074(1)
C3*b*	0.1576(2)	0.6310(4)	0.3838(1)	0.089(1)
C4*b*	0.1687(2)	0.5407(4)	0.3994(1)	0.085(1)
C5*b*	0.1672(2)	0.3401(4)	0.4039(1)	0.082(2)

C6*b*	0.1549(2)	0.2421(3)	0.3929(1)	0.084(2)
C7*b*	0.1171(2)	0.1295(3)	0.3533(1)	0.088(2)
C8*b*	0.0939(2)	0.1227(3)	0.3269(1)	0.087(2)
C9*b*	0.0837(2)	0.2204(4)	0.3121(1)	0.068(2)
N10*b*	0.0959(1)	0.3182(3)	0.3230(1)	0.054(1)
C11*b*	0.1322(1)	0.4298(3)	0.3611(1)	0.055(1)
C12*b*	0.1190(1)	0.3245(3)	0.3493(1)	0.055(1)
C13*b*	0.1564(1)	0.4378(4)	0.3885(1)	0.069(1)
C14*b*	0.1304(1)	0.2303(3)	0.3653(1)	0.071(2)
Sn1*c*	0.88819(2)	0.57183(4)	0.10905(1)	0.0470(1)
Cl1*c*	1.0077(1)	0.5938(2)	0.1131(1)	0.064(1)
O1*c*	0.7734(1)	0.5381(2)	0.1026(1)	0.056(1)
C21*c*	0.8672(1)	0.5723(2)	0.0671(1)	0.050(2)
C22*c*	0.8512(2)	0.6679(3)	0.0531(1)	0.076(2)
C23*c*	0.8374(3)	0.6684(4)	0.0257(1)	0.092(3)
C24*c*	0.8395(2)	0.5732(4)	0.0121(1)	0.080(3)
C25*c*	0.8552(3)	0.4776(4)	0.0255(1)	0.086(2)
C26*c*	0.8690(2)	0.4772(3)	0.0529(1)	0.072(2)
C31*c*	0.8970(1)	0.4293(2)	0.1330(1)	0.050(2)
C32*c*	0.8569(2)	0.3401(3)	0.1262(1)	0.054(2)
C33*c*	0.8628(2)	0.2474(3)	0.1419(1)	0.062(2)
C34*c*	0.9087(2)	0.2428(3)	0.1646(1)	0.082(3)
C35*c*	0.9489(2)	0.3299(4)	0.1717(1)	0.109(3)
C36*c*	0.9431(2)	0.4227(3)	0.1560(1)	0.085(2)
C41*c*	0.8735(1)	0.7218(2)	0.1282(1)	0.051(2)
C42*c*	0.9223(2)	0.7681(3)	0.1468(1)	0.067(2)
C43*c*	0.9128(2)	0.8652(3)	0.1593(1)	0.081(3)
C44*c*	0.8543(2)	0.9171(3)	0.1534(1)	0.080(3)
C45*c*	0.8053(2)	0.8729(3)	0.1351(1)	0.082(3)
C46*c*	0.8149(2)	0.7758(3)	0.1226(1)	0.067(2)
N1*c*	0.7154(1)	0.5147(3)	0.1477(1)	0.056(1)
C2*c*	0.7278(2)	0.6128(3)	0.1585(1)	0.078(1)
C3*c*	0.7512(2)	0.6279(4)	0.1858(1)	0.101(2)
C4*c*	0.7614(2)	0.5383(5)	0.2016(1)	0.099(2)
C5*c*	0.7589(2)	0.3381(4)	0.2067(1)	0.093(2)
C6*c*	0.7465(2)	0.2396(4)	0.1960(1)	0.093(2)
C7*c*	0.7096(2)	0.1254(3)	0.1566(1)	0.095(3)
C8*c*	0.6871(2)	0.1174(3)	0.1301(1)	0.097(2)
C9*c*	0.6778(2)	0.2143(4)	0.1151(1)	0.074(2)
N10*c*	0.6900(1)	0.3126(3)	0.1257(1)	0.054(2)
C11*c*	0.7257(1)	0.4258(3)	0.1636(1)	0.055(1)
C12*c*	0.7124(1)	0.3201(3)	0.1521(1)	0.054(1)
C13*c*	0.7490(1)	0.4350(4)	0.1910(1)	0.076(1)
C14*c*	0.7228(1)	0.2266(3)	0.1683(1)	0.074(2)
Sn1*d*	0.50030(2)	0.56795(4)	0.91038(1)	0.0469(1)
Cl1*d*	0.6184(1)	0.5778(2)	0.9099(1)	0.064(1)
O1*d*	0.3864(1)	0.5368(2)	0.9081(1)	0.060(1)
C21*d*	0.4705(1)	0.5711(2)	0.8688(1)	0.052(3)
C22*d*	0.4683(2)	0.6680(3)	0.8549(1)	0.091(3)
C23*d*	0.4486(3)	0.6705(4)	0.8277(1)	0.112(4)
C24*d*	0.4307(2)	0.5761(4)	0.8140(1)	0.088(4)
C25*d*	0.4325(3)	0.4793(4)	0.8273(1)	0.091(3)
C26*d*	0.4523(2)	0.4768(3)	0.8545(1)	0.076(3)
C31*d*	0.5123(1)	0.4287(3)	0.9352(1)	0.047(2)
C32*d*	0.5336(2)	0.3305(3)	0.9269(1)	0.071(2)
C33*d*	0.5419(2)	0.2394(3)	0.9432(1)	0.086(3)
C34*d*	0.5288(2)	0.2457(3)	0.9680(1)	0.071(3)
C35*d*	0.5076(2)	0.3420(4)	0.9767(1)	0.067(2)
C36*d*	0.4994(2)	0.4330(3)	0.9603(1)	0.058(2)
C41*d*	0.4955(1)	0.7197(3)	0.9306(1)	0.049(2)
C42*d*	0.5392(2)	0.8027(3)	0.9293(1)	0.060(2)
C43*d*	0.5362(2)	0.9010(3)	0.9424(1)	0.076(2)
C44*d*	0.4895(2)	0.9174(3)	0.9569(1)	0.081(3)
C45*d*	0.4457(2)	0.8365(4)	0.9584(1)	0.077(3)
C46*d*	0.4487(2)	0.7381(3)	0.9453(1)	0.061(2)
N1*d*	0.3064(1)	0.5256(3)	0.9485(1)	0.077(2)
C2*d*	0.2959(2)	0.6275(4)	0.9553(1)	0.119(2)
C3*d*	0.3044(2)	0.6610(4)	0.9819(1)	0.174(2)
C4*d*	0.3241(2)	0.5857(5)	1.0012(1)	0.178(2)
C5*d*	0.3562(2)	0.3965(5)	1.0141(1)	0.182(4)
C6*d*	0.3668(2)	0.2943(5)	1.0073(1)	0.185(5)
C7*d*	0.3684(2)	0.1571(4)	0.9725(1)	0.191(5)
C8*d*	0.3592(2)	0.1311(4)	0.9464(1)	0.187(4)
C9*d*	0.3387(2)	0.2140(4)	0.9277(1)	0.127(2)
N10*d*	0.3281(1)	0.3159(3)	0.9344(1)	0.081(2)
C11*d*	0.3260(1)	0.4511(3)	0.9677(1)	0.086(2)
C12*d*	0.3373(1)	0.3414(3)	0.9603(1)	0.089(2)
C13*d*	0.3354(1)	0.4789(5)	0.9946(1)	0.135(2)
C14*d*	0.3578(1)	0.2626(4)	0.9802(1)	0.141(3)
Sn1*e*	0.09401(2)	0.57006(4)	0.71640(1)	0.0457(1)
Cl1*e*	0.2133(1)	0.5799(2)	0.7181(1)	0.063(1)
O1*e*	-0.0206(1)	0.5395(2)	0.7123(1)	0.057(1)
C21*e*	0.0726(1)	0.5753(2)	0.6745(1)	0.053(3)
C22*e*	0.0934(2)	0.6614(3)	0.6610(1)	0.089(3)
C23*e*	0.0794(3)	0.6654(4)	0.6337(1)	0.111(4)
C24*e*	0.0445(2)	0.5835(4)	0.6195(1)	0.085(3)
C25*e*	0.0234(2)	0.4976(4)	0.6324(1)	0.077(3)
C26*e*	0.0374(2)	0.4935(3)	0.6598(1)	0.067(2)
C31*e*	0.1025(1)	0.4309(2)	0.7413(1)	0.053(3)
C32*e*	0.1315(2)	0.3359(3)	0.7349(1)	0.069(2)
C33*e*	0.1373(2)	0.2450(3)	0.7513(1)	0.088(3)
C34*e*	0.1142(2)	0.2481(4)	0.7742(1)	0.090(4)
C35*e*	0.0854(2)	0.3411(4)	0.7809(1)	0.083(3)
C36*e*	0.0796(2)	0.4320(3)	0.7645(1)	0.065(2)
C41*e*	0.0873(1)	0.7208(2)	0.7368(1)	0.048(2)
C42*e*	0.1328(2)	0.8025(3)	0.7373(1)	0.059(2)
C43*e*	0.1286(2)	0.9000(3)	0.7505(1)	0.076(2)
C44*e*	0.0789(2)	0.9170(3)	0.7634(1)	0.082(3)
C45*e*	0.0334(2)	0.8374(4)	0.7633(1)	0.078(3)
C46*e*	0.0376(2)	0.7398(3)	0.7500(1)	0.061(2)
N1*e*	-0.1019(1)	0.5065(3)	0.7530(1)	0.072(2)
C2*e*	-0.1153(2)	0.5995(3)	0.7640(1)	0.102(2)
C3*e*	-0.1201(2)	0.6072(4)	0.7907(1)	0.128(2)
C4*e*	-0.1106(2)	0.5155(5)	0.8058(1)	0.118(2)
C5*e*	-0.0861(2)	0.3184(4)	0.8100(1)	0.106(2)
C6*e*	-0.0736(2)	0.2250(4)	0.7991(1)	0.108(3)
C7*e*	-0.0541(2)	0.1237(3)	0.7600(1)	0.124(3)
C8*e*	-0.0503(2)	0.1229(4)	0.7341(1)	0.134(3)
C9*e*	-0.0608(2)	0.2215(4)	0.7198(1)	0.105(2)
N10*e*	-0.0742(1)	0.3148(3)	0.7306(1)	0.073(2)
C11*e*	-0.0925(1)	0.4155(3)	0.7681(1)	0.064(2)
C12*e*	-0.0780(1)	0.3152(3)	0.7564(1)	0.065(2)
C13*e*	-0.0965(1)	0.4173(4)	0.7950(1)	0.086(2)
C14*e*	-0.0680(1)	0.2196(3)	0.7719(1)	0.089(2)

*U_{eq} is defined as one-third the trace of the $\mathbf{U}_{ij}$ tensor.

in using symmetrized parameters defined by modulation vectors since all orders of satellites were well observed. The atomic coordinates and equivalent isotropic temperature factors are listed in Table 2.

Modulation functions could have been used to describe individual atom parameters but this is not a necessity. The concept of linear independence allows a multitude of choices for variables, provided they all span the same space. Modulation functions have the advantage that certain variables are associated with certain index conditions for their major contribution to observed intensities, but reflections with $2h + l = 5N \pm 1$ and $5N \pm 2$ had reasonably similar intensities, excluding the simple use of modulation functions as a basis for constrained refinement. We assumed that local object constraints were the most appropriate way of reducing the number of variables while maintaining the essential features of the structure. This allowed 524 degrees of freedom rather than the maximum 35 x 5 x 9 = 1575 for the 35 non-hydrogen atoms in the formula unit.

In the final refinement cycle, the change to the predicted sum of weighted residuals was found to be small although some shift/sigma values were still large (up to 0.5). This is a consequence of using highly correlated parameters, (rather than eigen functions of the least squares matrix) one at a time, evaluating the σ-values from the diagonal elements of the inverse of the least-squares matrix. The final difference Fourier map had peaks in the -0.90 to 1.00 eÅ^{-3} range. Selected bond dimensions are listed in Table 3. The unit cell contents are shown in Figure 1 (scheme).

calorimeter is maintained at atmospheric level. The time spent by any personnel near the calorimeter is kept to a minimum (less than a minute, the time taken to pass the meals through the air-lock window in the door); and the exhaust air is expelled at a considerable distance away from the location of the calorimeter.

The flow rate of air drawn out of the chamber can be adjusted through a by-pass (bleed) system on the outflow and it is usually fixed at 60±1 L/min as indicated on the LCD screen of the dry gas meter. This flow rate has been chosen such that the change in oxygen concentration of the chamber is less than 1% during a 24 hour experiment. As such it will prevent a high build up of carbon dioxide which is known to have adverse physiological effect on the subjects.

Temperature and humidity

The air inside the calorimeter is continuously mixed by a fan and the temperature is regulated to 25±0.5 ^{0}C by a split-unit thermostatical air-conditioner. Two sensors for temperature (HiTemp sensor, DCP Microdevelopments Ltd., UK) and humidity (HumiPro sensor, DCP Microdevelopments Ltd., UK) respectively are located inside the calorimeter. Both sensors are connected to a data-logger (LogIT Data Meter 1000, DCP Microdevelopments Ltd. UK) outside the chamber. The data-logger continuously records and displays temperature and humidity to the nearest ±0.1 ^{0}C and ±0.1%, respectively, via LogIT program (LogIT Data Logging System, DCP Microdevelopments Ltd., UK) in the computer. During human trials, it is known that air is neither dry nor fully saturated. However the use of a condenser (Hartmann & Braun CGEK 6) helps overcome the problem in the conversion of gas volume to STP.

Gas analysis

The oxygen concentration is measured using a T-piece junction connected on the main flow line immediately after the gas meter outlet (calorimeter air) and the atmospheric air (baseline) to a single flow through a solenoid valve (Herion 3/2 way solenoid valve). The valve is controlled by a time switch (Grasslin time switch) that alternates the opening and closing of two gas-tight valves at interval of 45 minutes (chamber air) and at 15 minutes interval (baseline air) per hour respectively, over the duration of the experiment. A small pump is installed to pull air sample at the rate of 150 cm^{3}/min through the condenser (for air drying) before it enters the oxygen analyzer (Servomex Xentra 4100 Gas Purity Analyzer, Servomex International Ltd., UK). Oxygen percentage is continuously displayed on the LCD monitor of the oxygen analyzer to the nearest value of 0.001% with a response time of 1 second. Prior to each experiment, the analyzer is calibrated using 99.8% oxygen and oxygen-free nitrogen (OFN) gases. The oxygen analyzer is interfaced to an on-line computer, which is installed with an application software (Labview version 5.1 Addendum, National Instruments Corporation, USA) to program the data output from the analyzer.

The output of the oxygen analyzer is transmitted into the computer by a 9-way D type (PL6) plug, which provides a communication serial configuration data frame output into the computer via data port RS232 in the computer processing unit (CPU). The communication provides a frequency of a one-way data transmission from the oxygen analyzer to the on-line computer by a single second, and can even be adjusted from 1 to 9999 seconds. For all the experiments, the data transmission frequency was adjusted to 10 seconds, hence for a 24-h measurement, there would be at least 8640 data points for oxygen concentration recorded in the computer. The application software continuously displays the oxygen level in sequential of 10 seconds interval, in numerical and graphical forms.

RESULTS AND DISCUSSION

Room volume test

The volume of the calorimeter was determined using 99.8% oxygen and oxygen-free nitrogen (OFN) which were injected into the calorimeter. If the volume of a gas injected displaces an equal volume of air in the room, then the volume of O_2 in the room after injection ($V_R.O_F$) will be equal to the volume of O_2 injected ($V_G.O_G$) plus the residual O_2 after displacement ($V_R - V_G)O_I$ [10], that is:

$$(V_R.O_F) = (V_G.O_G) + (V_R - V_G)O_I$$

hence,

$$V_R = \frac{V_G (O_G - O_I)}{O_F - O_I}$$

where, V_R = volume of the room
V_G = volume of gas injected
O_G = O_2 concentration in V_G
O_I = initial O_2 concentration in the room
O_F = final O_2 concentration in the room

Table 3. Selected bond distances and angles in $[(C_6H_5)_3SnCl{\cdot}H_2O{\cdot}C_{12}H_8N_2]_{2.*}$

Sn1*a*–Cl1*a*	2.501(2)	Sn1*b*–Cl1*b*	2.499(2)	Sn1*c*–Cl1*c*	2.504(2)	Sn1*d*–Cl1*d*	2.500(2)	Sn1*e*–Cl1*e*	2.505(2)
Sn1*a*–O1*a*	2.415(2)	Sn1*b*–O1*b*	2.415(2)	Sn1*c*–O1*c*	2.415(2)	Sn1*d*–O1*d*	2.415(2)	Sn1*e*–O1*e*	2.415(2)
Sn1*a*–C21*a*	2.104(3)	Sn1*b*–C21*b*	2.110(3)	Sn1*c*–C21*c*	2.125(3)	Sn1*d*–C21*d*	2.118(3)	Sn1*e*–C21*e*	2.124(3)
Sn1*a*–C31*a*	2.116(3)	Sn1*b*–C31*b*	2.116(3)	Sn1*c*–C31*c*	2.125(3)	Sn1*d*–C31*d*	2.117(3)	Sn1*e*–C31*e*	2.121(3)
Sn1*a*–C41*a*	2.131(3)	Sn1*b*–C41*b*	2.137(3)	Sn1*c*–C41*c*	2.137(3)	Sn1*d*–C41*d*	2.142(3)	Sn1*e*–C41*e*	2.144(3)
Cl1*a*–Sn1*a*–O1*a*	169.7(1)	Cl1*b*–Sn1*b*–O1*b*	172.3(1)	Cl1*c*–Sn1*c*–O1*c*	175.1(1)	Cl1*d*–Sn1*d*–O1*d*	172.9(1)	Cl1*e*–Sn1*e*–O1*e*	173.1(1)
Cl1*a*–Sn1*a*–C21*a*	90.4(1)	Cl1*b*–Sn1*b*–C21*b*	93.6(1)	Cl1*c*–Sn1*c*–C21*c*	94.9(1)	Cl1*d*–Sn1*d*–C21*d*	94.8(1)	Cl1*e*–Sn1*e*–C21*e*	92.4(1)
Cl1*a*–Sn1*a*–C31*a*	92.6(1)	Cl1*b*–Sn1*b*–C31*b*	93.5(1)	Cl1*c*–Sn1*c*–C31*c*	94.0(1)	Cl1*d*–Sn1*d*–C31*d*	92.6(1)	Cl1*e*–Sn1*e*–C31*e*	93.1(1)
Cl1*a*–Sn1*a*–C41*a*	97.9(1)	Cl1*b*–Sn1*b*–C41*b*	96.1(1)	Cl1*c*–Sn1*c*–C41*c*	96.1(1)	Cl1*d*–Sn1*d*–C41*d*	96.1(1)	Cl1*e*–Sn1*e*–C41*e*	96.1(1)
O1*a*–Sn1*a*–C21*a*	84.8(1)	O1*b*–Sn1*b*–C21*b*	80.2(1)	O1*c*–Sn1*c*–C21*c*	82.0(1)	O1*d*–Sn1*d*–C21*d*	82.1(1)	O1*e*–Sn1*e*–C21*e*	84.8(1)
O1*a*–Sn1*a*–C31*a*	83.2(1)	O1*b*–Sn1*b*–C31*b*	86.4(1)	O1*c*–Sn1*c*–C31*c*	84.8(1)	O1*d*–Sn1*d*–C31*d*	84.3(1)	O1*e*–Sn1*e*–C31*e*	83.8(1)
O1*a*–Sn1*a*–C41*a*	92.4(1)	O1*b*–Sn1*b*–C41*b*	90.8(1)	O1*c*–Sn1*c*–C41*c*	88.7(1)	O1*d*–Sn1*d*–C41*d*	91.0(1)	O1*e*–Sn1*e*–C41*e*	90.8(1)
C21*a*–Sn1*a*–C31*a*	127.7(1)	C21*b*–Sn1*b*–C31*b*	124.7(1)	C21*c*–Sn1*c*–C31*c*	124.9(1)	C21*d*–Sn1*d*–C31*d*	127.3(1)	C21*e*–Sn1*e*–C31*e*	128.2(1)
C21*a*–Sn1*a*–C41*a*	116.2(1)	C21*b*–Sn1*b*–C41*b*	116.8(1)	C21*c*–Sn1*c*–C41*c*	116.8(1)	C21*d*–Sn1*d*–C41*d*	116.5(1)	C21*e*–Sn1*e*–C41*e*	117.0(1)
C31*a*–Sn1*a*–C41*a*	115.1(1)	C31*b*–Sn1*b*–C41*b*	116.8(1)	C31*c*–Sn1*c*–C41*c*	116.1(1)	C31*d*–Sn1*d*–C41*d*	114.4(1)	C31*e*–Sn1*e*–C41*e*	113.5(1)
Intradimer contacts									
O1*a*···N1*a*	3.241(4)	O1*b*···N1*b*	2.833(4)*	O1*c*···N1*c*	2.860(4)*	O1*d*···N1*d*	2.938(4)*	O1*e*···N1*e*	3.000(4)*
O1*a*···N10*a*	3.030(4)*	O1*b*···N10*b*	3.566(4)	O1*c*···N10*c*	3.604(4)	O1*d*···N10*d*	3.368(4)	O1*e*···N10*e*	3.190(4)
O1*a*···N1*a*^{i}	3.073(4)*	O1*b*···N1*e*^{ii}	3.131(4)*	O1*c*···N1*d*^{i}	2.940(4)*	O1*d*···N1*c*^{i}	3.299(4)	O1*e*···N1*b*^{ii}	3.382(4)
O1*a*···N10*a*^{i}	3.173(4)	O1*b*···N10*e*^{ii}	3.205(4)	O1*c*···N10*d*^{i}	3.131(4)	O1*d*···N10*c*^{i}	2.816(4)*	O1*e*···N10*b*^{ii}	2.780(4)*

^{i} Symmetry transformation: *i* = 1- *x*, 1 - *y*, 1 - *z*; *ii* = -*x*, 1 - *y*, 1 - *z*.
*Hydrogen bond

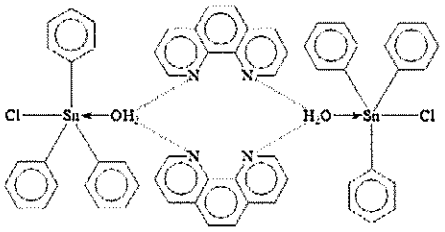

Scheme 1. Bis(aquachlorotriphenyltin.1,10-phenanthroline).

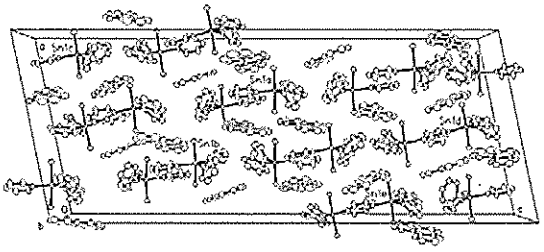

Figure 1. Projection of the cell contents down the **b**-axis. Labels *a*, *b*, *c*, *d* and *e* distinguish pseudo translationally-related molecules. Hydrogen bonds are not shown.

RESULTS AND DISCUSSION

For the $P2_1/n$ cell, the reflections can be indexed as $h\mathbf{a}^* + k\mathbf{b}^* + l\mathbf{c}^*$ or $h_o\mathbf{a}_o^* + k_o\mathbf{b}_o^* + l_o\mathbf{c}_o^* + m_o\mathbf{q}$ where $\mathbf{a}_o^* = \mathbf{a}^* + 3\mathbf{c}^*$, $\mathbf{b}_o^* = -\mathbf{b}^*$, $\mathbf{c}_o^* = \mathbf{a}^* - 2\mathbf{c}^*$; the values for the indices depend on the choice of **q**. If $\mathbf{q} = \mathbf{c}^* = (\mathbf{a}_o^* - \mathbf{b}_o^*)/5$, then $h_o = h - N$, $k_o = -k$, $l_o = N$, $m_o = -3h + l + 5N$, where N is any integer which can be chosen so that m_o lies in the -2 to +2 range. The *n*-glide special reflection condition of $h + l$ even for the $h0l$ reflections now corresponds to $l_o + m_o$ even for the $h_o0l_om_o$ reflections, but this does not correspond to a standard setting for a (3+1)-dimensional superspace group number 14.1 in Table 9.8.3.5, Section 9.8 of the *International Tables for Crystallography*, Volume C [16]. However, if we let $\mathbf{q} = \mathbf{c}^* + \mathbf{c}_o^* = \mathbf{a}^* - \mathbf{c}^* = (\mathbf{a}_o^* + 4\mathbf{c}_o^*)/5$, then $h_o = N$, $k_o = -k$, $l_o = -h - l + 4N$, $m_o = 2h + l - 5N$, where N is any integer. The *n*-glide special reflection condition ($h + l$ even for $h0l$ reflections) now corresponds to l_o even for $h_o0l_om_o$ reflections. This is seen to correspond to swapping **b** for **c** in the (3+1)-dimensional superspace group number 14.1. We can therefore describe the (3+1)-dimensional superspace group as $P2_1/c(\alpha 0\gamma)$ with $\alpha = 1/5$, $\gamma = 4/5$ and symmetry elements (**1**, 1 | 0, 0, 0, 0), (**m**, 1 | 0, 1/2, 1/2, 0), (**-1**, -1 | 0, 0, 0, τ_4), (**2**, -1 | 0, 1/2, 1/2, τ_4) with $\tau_4 = 0$ if we wish to have a true center of inversion at the origin.

A (3+1) dimensional superspace group is described by operators ($\mathbf{R}_j$, ε_j | τ_{j1}, τ_{j2}, τ_{j3}, τ_{j4}) or ($\mathbf{R}_j$, ε_j | τ_j, τ_{j4}) where R_j is a 3-dimensional symmetry operator with an associated 3-dimensional translation $\mathbf{t}_j = \tau_{j1}\mathbf{a}_o + \tau_{j2}\mathbf{b}_o + \tau_{j3}\mathbf{c}_o$. Allowed values of $\mathbf{R}_j$ satisfy the condition that $\mathbf{R}_j\mathbf{q} = \varepsilon_j\mathbf{q} + \mathbf{g}_o$ where $\varepsilon_j = \pm 1$ and $\mathbf{g}_o$ is a Bragg reflection of the parent structure.

There is a choice of global phase φ associated with a modulated structure corresponding to a translation of the crystal contents by (**1**, 1 | 0, 0, 0, φ). This leaves unchanged symmetry elements with $\varepsilon_j = 1$ but changes the value of τ_{4j} to $\tau_{4j} - 2\varphi$ for symmetry elements with $\varepsilon_j = -1$. This is analogous, for example, to changing the 3-dimensional symmetry elements *x*, -*y*, *z* and *x*, *y*, -*z*+1/3 to *x*, -*y*, *z* and *x*, *y*, -*z* by translating the unit cell contents by 0,0,1/6.

We can describe the scattering density of a (3+1)-dimensional incommensurate crystal structure as

$\Sigma_m \rho_m(\mathbf{r})$ where $\rho_m(\mathbf{r})$ is the Fourier transform of the mth subset of reflections $\{F_m(\mathbf{H})\}$, where $\mathbf{H} = \mathbf{G}_o + m\mathbf{q}$ and $\mathbf{G}_o$ is any Bragg reflection of the parent structure. When a (3+1)-dimensional operator $(\mathbf{R}_j, \varepsilon_j \mid \mathbf{t}_j, \tau_{j4})$ operates on $\rho(\mathbf{r})$, we change $F(\mathbf{H})$ to $\exp[2\pi i(h\tau_{j1} + k\tau_{j2} + l\tau_{j3} + m\tau_{j4})]F(\mathbf{HR}_j)$ and so $(\mathbf{1}, 1 \mid 0, 0, 0, \varphi)$ operating on the cell contents changes $\rho_m(\mathbf{r})$ to $\exp(2\pi i m\varphi)\rho_m(\mathbf{r})$ and any value of $F_m(\mathbf{H})$ to $\exp(2\pi i m\varphi)F_m(\mathbf{H})$. For real scattering density, $\rho_{-m}(\mathbf{r}) = \rho_m(\mathbf{r})^*$ and $F(-\mathbf{H}) = F(\mathbf{H})^*$.

The consequences of the structure being commensurate

When a structure is commensurate, $N\mathbf{q} = N_1\mathbf{a}_o^* + N_2\mathbf{b}_o^* + N_3\mathbf{c}_o^*$, where N, N_1, N_2 and N_3 are integers and we can write $\mathbf{H} = (h - nN_1)\mathbf{a}_o^* + (k - nN_2)\mathbf{b}_o^* + (l - nN_3)\mathbf{c}_o^* + (m + nN)\mathbf{q}$, where n is any integer. Consequently, $F(\mathbf{H})$ becomes $\Sigma_n F_{m+nN}(\mathbf{H})$ and reflections related by (3+1) dimensional symmetry elements now have the relationship $\Sigma_n F_{m+nN}(\mathbf{H}) = \Sigma_n \exp[2\pi i \Phi_{nj}(\mathbf{H})]F_{e(m+nN)}(\mathbf{HR}_j)$, where $\Phi_{nj}(\mathbf{H}) = (h - nN_1)\tau_{j1} + (k - nN_2)\tau_{j2} + (l - nN_3)\tau_{j3} + (m + nN)\tau_{j4}$.

Equivalence of reflection intensities, and hence the true maintenance of a (3+1) dimensional symmetry element, can only occur if $\exp[2\pi i(N_1\tau_{j1} + N_2\tau_{j3} + N_3\tau_{j3} - N\tau_{j4})]$ is exactly 1.0. For our system, $N = 5$, $N_1 = 1$, $N_2 = 0$ and $N_3 = 4$, so that this condition is always satisfied for $(\mathbf{1}, 1 \mid 0, 0, 0, 0)$ and $(\mathbf{m}, 1 \mid 0, 1/2, 1/2, 0)$, but is only satisfied for $(\mathbf{-1}, -1 \mid 0, 0, 0, \tau_4)$ and $(\mathbf{2}, -1 \mid 0, 1/2, 1/2, \tau_4)$ if τ_4 is an integer multiple of 1/5. The options simply correspond to having alternative origins.

Alternative origins that do not change the symmetry elements

We can have alternative origins for a structure in three dimensions without changing the symmetry elements or the magnitudes of structure factors, i.e., we can make certain translations of the cell contents without changing the phase relationships between equivalent reflections. For example, translations by $\mathbf{a}/2$, $\mathbf{b}/2$ or $\mathbf{c}/2$ of the contents of a $P2_1/c$ structure change the phases of reflections but not the relationships between equivalent reflections. Likewise, a translation in (3+1) dimensional space using the operator $(\mathbf{1}, 1 \mid 0, 0, 0, 1/2)$ leaves values of τ_{4j}, modulo 1, unchanged but changes values of $F_m(\mathbf{H})$ to $(-1)^m F_m(\mathbf{H})$. This is of no consequence if the structure is incommensurate but must be considered when $(2M+1)\mathbf{q} = \mathbf{g}_o$, a Bragg reflection of the parent structure.

We now have a number of possible commensurate structures derived from the same incommensurate prototype, differing only in the choice of global phase corresponding to a translation of the crystal contents by $(\mathbf{1}, 1 \mid 0, 0, 0, j)$ to give structure factors $F(\mathbf{H}) = \Sigma_n \exp[2\pi i(m+nN)\varphi]F_{m+nN}(\mathbf{H})$.

We can consider only those terms with the two smallest values of $|m+nN|$, and choose $\varphi = 0$ to correspond to having a true center of inversion at the origin. Then, as φ varies, we obtain $|F(\mathbf{H})|^2 = |F'(\mathbf{H})|^2 + |F''(\mathbf{H})|^2 + \cos(2\pi N\varphi)[F'(\mathbf{H})^*F''(\mathbf{H}) + F'(\mathbf{H})F''(\mathbf{H})^*]$ with $N = 5$. The $\cos(2\pi N\varphi)$ factor is 1.0 when $\varphi = 0$, -1.0 when $\varphi = 1/2$ and 0.0 when $\varphi = 1/4$. In there was no anomalous scattering $F'(\mathbf{H})$ and $F''(\mathbf{H})$ would both be real. If the structure is truly incommensurate but intensities accidentally overlap, then we obtain intensities that effectively are indistinguishable from those obtained for the commensurate $\varphi = 1/4$ case, which has space group Pn and has $\exp[2\pi i(m+nN)\varphi]$ real if $m+nN$ is even and imaginary if $m+nN$ is odd. Intensities for the $\varphi = 0$ and $\varphi = 1/2$ cases would then fit equally badly. However, if the $\varphi = 0$ case is correct, then the $\varphi = 1/2$ case fits twice as badly as does the $\varphi = 1/4$ case.

We determined the crystal structure by using standard 3-dimensional methods, and then refined the $P2_1/n$ structure by using constrained refinement techniques. Our first solution corresponded to the worst scenario. We obtained an initial model for the best scenario by simply multiplying calculated structure factors by -1.0 for of all $m = \pm 1$ reflections and then re-determining the structure from the resulting Fourier map using the same $P2_1/n$ symmetry elements.

Atom labeling and structure description

When a (3+1)-dimensional operator $(\mathbf{R}, \varepsilon \mid \mathbf{t}, \tau_4)$ operates on $\rho(\mathbf{r})$, we change $F_m(\mathbf{H})$ to $\exp[2\pi i(h\tau_1 + k\tau_2 + l\tau_3 + m\tau_4)]F_{em}(\mathbf{HR})$, which does not change in value when the values of the τ_n are changed by any integer. This requires that the operator changes $\rho_m(\mathbf{r})$ to $\exp[2\pi i m(\tau_4 - \mathbf{q}.\mathbf{t})]\rho_{em}(\mathbf{Rr} + \mathbf{t})$.

For our structure, $\mathbf{q} = (\mathbf{a}_o^* + 4\mathbf{c}_o^*)/5 = \mathbf{a}^* - \mathbf{c}^*$. The asymmetric unit contains five $(C_6H_5)_3SnCl{\cdot}H_2O$ and five $C_{12}H_8N_2$ entities. Atoms whose labels end in a are in molecules closest to the true inversion at (1/2, 1/2, 1/2) for the cell $\mathbf{a}$, $\mathbf{b}$, $\mathbf{c}$. Pseudo translation relates the molecules in the asymmetric unit. The remaining atoms are related by the pseudo translations $(\mathbf{1}, 1 \mid -\mathbf{a}_o, 0)^n = (\mathbf{1}, 1 \mid -n\mathbf{a}_o, 0)$, $n = 1,2,3,4$ and are distinguished by the b, c, d and e labels, respectively. The smallest

phase shifts for the primary modulation wave associated with ±**q** are associated with the sequence [*a* — *b* — *c* — *d* — *e*]. The sequence [*a* — *c* — *e* — *b* — *d*] etc., shows the smallest phase shifts for the modulation wave associated with ±2**q**.

The use of the operators (**m**, 1 | $\mathbf{c}_o/2$, 0)^n = (**m**^{n}, 1 | $n\mathbf{c}_o/2$, 0), n = 0 to 9, creates the sequence [*a* — *c*' — *e* — *b*' — *d* — *a*' — *c* — *e*' — *b* — *d*' —] where the molecules that are five apart in the sequence are related by the true glide operation, (**m**, 1 | 5$\mathbf{c}_o/2$, 0).

The close contacts between the oxygen atoms of the coordinated water molecule and the nitrogen atoms of the 1,10-phenanthroline heterocycle (Table 2) reveal the evolution of the title compound as hydrogen-bonded dimers (Fig. 2). The *i* and *ii* labels denote a true inversion. There are two shortest contacts for each water molecule to the nitrogen atoms belonging to different heterocycles. We also note that the evolution with pseudo translation for labels obtained by using the ε = -1 operations is in the reverse sequence to that applying to the other atoms. There are also possible interactions about other pseudo inversion centers, and atoms whose labels end in *d* are closest to the true inversion at 0, 1/2, 1/2. We also note the evolution of interactions about the pseudo screw axis. Molecules nearest the true screw axis at 1/4, *y*,1/4 have labels that end in *b* for the aquachlorotriphenyltin moiety but end in *e* for the 1,10-phenanthroline moiety, whereas molecules nearest the true screw axis at 1/4, *y*, 3/4 have labels that end in *e* for the organotin moiety but end in *c* for the heterocycle.

Acknowledgements – We thank the University of Malaya, Suranaree University of Technology and the Australian National University for supporting this work.

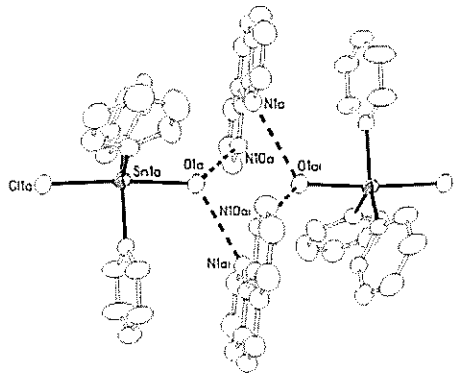

Figure 2a. *ORTEP* plot of the centrosymmetric (1 - *x*, 1 - *y*, 1 - *z*) hydrogen-bonded *a* dimer at the 30% probability level when viewed down the **b**-axis.

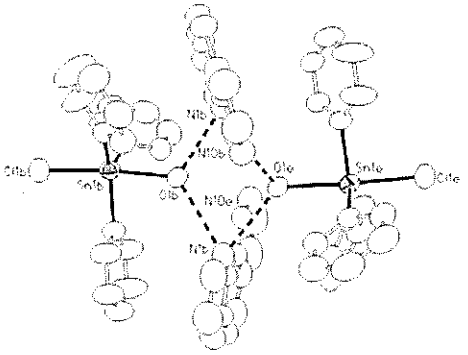

Figure 2b. *ORTEP* plot of the hydrogen-bonded *b* molecule and the symmetry-transformed (-*x*, 1 - *y*, 1 - *z*) *e* molecule at the 30% probability level when viewed down the **b**-axis. Hydrogen atoms are not shown.

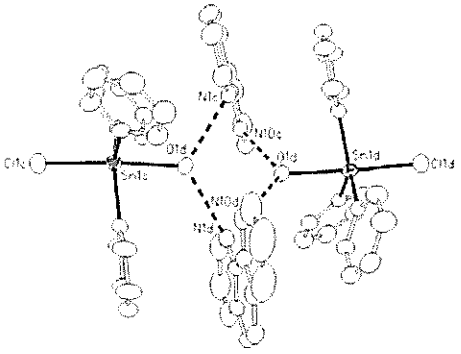

Figure 2c. *ORTEP* plot of the hydrogen-bonded *c* molecule and the symmetry-transformed (1 - *x*, 1 - *y*, 2 - *z*) *e* molecule at the 30% probability level when viewed down the **b**-axis. Hydrogen atoms are not shown.

REFERENCES

1 Gabe E.J., Lee F.L. and Smith F.E. (1984) Outer-sphere coordination in the phenanthroline and bipyridine complexes of triphenyltin chloride. *Inorg. Chim. Acta* **90**: L11-L13.

2 Ng S.W. and Kumar Das V.G. (1996) Outer-sphere coordination of *o*-phenanthroline in bis[aquachlorotri(*p*-chlorophenyl)tin·*o*-phenanthroline]. *J. Organomet. Chem.* **513**: 105-108.

3 Ng S.W., Yap C.K., Chen W., Kumar Das V.G. and Sinn, E. (1997) Outer-sphere coordination of *o*-phenanthroline in aquabromotri-*p*-tolyltin·*o*-phenanthroline. *Main Group Met. Chem.* **20**: 531-534.

4 Ng S.W. (1997) Bis[aqua(chlorodifluoroacetato-*O*)triphenyltin-1,10-phenanthroline. *Acta Crystallogr.* **C53**: 1059-1061.

5 Ng S.W., Kumar Das V.G. and Kennard C.H.L. (1996) Outer-sphere coordination of 1,10-phenanthroline in bis(aquatrifluoroacetatotriphenyltin·1,10-phenanthroline). *Main Group Met. Chem.* **19**: 107-111.

6 Chee C.F., Lo K.M. and Ng S.W. (2003) μ-Succinato-bis(triphenyltin)bis(*o*-phenanthroline). *Acta Crystallogr.* **E59**: m36-m37.

7 Ng S.W. (1996) A 1,1 adduct of aquachlorotriphenyltin with 3,4,7,8-tetramethyl-1,10-phenanthroline. *Acta Crystallogr.* **C52**: 354-356.

8 Prasad L., Lee F.L., Le Page Y. and Smith F.E. (1982) 2,2':6'2"-Terpyridyl-aquachlorotriphenyltin(IV) (1:1). *Acta Crystallogr.* **1983**, 259-262.

9 Chee C.F., Lo K.M. and Ng S.W. (2002) Aquatrifluoroacetatotriphenyltin·2,4,6-tris(2-pyridyl)-1,3,5-triazine (1/1). *Acta Acta Crystallogr.* **E58**: m661 -m662.

10 Chee C.F., Lo K.M. and Ng, S.W. (2003) Aquatrifluoroacetatotriphenyltin–2,2':6',2"-terpyridine (1/1). *Acta Crystallgor.* **E59**: m173-m174.

11 Sheldrick G.M. (1997) *SHELXS-97* and *SHELX-97*. Programs for crystal structure analysis (Release 97-2). University of Göttingen, Germany.

12 Rae A.D. (2000) *RAELS00*, A comprehensive constrained least squares refinement program. Australian National University, Canberra, Australia.

13 Coppens P., Leiserowitz L. and Rabinovich D. (1965) Calculation of absorption corrections for camera and diffractometer data. *Acta Crystallogr.* **18**: 1035-1038.

14 Otwinowski Z. and Minor W. (1997) *DENZO-SCALEPACK*. Processing of X-ray diffraction data collected in oscillation mode. *In*: Carter C.W. and Sweet R.M. (eds.) Methods in enzymology, Volume 276: Macromolecular Crystallography, Part A, pp. 307-326, Academic Press.

15 Rae A.D. (1975) Crystal structure refinement using a number of orthonormal axial systems. *Acta Crystallogr.* **A31**: 560-570. Rigid-body motion in crystals - the application of constraints on the TLS model. *Acta Crystallogr.* **A31**: 570-574.

16 Janssen T., Janner A., Looijenga-Vos A. and de Wolff P.M. (1995) Incommensurate and commensurate modulated structures. Section 9.8 of the *International Tables for Crystallography*, Volume C, pp. 797-835.

Journal of Science and Technology in the Tropics (2005) **1:** 165-169

The structures and absolute configurations of aglaxiflorin A and new aglaxiflorins E and F from *Aglaia laxiflora* (Meliaceae)

Y. J. Xu,[a,b] Y. H. Lai[b] and S. H. Goh[b,c]

[a] Merlion Pharmaceuticals Pte. Ltd. 59A Science Park Drive, The Fleming, Singapore Science Park, Singapore 118240

[b] Department of Chemistry, National University of Singapore, Singapore 117543

[c] Forest Research Institute of Malaysia, Kuala Lumpur, Malaysia

(chmgsh@yahoo.com)

Received: 1 July 2005; Accepted: 30 September 2005

Abstract Two new aglaxiflorins E and F were isolated from the leaf extracts of the Malaysian plant *Aglaia laxiflora*. Their structures were elucidated primarily by 2D NMR spectroscopy and the absolute stereochemistry of the aglaxiflorins was confirmed by single-crystal X-ray crystallography. Similarly the absolute stereochemistry of previously isolated aglaxiflorin A was determined from its brominated derivative.

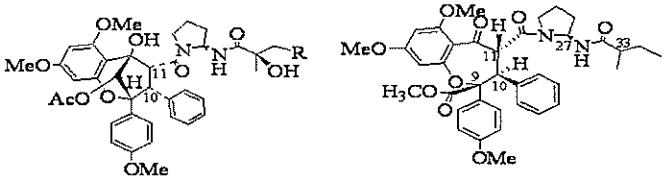

Aglalaxiflorin A 10R, 11S, R=Me
Aglalaxiflorin E 10R, 11R, R=H

Aglalaxiflorin F
Forbaglin A: 27*S*, 33*S*
Forbaglin B: 27*R*, 33*S*

Keywords aglaxiflorin A – aglaxiflorins E and F – *Aglaia laxiflora* - Meliaceae

Aglaia species of the family Meliaceae are of ethnomedicinal value [1,2] and have insecticidal [3] and cytotoxic properties [4]. Study of the Malaysian plant *aglaia laxiflora* has led to the isolation of cytotoxic cyclopentatetrahydobenzofurans and several bicyclic diamides aglaxiflorins A – D [5]. Here we report the further isolation and structure elucidation of two minor compounds Agalaxiflorins E and F, and the absolute stereochemistry of previously isolated aglaxiflorin A [5].

Aglaxiflorin E was isolated as an amorphous powder. The HRFAB-MS pseudo-molecular ion peak $[M+H]^+$ 675.2930 (calcd for $C_{37}H_{43}N_2O_9$, 675.2918) established its molecular formula as $C_{37}H_{42}N_2O_{10}$. The IR and UV were quite similar to those of aglaxiflorins A – D [5] indicating aglaxiflorin E had a similar structural skeleton. But two sets of peaks (of ratio about 9 : 10) were observed in the 1D NMR data of aglaxiflorin E when methanol-d_4 was used as solvent. More sets of peaks were observed in $CDCl_3$. Fortunately, most of the protons and carbons can be differentiated into two sets by careful analysis of the spectral data. The ^1H and ^{13}C resonances within one set were assigned by ^1H-^1H COSY, HMQC, HMBC and ROESY spectra (Tables 1 and 3). The bicyclic system as in aglaxiflorins A was deduced from the HMBC connections H-12/C-9,10,11; H-10/C-9,11,13,19,25; H-11/C-1,2,10,19,25 (Fig. 1). No doublet methyl group was observed in ^1H NMR and the molecular formula of aglaxiflorin E has less one CH_2 than aglaxiflorin A indicating that the side chain linked to the C-32 amide carbonyl was 2-propanol. This group was confirmed

by the HMBC between the oxygenated carbon at d_C 73.5 (73.4) and the methyl groups [d_H 1.07, 0.82 (Me-34); 1.18, 1.14 (Me-35)]. The relative stereochemistry of aglaxiflorin E was deduced from the 2D ROESY spectrum data. Clear and strong ROESY cross-peaks H-12/H-10,11 indicated H-10 and H-11 were of a *cis* configuration, which was different from aglaxiflorins A–D [5]. The structure of aglaxiflorin E was determined as drawn in Figure 1. The ROESY correlation between H-27 and H-10,11, observed for both rotamers, revealed that the structures represented by these two sets of signals have the same conformation of the C-25/N-26 amide bond but different conformation of the C-32/N-31.

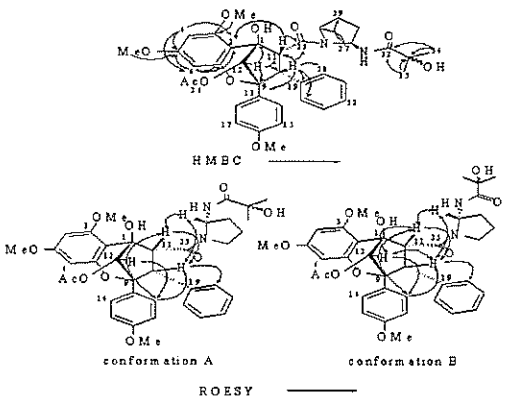

Figure 1. Selected HMBC and ROESY correlations of aglaxiflorin E.

Table 1. ^{1}H, HMBC and ROESY NMR data of **aglaxiflorin E.**

#	δ_H[a]	HMBC[b]		ROESY
		^2J	^3J	
4	6.08 (1H, d, J = 2.2 Hz)[c]	5	2, 6	MeO-3, MeO-5
	6.25 (1H, d J = 2.3 Hz)	3, 5	2, 6	MeO-3, MeO-5
6	6.01 (1H, d, J = 2.2 Hz)	5, 7	2, 4	MeO-5
	5.94 (1H, d, J = 2.3 Hz)	5, 7	2, 4	MeO-5
10	4.42 (1H, dd, J = 9.7 0.9 Hz)	9, 11, 19	13, 20, 24, 25	11, 20, 24, 27
	4.29 (1H, d, J = 5.0 Hz)	9, 11, 19	13, 20, 24, 25	11, 12, 14, 18, 27
11	4.23 (1H, d, J = 9.7 Hz)	1, 10, 25	2, 12, 19	10, 14, 18, 27
	3.92 (1H, d, J = 5.0 Hz)	1, 10, 25	2, 12, 19	10, 12, 14, 18, 20, 24, 27
12	5.75 (1H, d, J = 0.9 Hz)	9	10, 11, 36	14, 18
	6.36 (1H, s)	1	2, 36	11, 12, 14, 18
14, 18	6.91 (2H, d, J = 9.0 Hz)		9, 16	10, 11, 12, 15, 17
	7.37 (2H, d, J = 9.0 Hz)		9, 16	10, 11, 12, 15, 17
15, 17	6.50 (2H, d, J = 9.0 Hz)	16	13	14, 18, MeO-16
	6.78 (2H, d, J = 9.0 Hz)	16	13	14, 18, MeO-16
20, 24	6.87-6.97[d]			
	6.39 (2H, br. d, J = 7.4 Hz)	21, 23	10, 22	10, 21, 23
21, 23	6.87-6.97[d]			
	6.87-6.97[d]			
22	6.87-6.97[d]			
	6.87-6.97[d]			
27	6.20 (1H, br d, J = 5.9 Hz)		29, 30	10, 11, 29, 30
	6.70 (1H, br d, J = 5.8 Hz)		29, 30	10, 11
28	1.85-1.98 (2H, m)			
	1.85-1.98 (2H, m)			
29	1.73-1.85 (2H, m)			
	2.02-2.20 (2H, m)			
30	3.36-3.41 (1H, m); 2.95-3.11 (1H, m)			
	3.43-3.55 (2H, m)			
34	1.07 (3H, s)	33	32, 35	
	0.82 (3H, s)	33	32, 35	
35	1.18 (3H, s)	33	32, 34	
	1.14 (3H, s)	33	32, 34	
MeO-3	3.85 (3H,s)		3	4
	3.72 (3H, s)		3	4
MeO-5	3.67 (3H, s)		5	4, 6
	3.69 (3H, s)		5	4, 6
MeO-16	3.57 (3H, s)		16	15, 17
	3.70 (3H, s)		16	15, 17
Me-C_{36}	2.25 (3H, s)	36		
	1.69 (3H, s)	36		

[a] 500 MHz, chemical shift (δ) in ppm; resonances (2 sets) for two rotamers. [b] carbons correlated with proton [c] coupling constant (J) in Hz; s: singlet, d: doublet, m: multiplet. [d] overlapped protons.

Similar to aglaxiflorin E, 1D NMR data of aglaxiflorin F (Tables 2 and 3) showed two sets of peaks in methanol-d_4 and most of the protons and carbons were assignable. The ^{1}H and ^{13}C NMR data of aglaxiflorin F showed many characteristic features of the aglaxiflorins A and E, e.g. a *meta*-dimethoxy substituted aromatic ring A, a *para*-methoxyphenyl ring B, a phenyl ring C, and a methine pair (H-10 and H-11) coupling with each other. Compared to aglaxiflorins A and E, the methyl group of an acetyl was missing; however, new resonances typical for a -COOCH3 group appeared in the ^{13}C and ^{1}H NMR spectra (methoxycarbonyl group; compare Tables 1 and 2) This suggested a structure which could be derived from cyclopenta[*bc*]bezopyran type aglaxiflorin by an oxidative opening of the 1,9-methano-bridge. Five

Table 2. ^{1}H, HMBC and ROESY NMR data of **138**.

#	δ_H[a]	HMBC[b]		ROESY
		^2J	^3J	
4	6.03 (1H, d, J = 2.5 Hz)[c]	3, 5	2, 6	MeO-3, MeO-5
	6.10 (1H, d J = 2.3 Hz)	3, 5	2, 6	MeO-3, MeO-5
6	6.53 (1H, d, J = 2.5 Hz)	5, 7	2, 4	14, 18, MeO-5
	6.58 (1H, d, J = 2.3 Hz)	5, 7	2, 4	14, 18, MeO-5
10	4.87 (1H, d, J = 10.3 Hz)	11, 19	25	11, 20, 24
	5.16 (1H, d, J = 9.4 Hz)	11, 19	20, 24, 25	11, 14, 18, 20, 24
11	4.59 (1H, d, J = 10.3 Hz)	1, 10, 25	19	10, 20, 24, 27
	4.42 (1H, d, J = 9.4 Hz)	1, 10, 25	19	10, 20, 24, 30a, 30b
14, 18	7.28 (2H, d, J = 9.1 Hz)		16	15, 17
	7.28 (2H, d, J = 9.1 Hz)		16	10, 15, 17
15, 17	6.64 (2H, d, J = 9.1 Hz)	14, 16, 18		14, 18, MeO-16
	6.64 (2H, d, J = 9.1 Hz)	14, 16, 18		14, 18, MeO-16
20, 24	7.18-7.25[a]			10, 11, 21, 23
	7.28 (2H, br. d, J = 7.1 Hz)			10, 11, 21, 23
21, 23	7.10-7.18[d]			
	7.18-7.25[d]			
22	7.10-7.18[d]			
	7.18-7.25[d]			
27	4.98 (1H, br. dd, J = 6.3, 1.5 Hz)			11, 28a, 28b
	5.80 (1H, br. dd, J = 6.5, 2.2 Hz)			28a, 28b
28	1.3-1.48 (2H, m)			27
	1.62-1.67 (1H, m, H-28a);			27
	1.90-2.00 (1H, m, H-28b)			
29	1.58-1.64 (1H, m, H-29a)			30a
	1.78-1.85 (1H, m, H-29b)			30b
	1.75-1.79 (1H, m, H-29a)			30a
	1.86-1.93 (1H, m, H-29b)			30b
30	3.07 (1H, ddd, J = 11.6, 7.7, 4.6 Hz, H-30a)			29a, 30b
	3.23 (1H, ddd, J = 11.6, 8.1, 2.4 Hz, H-30b)			29b, 30a
	2.78 (1H, br dd, J = 16.1, 9.0 Hz, H-30a)			11, 29a, 30b
	3.46 (1H, ddd, J = 16.1, 7.8, 2.8 Hz, H-30b)			11, 29b, 30a
33	1.68-1.75 (1H, m)			
	1.92-1.98 (1H, m)			
34	0.9-1.2 (2H, m)			
	1.24-1.31 (1H, m); 1.48-1.55 (1H, m)			
35	0.52 (3H, t, J = 7.4 Hz)	34	33	MeO-3
	0.75 (3H, t, J = 6.9 Hz)	34	33	
36	0.76 (3H, d, J = 7.4 Hz)	33	32, 34	
	0.86 (3H, d, J = 6.9 Hz)	33	32, 34	
MeO-3	3.51 (3H, s)		3	4, 35
	3.55 (3H, s)		3	4
MeO-5	3.77 (3H, s)		5	4, 6
	3.80 (3H, s)		5	4, 6
MeO-12	3.08 (3H, s)		12	
	3.11 (3H, s)		12	
MeO-16	3.61 (3H, s)		16	15, 17
	3.62 (3H, s)		16	15, 17

[a] 500 MHz, chemical shift (δ) in ppm; resonances (2 sets) for two rotamers. [b] carbons correlated with proton [c] coupling constant (J) in Hz; s: singlet, d: doublet, m: multiplet. [d] overlapped protons.

Table 3. ^{13}C NMR data of aglaxiflorin E and aglaxiflorin F in methanol-d^4.[a]

#	aglaxiflorin E	aglaxiflorin F	#	aglaxiflorin E	aglaxiflorin F	#	aglaxiflorin E	aglaxiflorin F
1	82.5 80.1	190.5 193.3	13	130.3 131.9	63.4 63.4	29	22.3 23.0	21.2 22.7
2	106.7 108.3	113.8 113.6	14, 18	128.3 129.2	129.3 129.3	30	47.2 47.1	46.1 46.0
3	159.5 159.9	164.7 164.8	15, 17	113.7 114.3	113.7 113.7	32	178.0 177.9	177.8 177.1
4	93.2 93.5	94.3 93.5	16	160.3 160.6	161.0 159.8	33	73.5 73.4	41.4 42.5
5	163.0 162.5	160.3 160.4	19	142.0 137.5	139.8 140.6	34	27.5 27.8	25.1 27.4
6	95.2 94.7	100.1 98.9	20, 24	131.1 130.5	129.5 129.9	35	27.9 28.1	10.7 11.3
7	155.6 154.7	159.9 159.9	21, 23	128.8 130.7	128.3 128.2	36		15.8 16.5
9	89.0 86.8	90.6 91.0	22	127.3 127.8	127.8 127.8	3-OMe	56.7 56.6	55.2 55.2
10	57.9 56.4	52.2 50.3	25	171.1 172.5	168.6 167.2	5-OMe	55.7 55.88	55.3 55.6
11	62.8 57.7	63.3 65.7	27	64.8 64.9	63.4 63.4	16-OMe	55.5 55.92	51.2 51.4
12	81.7 74.7	171.0 171.1	28	35.0 34.8	33.9 32.4	36-Me[b]	21.5 19.8	54.6 54.6

[a] 125 MHz, chemical shift (δ) in ppm; every carbon has two sets of signals, the first number belongs to one set and the second number belongs to the other set. [b]12-OMe for aglaxiflorin F.

similar derivatives, forbaglin A and B, and thapoxepine A – C have recently been reported [6,7]. Forbaglin A and B were C-27 epimers, and thapoxepine A and C were isolated as C-27 epimeric mixtures. The ^{13}C NMR shifts of C-28 and C-29 showed some characteristic differences between two epimers, which seems to be well suited for distinguishing the 27-*S* and 27-*R* configurations [C-28: 33.6-34.4 (27 *S*), 30.8-31.7 (27 *R*); C-29: 21.2-21.8 (27 *S*), 23.0-23.7 (27 *R*)] [7]. In our case, the chemical shift of C-28 was 32.4-33.9 and the chemical shift of C-29 was 21.2-22.7, so the configuration of C-27 of aglaxiflorin F was determined to be *S*. Two different conformations of aglaxiflorin F were the two rotamers derived from the amide bond C-25/N-26, which was deduced from the ROESY correlations H-11/H-27 in one set of signal and H-11/H-30 in the other set of signal as drawn in Figure 2.Although many flavonol-cinnamate cycloadducts similar to aglaxiflorin A and F have been isolated from *aglaia* specie [6-8], the absolute stereochemistry of this type of compound was not determined. We tried to crystallize the brominated aglaxiflorin A derived from Br_2 direct bromination. The single crystal X-ray structure determination of 6-bromo-aglaxiflorin A obtained showed the absolute stereochemistry of aglaxiflorin A as illustrated as in Figure 3.

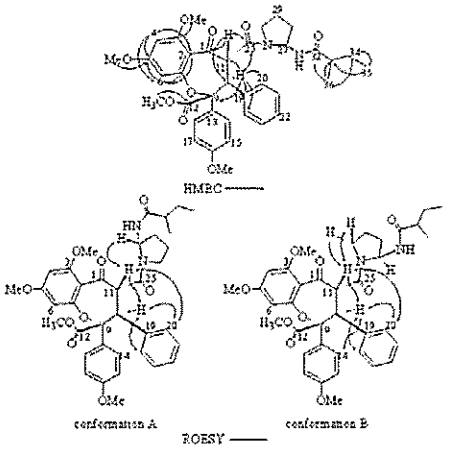

Figure 2. Selected HMBC and ROESY of aglaxiflorin F.

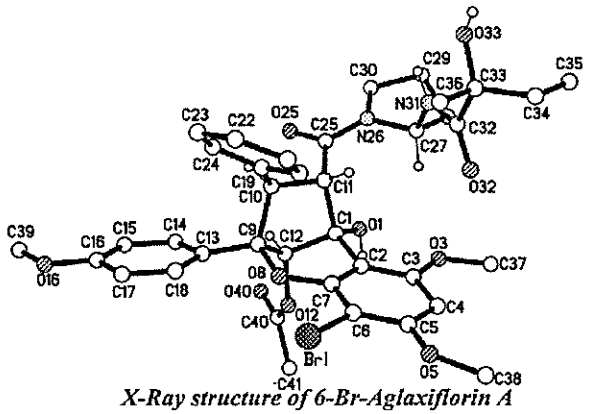

Figure 3. Structure of 6-Bromoglaxiflorin A

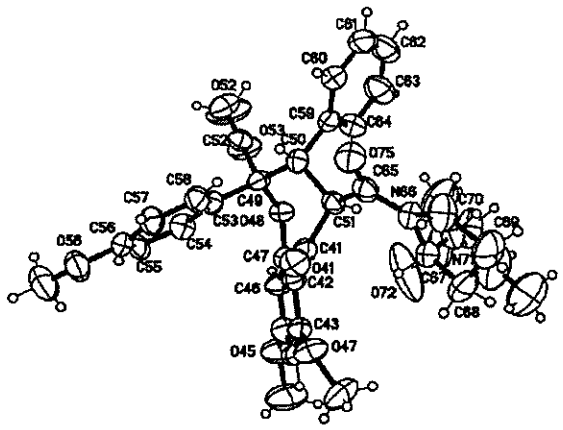

Figure 4. Structure of Aglaxiflorin G, 27-Epimer of Aglaxiflorin F

The same method was applied to aglaxiflorin F. The product aglaxiflorin G obtained by epiemerization by (treatment by bromine) was slightly less polar on silica gel TLC and had a more highly preferred conformation than aglaxiflorin F and showed only one set of signals in the 1H NMR spectrum when methanol-d_4 was used as solvent. The FABMS of aglaxiflorin G showed the same molecular ion as aglaxiflorin F indicating it was an isomer of aglaxiflorin F. X-Ray crystallography established its structure as the 27-epimer of aglaxiflorin F (Fig. 4).

Ackowledgment – We thank the National University of Singapore for a grant (RP) for this research and Ms. X. H. Wu for the cytoxicity determination.

REFERENCES

1. Hayashi N, Lee K H, Hall I H, McPhail, A T, *Phytochemistry* (1982), 21(9), 2371-2373.
2. Pursuhothaman K K, Sarada A, Connolly J D, Akinniyi J A, *Chem. Soc.Perkin. Trans.* (1979), 1, 3171-3179.
3. Duh C Y, Wang S K, Hou R S, Wu Y C, Yu W, Cheng M C, Chang T T, *Phytochemistry* (1993) 34(3), 857-858.
4. Wu T S, Liou M J, Kuoh C S, Teng C M, Nagao T, Lee D H, *J. Nat. Prod.* (1997) 60, 606-608.
5. Xu Y J, Wu X H, Tan B K H, Lai Y H, Vittal J J, Imiyabir Z, Madani L, Khozirah K S, Goh S H, *J. Nat. Prod.* (2000) 63, 473-476.
6. Dumontet, V, Thoison, O., Omobuwajo, O. R., Martin, M. T, Perromat, G., Chiaroni, A., Riche, C., Pais, M., Sevenet, T, *Tetrahedron* (1996) 52(20), 6931-6942.
7. Bacher, M., Hofer, O., Brader, G., Vajrodaya, S., Greger, H. *Phytochemistry* (1999) 52, 253-263.
8. Nugroho, B. W., Edrada, R. A., Wray, V., Witte, L., Bringmann, G., Gehling, M., Proksch, P. *Phytochemistry* (1999) 51, 367-376.

Journal of Science and Technology in the Tropics (2005) 1: 95-101

Table 1 shows the results of the calorimeter volume assessed by the two gases and the results indicate a mean value of 18112±993 L. This figure is slightly lower than that obtained by multiplying the length, width and height of the room, which was 18400 cm^3. Taking into account the furniture, objects and the subject found in the room during the measurements, the net volume of the calorimeter or V value for all related calculation was rounded to 18 000 L.

Table 1. Determination of room calorimeter volume by two different gases.

99.8% oxygen		OFN	
Volume injected (L)	Room volume (L)	Volume injected (L)	Room volume (L)
50	17 268	150	15 936
100	17 606	200	18 182
150	17 932	250	18 668
200	18 662	300	18 453
250	19 156	350	19 256
Mean ± SD	18 125 ± 773	Mean ± SD	18 099 ± 1272

* Mean ± SD for the room calorimeter volume as assessed by all 2 gases = 18 112 ± 993L.

An overestimation or underestimation of the volume of the calorimeter by ±1000 L would result in less than 1% error in the measurement of energy expenditure. This could be explained as follows: the difference in O_2 concentration between the room air (O_i) and the ambient air (O_e) is equal to zero when a subject first enters the calorimeter (or at the start of butane combustion). As respiration proceeds, $O_i - O_e$ increases from zero to values ranging from 0.4% to 5%, depending on the flow rate and the magnitude of energy expenditure (EE) of the subject. Substituting typical values for flow rate (e.g. 60 L/min) and for $O_i - O_e$ (e.g. 0.5%) and using the Weir equation [11], the 24-hour EE could be derived as follows:

$$EE = 1.50 + 0.00001736\ (V)$$

For V = 18 000 L, then EE = 1.812 kcal/min. If V = 18 000 ± 1000 L, EE calculated ranges from 1.795 kcal/min to 1.830 kcal/min. Thus if V is ±1000 L, the error for a 24-h EE run is negligible, less than 1%.

Butane standardization test

A series of tests by burning butane gas (Campingaz C206, Kolon International Corp., Korea) was carried out to assess the reliability and accuracy of the calorimeter. The equation for the combustion of butane gas is as follows:

$$\underset{(116)}{2\,C_4H_{10}} + \underset{(416)}{13\,O_2} \rightarrow \underset{(352)}{8\,CO_2} + \underset{(180)}{10\,H_2O}$$

Hence,

116g butane requires (13 x 22.4) O_2 = 291.2L O_2

Thus,

$$1\text{g butane requires } \frac{291.2}{116} = 2.51\text{L } O_2$$

Assuming that the content of the butane gas canister is not entirely pure butane, for example an equal mixture of butane and propane (50:50), it produces only a small error of 0.8%. By calculation, the combustion of 1 g butane requires 2.51 L O_2 with an assumption of 100% combustion of the gas including that from the condensation of water formed during the combustion. Practically in the open-circuit system, butane is unlikely to attain 100% combustion under normal atmospheric conditions. In fact, the net value for the volume of O_2 required for combustion of butane is lower than the gross calculated value by 8% [12]. In line with previous studies [3,4], a value of 2.31 L O_2 for net combustion of 1 g of butane was used in the calculation.

The butane canister was initially weighed prior to burning. The flame could be adjusted to mimic slow or high respiratory rates of man. The amount of butane used in the combustion could be determined either by subtracting the initial and final weights of the butane canister or by calculation using the formula derived by Boroumand [13].

$$\text{Volume } O_2 \text{ used (L)} = \frac{MO_2 \times F \times a}{100} + \frac{b \times V}{100}$$

where:

- MO_2 = mean change O_2 concentration (%)
- F(STP) = air flow through the room (L/min)
- V(STP) = volume of the room (L)
- a = experimental time (min)
- b = O_2 deficit in the room at the end of experiment (%)

Thus,

$$\text{calculated g butane used} = \frac{\text{Volume } O_2 \text{ used (L)}}{2.31}$$

The reliability and accuracy of the calorimeter were assessed by measuring the differences between the gross weight loss and the calculated values of the butane used. Results of butane standardization tests are shown in

JOURNAL OF SCIENCE AND TECHNOLOGY OF THE TROPICS

NOTICE TO CONTRIBUTORS

JOSTT is a multi-disciplinary journal. It publishes original research articles and reviews on all aspects of science and technology relating to the tropics. All manuscripts are reviewed by at least two referees, and the editorial decision is based on their evaluations.

Manuscripts are considered on the understanding that their contents have not been previously published, and they are not being considered for publication elsewhere. The authors are presumed to have obtained approval from the responsible authorities, and agreement from all parties involved, for the work to be published.

Submission of a manuscript to JOSTT carries with it the assignment of rights to publish the work. Upon publication, the Publisher (COSTAM) retains the copyright of the paper.

Manuscript preparation

Manuscripts must be in English, normally not exceeding 3500 words. Type double spaced, using *MS Word*, on one side only of A4 size with at least 2.5 cm margins all round. Number the pages consecutively and arrange the items in the following order: title page, abstract, key words, text, acknowledgements, references, tables, figure legends.

Title page

Include (i) title, (ii) names, affiliations and addresses of all authors, (iii) running title not exceeding five words, and (iv) email of corresponding author.

Abstract and key words

The abstract, not more than 250 words, should be concise and informative of the contents and conclusions of the work. A list of not more than five key words must immediately follow the abstract.

Text

Original research articles should be organized as follows: Introduction, Materials and Methods, Results, Discussion, Acknowledgements, References. The International System of Units (SI) should be used. Scientific names and mathematical parameters should be in italics.

References

References should be cited in the text as numbers enclosed with square [ ] brackets. The use of names in the text is discouraged. In the reference section, the following examples should be followed:

1 Yong H.S., Dhaliwal S.S. and Teh K.L. (1989) A female Norway rat, *Rattus norvegicus*, with XO sex chromosome constitution. *Naturwissenchaften* **76:** 387-388.
2 Beveridge W.I.B. (1961) *The Art of Scientific Investigation*. Mercury Book, London.
3 Berryman A.A. (1987) The theory and classification of outbreaks. *In* Barbosa P. and Schultz J.C. (eds.) *Insect outbreaks* pp. 3-30. Academic Press, San Diego.

Tables

Tables should be typed on separate sheets with short, informative captions, double spacing, numbered consecutively with Arabic numerals, and do not contain any vertical lines. A table should be set up to fit into the text area of at most the entire page of the Journal.

Illustrations

Black-and-white figures (line drawings, graphs and photographs) must be suitable for high-quality reproduction. They must be no bigger than the printed page, kept to a minimum, and numbered consecutively with Arabic numerals. Legends to figures must be typed on a separate sheet. Colour illustrations can only be included at the author's expense.

Proofs and reprints

Authors will receive proofs of their papers before publication. Ten reprints of each paper will be provided free of charge.

Submission

Manuscripts should be submitted in triplicate (including all figures but not original artwork), together with a floppy diskette version of the text, to:

The Managing Editor
JOSTT
C-3A-10, 4th Floor Block C
No. 1 Jalan SS20/27
47400 Petaling Jaya
Selangor Darul Ehsan
Malaysia

Table 2. The differences in weight of butane used between the observed and calculated values ranged from -1.2% to +1.8%; the measured value was 98.77±0.21% of that obtained by theoretical calculation. These results suggest that the problem of diffusion was minimal despite long experimental periods as well as high ventilation rates, neither of which seems to affect the sensitivity of the system.

Table 2. Butane standardization tests.

Experimental time (hour)	Flow rate (L/min)	Amount of butane used (g) By weight	By calculation	% difference
4	50.5	30.1	30.5	1.3
6	66.0	62.5	61.8	-1.1
12	62.5	89.7	90.8	1.2
15	58.0	105.8	104.5	-1.2
18	67.0	122.8	124.9	1.7
19	56.0	142.8	141.2	-1.1
24	59.4	49.6	49.0	-1.2
24	50.0	192.0	189.7	-1.2
24	50.0	196.3	198.3	1.0
24	50.5	135.3	137.1	1.3
24	52.0	208.1	205.8	-1.1
24	66.8	41.5	42.2	1.8
24	69.0	190.0	192.2	1.2
24	67.0	184.4	182.8	-0.9
25	66.0	201.7	204.4	1.3

Air and gas permeability tests

Tests were carried out to validate the assumption that during the EE measurements there was no diffusion or leakage of air/gases through the walls, ceiling or floor except through the main outflow and the sample tubes. The O_2 concentration in the room was first reduced by butane combustion using standard butane canister (Campingaz C206, Kolon International Corp., Korea). After $O_i - O_e$ had reached values of 0.3 to 0.6% the combustion was stopped and the subsequent fall in $O_i - O_e$ was recorded for several hours. As EE = 0, the general equation for the EE calculation, Weir equation [11] can be written as follows:

$$d(O_i - O_e)/dt = -F/V\ (O_i - O_e)$$

or

$$d(O_i - O_e)/(O_i - O_e) = -(F/V)dt$$

After integration on both sides of the equation, it is written:

$$\ln (O_i - O_e) = -(F/V)t$$

By plotting $\ln (O_i - O_e)$ against time (t), a straight line is obtained, where $O_i - O_e$ gradually dropped and the gradient of the graph is equal to the value of F/V. The values for F/V from the graph were then compared with those obtained by theoretical calculation. At a typical flow rate of 60.0 to 62.5 L/min, the values of F/V from the graph were less than 2% of the theoretical F/V values; the measured value was 99.01±0.10% of that obtained by calculation. These differences suggest that the error is sufficiently small and that the assumptions mentioned above are valid.

Estimation of energy expenditure

Based on Weir equation [11], energy expenditure was calculated using the following equation: in 5-minute time respective moving average

$$EE = [(0.05)\ (F)\ (O_i - O_e)] + [(0.05)\ (V)\ (d(O_i - O_e)/dt)]$$

where,

- EE = energy expenditure (kcal/min)
- F = rate of air exhausted from the calorimeter (L/min)
- V = air volume of calorimeter (L)
- O_i = oxygen concentration of baseline (outdoor)
- O_e = oxygen concentration of calorimeter
- $d(O_i - O_e)/dt$ = reduction rate of $(O_i - O_e)$
- 0.05 = the Weir factor

Thus, calculation of EE can be programmed in the computer using the following equation:

$$EE = [(F)\ (O_i - O_e)\ (0.05)] + [(V)\ (O_a - O_b)\ (0.05)]$$

where,

- EE = energy expenditure (kcal/min)
- F = rate of air exhausted from the calorimeter (L/min)
- O_i = oxygen concentration of baseline (outdoor)
- O_e = oxygen concentration of calorimeter
- V = air volume of calorimeter (L)
- O_a = initial oxygen concentration of calorimeter
- O_b = final oxygen concentration of calorimeter
- 0.05 = the Weir factor

From the above equation, the reproducibility of the calorimeter was tested using several 24 hour EE trial runs. Seven subjects (3 lean and 4 obese), respectively, participated in 2 trials of sedentary 24-h EE within 1 week (Table 3). By paired samples t-test analysis, the results showed that all normal and obese subjects recorded small and no significant differences in EE over 24-h between the first and second trials. The above trials have also provided us with useful information on the calorimeter. Besides being viable for comparative studies, it has also proven to be comfortable since no